AD NUMBER: AD0371261
CLASSIFICATION CHANGES
TO: Unclassified
FROM: Confidential
LIMITATION CHANGES
TO: Approved for public release; distribution is unlimited.
FROM: Distribution authorized to U.S. Government Agencies and their Contractors; Export Control; 5 Mar 1966. Other requests shall be referred to US Army Missile Command, Redstone Arsenal, AL, 35898.
AUTHORITY
U per DoDD 5200.10, GP-4 dtd 31 Dec 1978; ST-A per USASSC ltr dtd 10 May 1974

GENERAL DECLASSIFICATION SCHEDULE

IN ACCORDANCE WITH
DOD 5200.1-R & EXECUTIVE ORDER 11652

THIS DOCUMENT IS:

CLASSIFIED BY_____

Subject to General Declassification Schedule of Executive Order 11652-Automatically Downgraded at 2 Years Intervals- DECLASSIFIED ON DECEMBER 31,____.

BY

Defense Documentation Center
Defense Supply Agency
Cameron Station
Alexandria, Virginia 22314

SECURITY MARKING

The classified or limited status of this report applies to each page, unless otherwise marked.
Separate page printouts MUST be marked accordingly.

THIS DOCUMENT CONTAINS INFORMATION AFFECTING THE NATIONAL DEFENSE OF THE UNITED STATES WITHIN THE MEANING OF THE ESPIONAGE LAWS, TITLE 18, U.S.C., SECTIONS 793 AND 794. THE TRANSMISSION OR THE REVELATION OF ITS CONTENTS IN ANY MANNER TO AN UNAUTHORIZED PERSON IS PROHIBITED BY LAW.

NOTICE: When government or other drawings, specifications or other data are used for any purpose other than in connection with a definitely related government procurement operation, the U. S. Government thereby incurs no responsibility, nor any obligation whatsoever; and the fact that the Government may have formulated, furnished, or in any way supplied the said drawings, specifications, or other data is not to be regarded by implication or otherwise as in any manner licensing the holder or any other person or corporation, or conveying any rights or permission to manufacture, use or sell any patented invention that may in any way be related thereto.

CONFIDENTIAL

7

3771261

BOEING

DDC AVAILABILITY NOTICES

a. Foreign announcement and dissemination of this report by DDC is not authorized.

b. U.S. Gov't. agencies may obtain copies of this report directly from DDC. Other qualified DDC users shall request through U.S. Army Missile Command, AMSMI-RNT.

c. Release or announcement to the public is not authorized.

This document contains information affecting the National defense of the United States within the meaning of the Espionage Laws, Title 18, U.S.C., Section 793 and 794, its transmission to or the revelation of its contents in any manner to an unauthorized person is prohibited by law.

SEATTLE, WASHINGTON

CONFIDENTIAL

CONFIDENTIAL

THE BOEING COMPANY

REV LTR

CODE IDENT. NO. 81205

NUMBER D2-99603-1

TITLE: HiBEX Silo Design and Test Firing Results(U)

FOR LIMITATIONS IMPOSED ON THE USE OF THE INFORMATION CONTAINED IN THIS DOCUMENT AND ON THE DISTRIBUTION OF THIS DOCUMENT, SEE LIMITATIONS SHEET.

MODEL HiBEX CONTRACT DA-01-021-10696(Z)

ISSUE NO. _____ ISSUED TO: _____

PREPARED BY HiBEX Engineering

SUPERVISED BY C. R. Smith
N. O. Kinyon

APPROVED BY C. R. Smith 3/5/66
C. R. Smith

APPROVED BY _____

CONFIDENTIAL

D3 4802 1430 ORIG. 4/65

HIBEX SILO DESIGN AND TEST FIRING RESULTS

This Project HiBEX Research effort is a part of PROJECT DEFENDER, sponsored by the Advanced Research Projects Agency, Department of Defense, under ARPA Order No. 510, Program Code No. 4730.

Project Code Number	5900.21.21414.01
Name of Contractor	The Boeing Company
Date of Contract	10 January 1964
Contract Number	DA-01-021-AMC-10696(Z)
Contract Expiration Date	Approximately 25 March 1966
Project Engineer	HiBEX Program Manager Elliot V. Mock Telephone - Area Code 206 656-6774
Short Title of Work	HiBEX

DISTRIBUTION LIMITATIONS

Distribution outside The Boeing Company shall not be made except as required to execute HiBEX Contract DA-01-021-AMC-10696(Z) or as approved by the U. S. Army Missile Command.

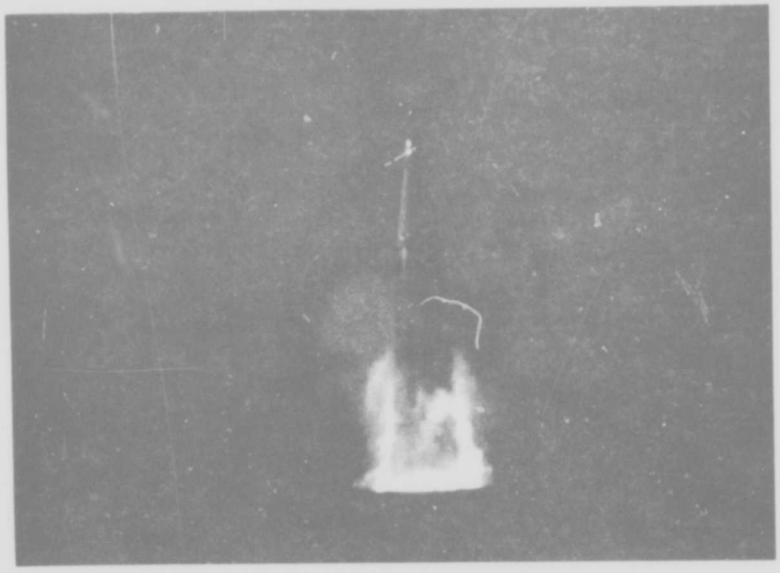

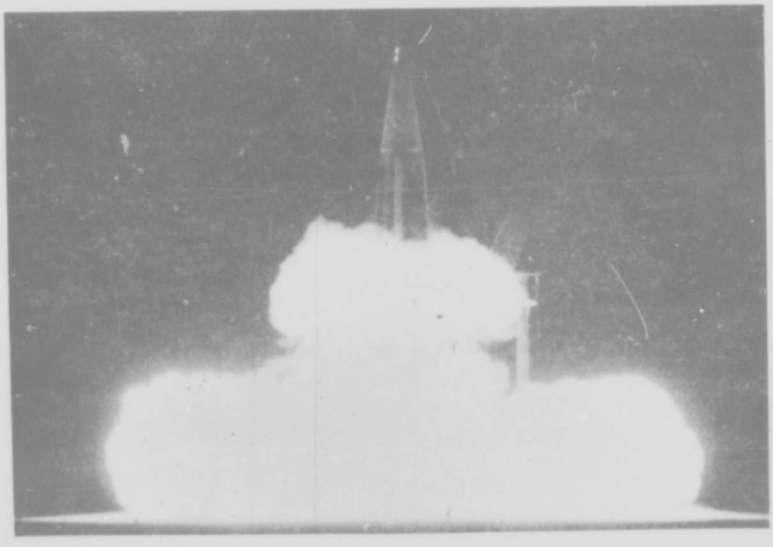

D-3 LAUNCH

The two views above show the HiBEX D-3 vehicle launch just before and just after sabot separation.

ABSTRACT AND KEY WORDS

Mathematical models were developed to predict the silo environment and the effects of a silo launch on a high-performance vehicle. Based upon the results of theoretical analyses using those models, equipment was designed to explore launch effects with three different silo configurations, namely:

1. Closed breech, low plenum pressure.
2. Closed breech, high plenum pressure
3. Vented

HiBEX vehicles were successfully launched from the low- and high-pressure closed-breech configurations. Utilization of the vented configuration was planned in the event that insurmountable difficulties were encountered with the other configurations. Since no difficulties were encountered, the vented configuration was not required.

The silo thermal and pressure environment measured during the silo launches compared well with the analytical results. The effects of silo launches on the vehicle were not significantly different from those encountered during a surface launch. The acoustic environment in the vicinity of the silo correlated well with blast wave theory.

Acoustic overpressure

ARPA Project HiBEX

Closed breech silo launch

High g Boost Experiment

Sabot

Silo pressure

Silo heating rate

Vehicle skirt strain

TABLE OF CONTENTS

REFERENCES

1. ARPA Project HiBEX Technical Requirement Nr. 506, Revision Nr. 2, 5 October 1964, with Contractual Modifications to March 5, 1966 (Confidential).

2. Boeing Document D2-99513, ARPA Project HiBEX Task I Final Report (U), April 28, 1964 (Confidential).

3. Boeing Document D2-99600-1, HiBEX Final Technical Report (U), March 1966 (Confidential).

4. Boeing Document D2-99579-5, ARPA Project HiBEX Flight Test Report, Vehicle D-2 (U), December 10, 1965 (Confidential).

5. Boeing Document D2-99579-6, HiBEX Flight Test Report, Vehicle D-3 (U), January 17, 1966 (Confidential).

6. Boeing Document D2-99539-1, A Program for Calculating the Vehicle Environment and Performance During a Silo Launch, August 1965 (Unclassified).

7. Boeing Document D2-99572-1, HiBEX Vibration and Shock Environment (U), March 1966 (Confidential).

8. Boeing Document D2-3617, Material and Structural Element Allowables - Minuteman, Revised May 1965 (Unclassified).

9. Boeing Document D2-99590-1, Development and Calibration of Heat Flux Transducers for HiBEX (U), February 1, 1966 (Confidential).

10. Boeing Document T2-1224, Boeing Test Report - Shear Test of 100° Counter-Sunk Head Rivets in 7075 and 2024-T3 Clad Sheet, June 1958 (Unclassified).

11. Shanley, F. R., Strength of Materials, McGraw-Hill, 1957 (Unclassified).

1.0 FOREWORD

This report is one of the series of special reports of significant scientific and technical findings during Project HiBEX as defined in paragraph 5.7 of Technical Requirement Nr. 506(1). The report describes analytical methods, equipment design, and test results for silo launch investigations conducted as part of Project HiBEX.

2.0 INTRODUCTION

The objectives of the HiBEX silo launch investigation were to determine the effects of launch from an underground silo on the HiBEX vehicle and the silo, and the resulting acoustic overpressure environment.

Studies were made of three silo types; open silo, closed breech silo, and vented silo. Two basic silo concepts were examined in detail. These were the closed breech silo and vented silo concepts. In both concepts, the rocket exhaust gases are expelled into a plenum chamber below the vehicle, and the vehicle is guided out of the silo by means of a sabot which had a close fit in the launch tube. In the case of a vented silo, the gas pressure in the plenum chamber is reduced by venting a portion of the exhaust gas to the atmosphere.

The closed breech launch, with the vehicle aft skirt riveted to a sabot which provided a gas seal and guidance in the silo was selected for the flight test program. The primary advantages of the closed breech launch are:

1) Rapid reaction time
2) Simplicity
3) Protection of the vehicle from pressure and thermal environments.

Vented silos were studied and hardware constructed, but not tested. The selected silo is shown in Figure 1.

The open silo launcher was dropped from primary consideration during Task I(2). The open silo would have subjected the vehicle to the disturbing effect of reverse flow of high velocity hot exhaust gases. No significant offsetting advantages were identified for the open silo design.

The vented silo test was dropped from the program when the number of silo launches to be attempted was reduced to two. The information value of the results of a second closed breech launch was judged to be greater than of the data from a single vented silo launch. The effects of a vented silo launch on the vehicle are not fundamentally different from the effects of a low pressure closed breech launch, except for the possibly disturbing effect of the vent exhaust, which can be controlled by the vent exit configuration.

The silo was a test device and was designed to accommodate the three modes of launches; closed breech, vented, and open. In keeping with the scope of the HiBEX Program, operational or tactical considerations were not included in the design. The silo and sabot were designed by using the analytical methods discussed in Section 4. No subscale or full scale development tests were performed prior to the two flight tests.

SILO CONFIGURATION

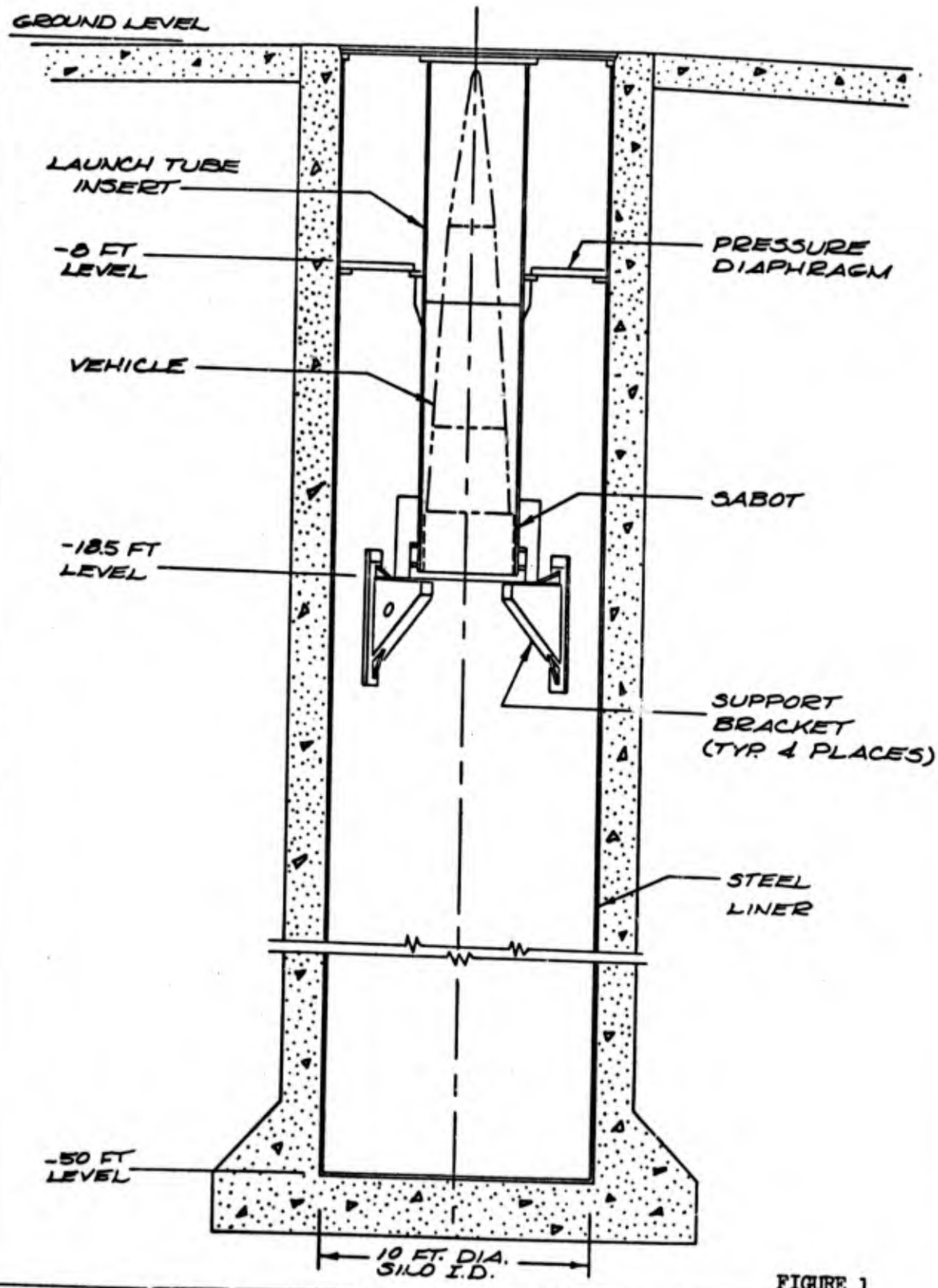

FIGURE 1

USE FOR DRAWING AND HANDPRINTING — NO TYPEWRITTEN MATERIAL

REV LTR _____

The silo structure was required to survive the heat, pressure, and exhaust gas flow of a launch without damage. The silo inside diameter of 10 ft was selected to permit an open silo fly-out launch and to allow adequate working space for in-silo operations during the experimental program. The silo depth of 50 ft was established to allow a closed-breech launch with a maximum back pressure of about 160 psi. Higher back pressures were obtained by filling in the lower portion of the silo to reduce the plenum volume.

Figure 2 shows an external view with principal dimensions of the HiBEX vehicle used in the launch tests. Other details of the vehicle are shown and described in Boeing Document D2-99600-1(3).

Particular objectives of the launch tests were:

1) Vehicle

   a) To determine the effects of the silo launch on the propulsion system performance and operation.

   b) To determine the effects of the silo launch on vehicle dynamics and performance.

   c) To determine the effects of the silo launch and sabot separation on vehicle structure and on equipment operation and survivability.

2) Silo

   a) To determine the silo internal environment, including pressures and heating rates, and compare the measured parameters with analytical values.

   b) To determine the effects of the launch on the silo and sabot structure, including the launch tube alignment and surface of the bore.

The acoustic and pressure levels in the launch area resulting from the silo launch were also measured and compared with analytical results and pad launch results.

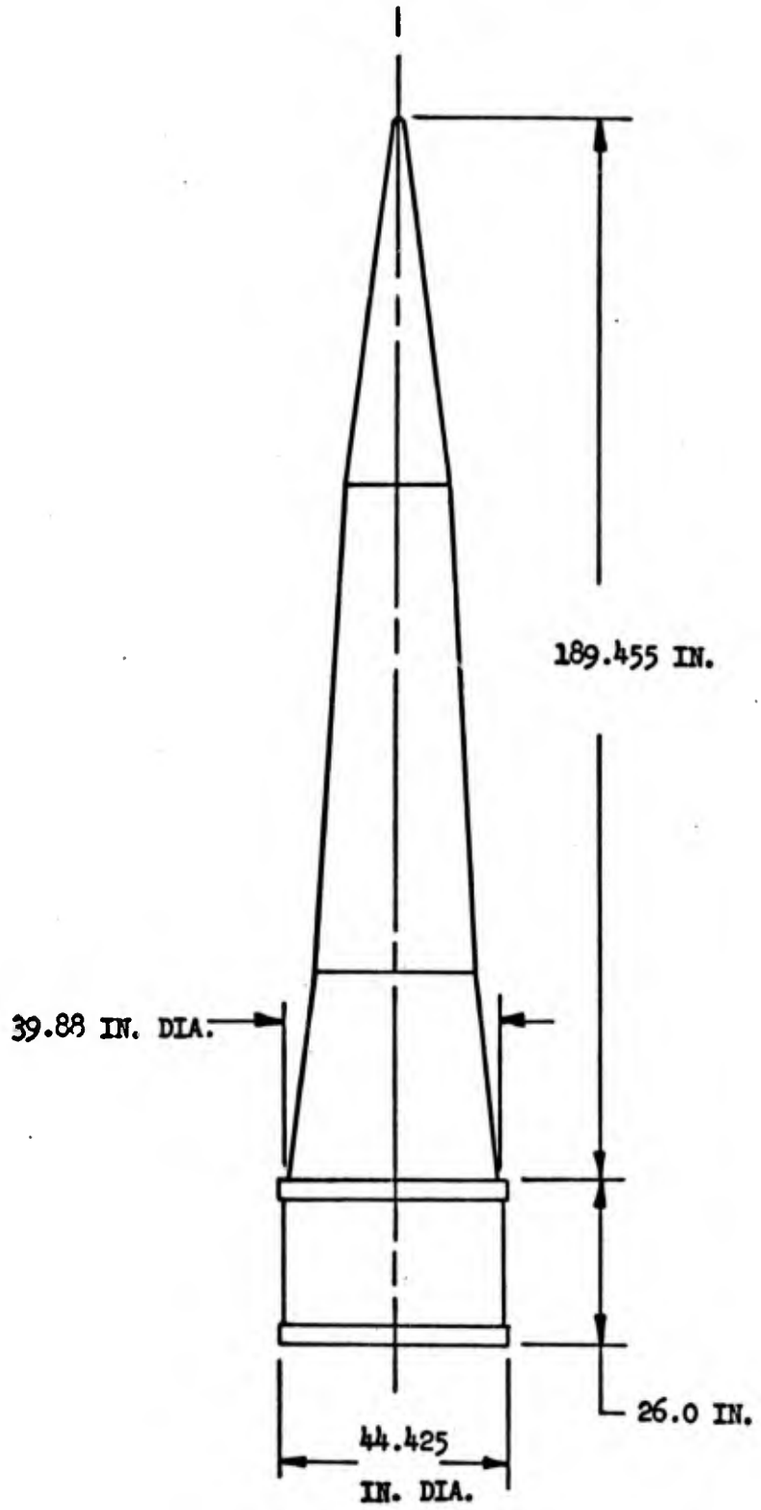

FIGURE 2 - PRINCIPAL DIMENSIONS OF SILO LAUNCH TEST VEHICLES

3.0 SUMMARY OF RESULTS AND CONCLUSIONS

Two HiBEX vehicles with overstrength rocket motor cases were successfully launched from closed breech silos, one at 169 and the other at 254 psia average silo pressures at vehicle emergence. Both launches were successful. The launches were part of the HiBEX D-2(4) and D-3(5) flight tests; they took place at WSMR on October 22, 1965 and on December 2, 1965.

The analytical model used to predict silo pressure and thermal environment, as well as vehicle performance, provided excellent correlation between the closed breech silo launch predictions and the launch test measurements.

There were no detrimental effects of the silo launch on either the vehicle or the silo. The dynamic structural analysis technique adequately predicted the structural effects, including sabot separation shock.

3.1 SILO ENVIRONMENT

The silo pressure histories during launch were essentially as predicted (see Figures 3 and 4.) Consequently, the analytical methods used during this program can be used with confidence for predicting pressure in other closed breech silos. The capability of these analytical methods to predict vented silo pressures cannot be firmly ascertained at this time since no launches were made from a vented silo.

The calculated average heating rates on the silo walls were in fairly good agreement with the measured average values. No attempt was made to calculate the heating rate distributions along the silo walls. The measured data showed a large variation in heating rates between the top and bottom of the silo, as shown in Figure 5. This large variation was partially caused by the incomplete mixing of rocket motor exhaust gases and air in the silo.

The flow within the launch tube remained attached to the launch tube walls for silo plenum pressures greatly in excess of the nozzle exit pressure. The flow became detached approximately 0.01 sec before the vehicle left the silo during the D-3 launch. Launching from a silo of lesser volume than the D-3 would probably result in a longer period of flow detachment during which high pressures would act on the base of the sabot.

3.2 VEHICLE PERFORMANCE

The effect of the silo launch on the vehicle performance is summarized below:

a) The rocket exhaust flow remained attached to the launch tube walls throughout launch on D-2 and for most of the launch period on the D-3 flight. As a result, the high silo pressure had only a small effect on the vehicle performance while the vehicle was in the silo.

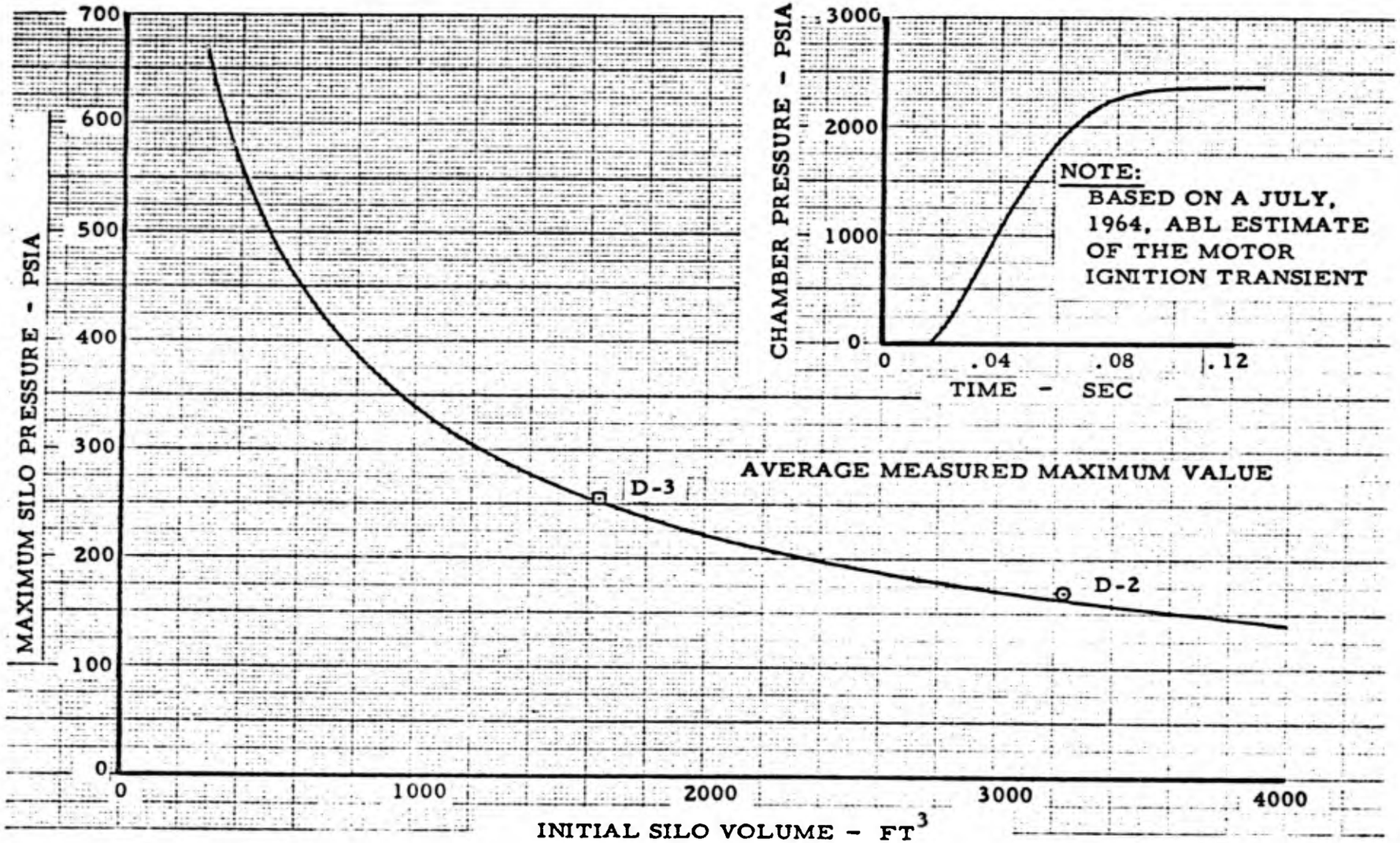
MAXIMUM SILO PRESSURE - PSIA
700
600
500
400
300
200
100
0
0
1000
2000
3000
4000
INITIAL SILO VOLUME - FT3
D-3
D-2
AVERAGE MEASURED MAXIMUM VALUE
CHAMBER PRESSURE - PSIA
3000
2000
1000
0
0
.04
.08
.12
TIME - SEC
NOTE:
BASED ON A JULY, 1964, ABL ESTIMATE OF THE MOTOR IGNITION TRANSIENT

FIGURE 3

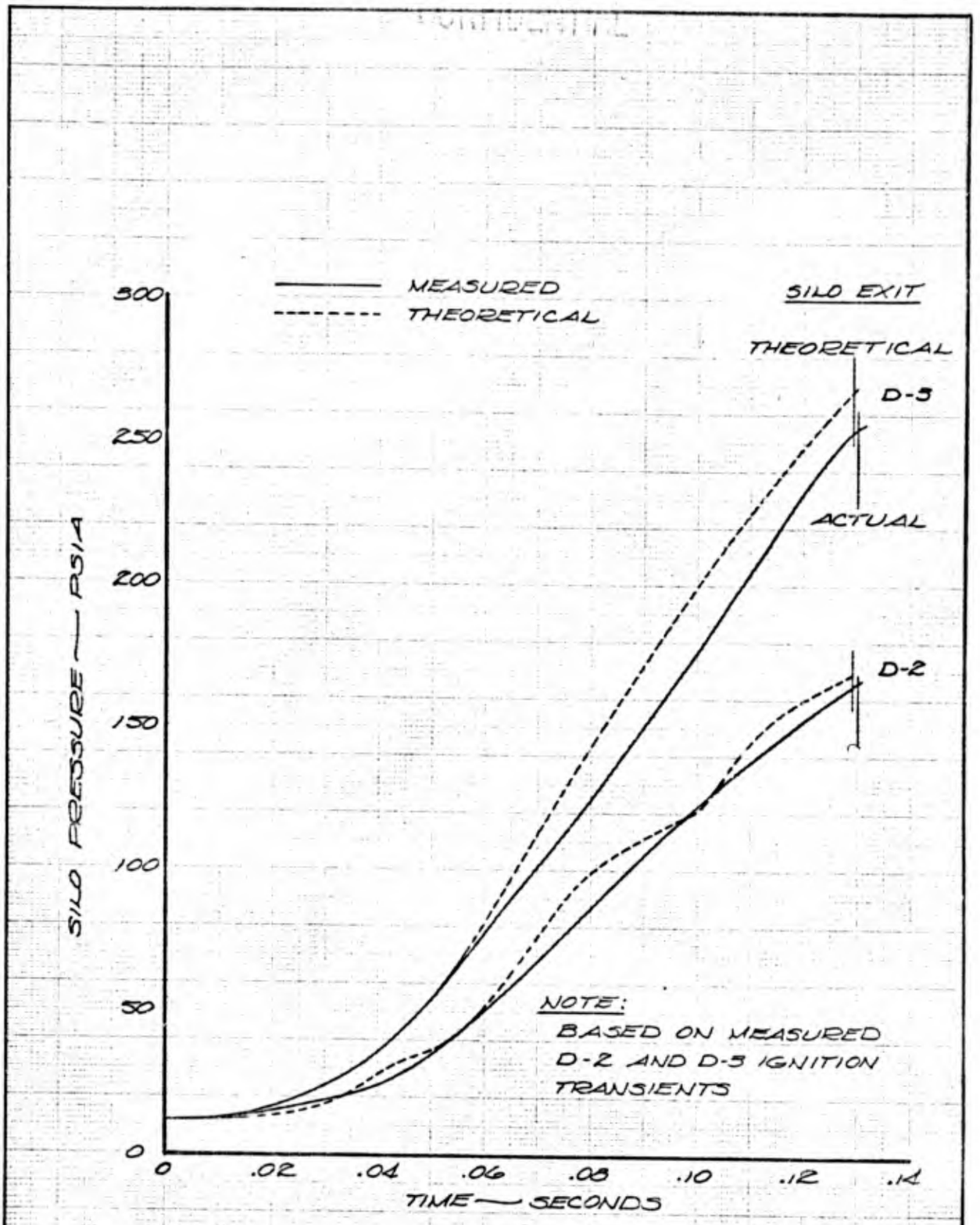

			REVISED	DATE
CALC				
CHECK				
APR				
APR				

COMPARISON OF MEASURED AND THEORETICAL SILO PRESSURES DURING LAUNCH

FIGURE 4

D2-99503-1

THE BOEING COMPANY

TD 461 C-R4

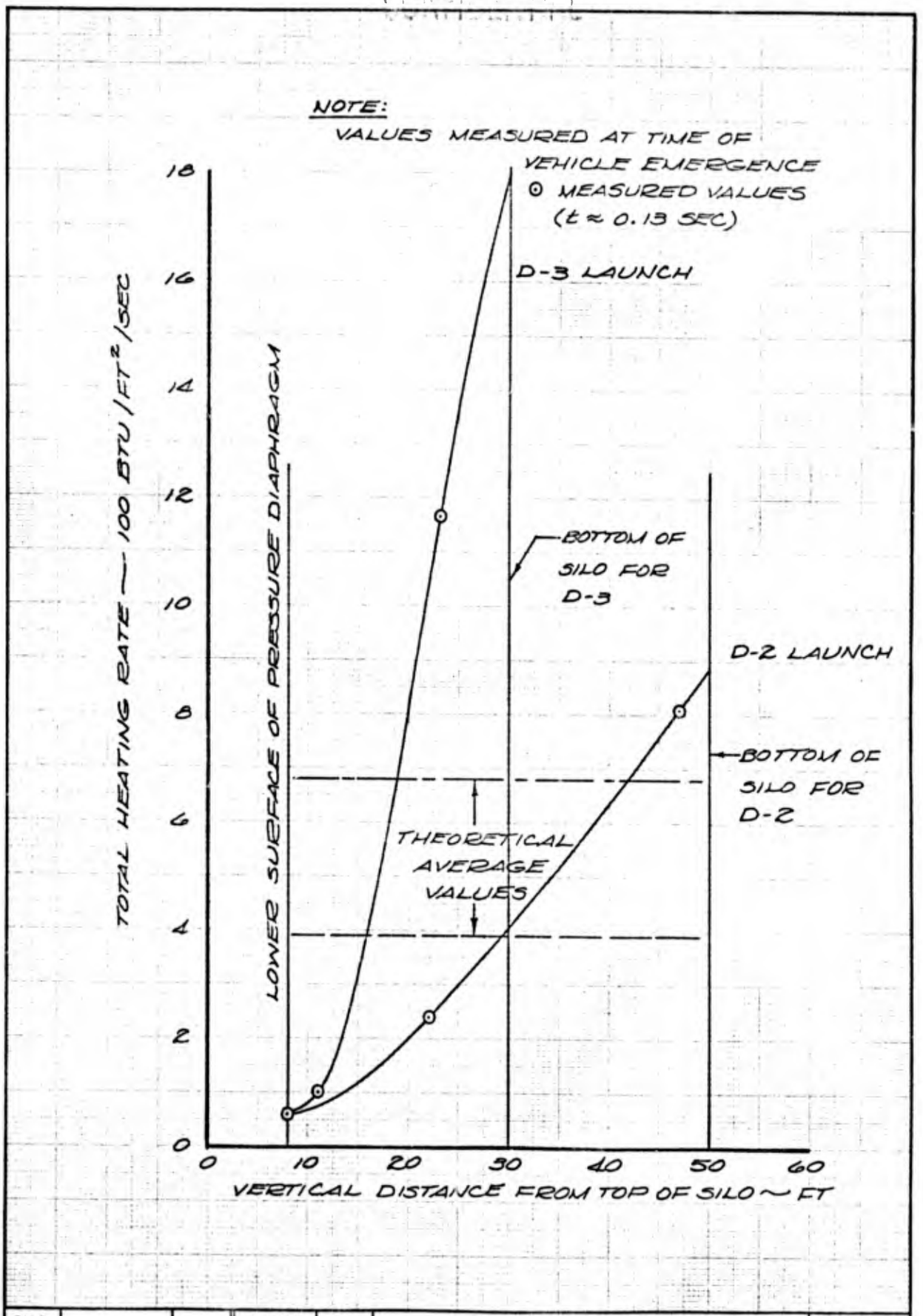

CALC			REVISED	DATE
CHECK				
APR				
APR				

FIGURE 5
TOTAL HEATING RATE DISTRIBUTIONS IN SILO

D2-99603-1

THE BOEING COMPANY

TD 461 C-R4

b) The rocket exhaust flow became detached from the launch tube walls just prior to vehicle emergence from the silo during the D-3 flight. This implies that launching from a silo of lesser volume than the D-3 would result in a larger effect of back pressure on vehicle performance.

c) The nozzle flowed full during the entire launch period of both D-2 and D-3 so that the rocket motor (including the nozzle) was not affected by the silo launch.

d) Pressures acting on the sabot slightly more than compensated for the sabot weight and friction, resulting in an 8 to 15 fps velocity gain at the time of vehicle exit from the silo as compared to a pad launch.

e) Velocity at burnout is influenced by the time of initiating pitchover; the rate is 10 fps per millisecond in the region of vehicle exit from the silo. Accordingly, further silo launch optimization should include compensation for known system delays so as to accomplish the maneuver as early as possible.

3.3 EFFECTS ON STRUCTURE AND EQUIPMENT

Conclusions regarding the effect on vehicle and launch equipment (sabot and silo) of the silo launch are as follows:

a) The vehicle was not adversely affected by the silo launch. Imposed pressure and acceleration loads on the skirt were less than the design loads, and less than other skirt load requirements. The vehicle vibration environment was no greater than for a pad launch.

b) The sabot performed as planned. Loads imposed were less severe than the design loads.

c) The sabot-vehicle separation method of shearing rivets verified that the axial loads from this type of impulse loading are predictable.

d) The silo structure was completely satisfactory--dimensional and angular tolerances were maintained for both launches, and the silo was easily refurbished after launch.

3.4 LAUNCH AREA EFFECTS

Comparison of the predictions with the results of overpressure measurements in the launch area indicate that the environment is predictable with good accuracy. The modified blast wave theory verified by D-3 launch measurements, can be used to derive overpressure design criteria for structure.

Any employment of this closed breech silo concept which requires structures near the launcher must include consideration of the overpressure environment. Non-conventional blast resistant construction would be required inside of 100 ft, and at least "gust type" design out of 1300 ft. Window breakage could be a problem out as far as 600 ft for normal blast incidence, compared to 150 ft for a surface launch.

The threshold of pain for unprotected personnel was 1500 ft from the launch site for silo launch compared with 850 ft for pad launch.

4.0 ANALYSIS AND DESIGN

4.1 THEORETICAL ANALYSIS - SILO PRESSURES AND HEATING RATES

4.1.1 Equations and Method of Solution

The methods and equations used to calculate the vehicle performance and environment during launch are presented in this section. The analytical approach was to establish mass rate and energy rate balances within the rocket motor chamber and within the silo reservoir, and to establish a force balance on the vehicle.

The analytical model developed to perform the calculations consisted of two major branches. The first branch solved the closed breech silo problems, and the second solved the vented silo problem. The second branch consisted of two sub-branches which were built around the assumptions of either no mixing or instantaneous complete mixing of the rocket exhaust gases and air in the silo.

The transient nature of the problem was considered in establishing the model, as were the energy transfer mechanisms which exist in the system.

4.1.1.1 Rocket Motor Combustion Chamber Equations

The thermodynamic properties within the rocket motor chamber were determined by the simultaneous solution of a mass rate balance equation and an energy rate balance equation.

a) Mass Rate Balance

The mass rate balance within the rocket motor combustion chamber is:

Rate of mass into motor combustion chamber from igniter,

plus

Rate of mass into motor combustion chamber from propellant burning surface,

equals

Mass flow rate through the rocket nozzle,

plus

Mass accumulation rate in the rocket chamber.

The rate balance is written symbolically as:

$$\dot{m}_o + A_b \rho_b r_b = C_w P_c A_t + \frac{M_e}{R} \frac{V_c}{P_c} \frac{d}{d\theta} \left(\frac{P_c}{T_c}\right)$$

where:

$\dot{m}_o$ = Mass flow rate of the igniter

A_b = Propellant burning area

ρ_b = Propellant density

r_b = Propellant burning rate

c_w = Rocket nozzle mass flow coefficient

P_c = Rocket motor chamber pressure

A_t = Cross-sectional area of nozzle throat

Me_{P_c} = Molecular weight of propellant gas in the chamber

V_c = Volume of rocket motor chamber

R = Universal gas constant

θ = Time

T_c = Rocket motor chamber temperature

b) Energy Rate Balance

The energy rate balance within the rocket motor chamber is:

Rate of energy into chamber from igniter,

plus

Rate of energy into chamber from burning propellant,

equals

Rate of heat transfer from chamber to surroundings,

plus

Rate of energy expelled through rocket nozzle,

plus

Rate of accumulation of energy in rocket motor chamber.

This is written symbolically:

USE FOR TYPEWRITTEN MATERIAL ONLY

$$\dot{m}_o c_{p_o} (T_o - T_R) + (-\Delta U_c A_b \rho_b r_b) =$$

$$(K_{24} \dot{q}_{c_c} + K_{25} \dot{q}_{r_c}) + c_v P_c A_t c_{p_{p_c}} (T_c - T_R) +$$

$$\frac{c_{v_{p_c}} M_{e_{p_c}} V_c}{R T_c} \left[(T_c - T_R) \frac{d\rho_c}{d\theta} + \frac{P_c T_R}{T_c} \frac{dT_c}{d\theta} \right]$$

Where the additional symbols are defined as follows:

c_{p_o} = specific heat at constant pressure for igniter gases

T_o = igniter exhaust gas temperature

T_R = reference temperature

ΔU_c = heat of combustion of propellant (negative value for an exothermic reaction)

K_{24} = control parameter to eliminate convective energy losses in the chamber if not desired

K_{25} = control parameter to eliminate radiant energy losses in the chamber if not desired

$\dot{q}_{c_c}$ = convective heating rate to inner surface of chamber

$\dot{q}_{R_c}$ = radiant heating rate to inner surface of chamber

$c_{p_{p_c}}$ = specific heat at constant pressure for propellant gases in the chamber

T_c = rocket motor chamber temperature

$c_{v_{p_c}}$ = specific heat at constant volume for propellant gases in the chamber

V_c = volume of rocket motor chamber

4.1.1.2 Silo Reservoir Equations

The thermodynamic properties within the silo reservoir were determined by the simultaneous solution of a mass balance equation, an energy rate balance equation, and a force balance equation. As measured values of chamber pressure and temperature data derived therefrom became available from rocket motor static firings, they were used as input to the silo reservoir portion of the analytical model in place of the foregoing equations.

a) Closed Breech Silo

It was assumed in the closed breech analysis that the rocket gas and air in the silo reservoir mixed instantaneously and completely. This assumption greatly simplified the calculations, and was believed to be valid because of the high velocity and turbulent nature of the rocket exhaust gas.

1. Mass Balance

The mass balance within the silo reservoir is:

Accumulation of mass in silo reservoir,

equals

Mass into silo reservoir from rocket nozzle,

plus

Original mass of air in the silo

Algebraically, this is written as:

$$m_{acc} = m_{p_o} + m_A$$

2. Energy Rate Balance

The energy rate balance within the closed breech silo reservoir is:

Rate of energy into silo reservoir from rocket,

equals

Rate of heat transfer from reservoir to surroundings,

plus

Rate of accumulation of energy in silo reservoir

plus

Rate of work done in expanding against the base of the vehicle and the atmosphere.

This is expressed algebraically as:

$$C_{30}\, C_W\, P_c\, A_t\, c_{p_{p_c}}\, (T_c - T_R) = (\dot{q}_{c_r} + \dot{q}_{r_r})$$

$$+ \frac{d}{d\theta}\left\{\frac{P_r\ V_r}{T_r}\left(\frac{c_{v_r}}{R_{eq}}\right)_{eq}(T_r - T_R)\right\}$$

$$+ \frac{1}{JA_b}\left[(P_{b_s} - P_\infty)(A_b - A_{sep_s}) + (P_{s_s} - P_\infty)\, A_{sep_s}\right]\frac{dV_r}{d\theta}$$

The symbols that have not been previously used are defined below:

C_{30} = A constant to account for energy losses in the nozzle

$\dot{q}_{c_r}$ = convective heating rate to inner surface of silo reservoir

$\dot{q}_{r_r}$ = radiant heating rate to inner surface of silo reservoir

P_r = silo reservoir pressure

V_r = silo reservoir volume

T_r = silo reservoir temperature

$c_{v_{r_{eq}}}$ = equivalent specific heat at constant volume for the gases in the silo reservoir

R_{eq} = equivalent gas constant for gases in the silo reservoir

J = mechanical equivalent of heat

A_b = base area of the vehicle including nozzle exit area

P_{b_s} = pressure acting on the base of the vehicle

P = ambient pressure

A_{sep_s} = nozzle cross-sectional area at the point where separation occurs

USE FOR TYPEWRITTEN MATERIAL ONLY

P_{s_s} = pressure acting on the nozzle exit for the silo case

The total convective heat transferred is given by:

$$\dot{q}_{c_r} = h_{r_{total}} (T_r - T_{w_r})$$

The total convective heat transfer coefficient is composed of three terms:

$$h_{r_{total}} = h_{r_1} + h_{r_2} + h_{r_3}$$

a. Heat transferred to surface of annular section of silo:

$$h_{r_1} = \frac{(0.0263)\, k_r \left(\dot{W}/A_{c_r}\right)^{0.8}}{D_{c_r}^{0.2}\, \mu_r^{0.8}}$$

b. Heat transferred to bottom of silo:

$$h_{r_2} = \frac{(0.0263)\, k_r \left(\dot{W}/A_s\right)^{0.8}}{D_s^{0.2}\, \mu_r^{0.8}}$$

c. Heat transferred to the inner surface of the launch tube:

$$h_{r_3} = \frac{(0.0263)\, k_r \left(\dot{W}/A_B\right)^{0.8}}{D_b^{0.2}\, \mu_r^{0.8}}$$

where:

$$\dot{w} = C_w\, P_c\, A_t$$

The radiant heating rate is given by:

$$\dot{q}_{r_r} = \sigma \left[\epsilon_{g_r}\, T_r^{\,4} - \epsilon_{w_r}\, T_{w_r}^{\,4} \right]$$

and, the emissivity of the aluminum oxide particles in the silo reservoir, ϵ_{g_r}, is obtained from:

$$\epsilon_{g_r} = 1 - e^{-3/2\left(\frac{C_{g_r}\, L_{g_r}}{D_{g_r}}\right)}$$

USE FOR TYPEWRITTEN MATERIAL ONLY

The additional symbols are defined as follows:

$\dot{q}_{c_r}$ = Convective heating rate to inner surface of silo reservoir

h_{r_1} =
h_{r_2} = } Convective heat transfer coefficient to various sections of inner surface of the silo reservoir
h_{r_3} =

T_{w_r} = Reservoir inner surface wall temperature

k_r = Thermal conductivity of exhaust gas in the silo reservoir

$\dot{W}$ = $\frac{dW}{dt}$ - weight flow rate

A_{c_r} = Cross-sectional area of the silo duct

D_{c_r} = Effective diameter of the chamber (silo reservoir)

μ_r = Exhaust gas viscosity in reservoir

A_s = Silo base (floor) area

D_s = Silo diameter

A_B = Propellant burning area

D_b = Vehi le base diameter

C_v = Rocket nozzle mass flow coefficient

A_t = Cross-sectional area of nozzle at throat

USE FOR TYPEWRITTEN MATERIAL ONLY

$\dot{q}_{r_r}$ = Radiant heating rate to inner surface of silo reservoir

σ = Stefan-Boltzmann constant

ϵ_{g_r} = Emissivity of propellant gas (and air mixture) in reservoir

ϵ_{w_r} = Emissivity of inner surface of reservoir walls

e(exp) = Natural logarithm base

C_{g_r} = Concentration of aluminum oxide particles in exhaust gas in the silo reservoir

L_{g_r} = Thickness of exhaust gas cloud in the silo reservoir

D_{g_r} = Diameter of aluminum oxide particles in exhaust gas in the silo reservoir

b) Vented Silo

Two methods were developed for analyzing the vented silo configurations. The first method was based upon the assumption of no mixing of the rocket motor exhaust gases and the air in the silo. The second method was based upon the assumption of instantaneous complete mixing of the gases and air which was similar to the method used in the closed breech analysis.

Details of the analytical model are presented in Boeing Document D2-99539-1(6).

4.1.2 Restrictions, Limitations, and Basic Assumptions

There were several inherent restrictions, limitations, and assumptions in the analytical method used to calculate silo pressure and heating rates, namely:

a) The basic silo geometry consisted of two concentric cylinders, the inner one being the launch tube; and the outer one, the silo. The silo floor was a flat plate and the pressure diaphragm was a flat plate with a center hole, and both were normal to the axis of the cylinders, as depicted in Figure 1. Minor modifications to the analytical model would be required if this basic geometry were changed.

b) The closed breech analysis and one alternate of the vented silo analysis were based on the assumption of instantaneous, complete mixing of the air and the rocket exhaust gases.

c) The second alternate for the vented silo analysis was based on the assumption of no mixing of the air and the rocket exhaust gases.

d) The analytical model calculated the average thermodynamic properties within the rocket motor chamber and silo reservoir. No spatial variation of these thermodynamic properties was included in the analysis.

e) Exhaust gas thermodynamic properties (specific heats, molecular weights, etc.) were obtained from chemical analyses.

f) Secondary burning within the silo reservoir was assumed to be small, and was neglected.

g) The propellant burning surface area and temperature were assumed constant during launch.

h) The heat transfer from the hot gases in the rocket motor chamber to the propellant subsurface was assumed negligible, since the propellant surface recession rate exceeded the rate of subsurface heat conduction.

i) The rocket motor chamber volume was assumed constant during the launch period.

j) Vehicle and launch tube wall temperatures were assumed to increase linearly with time.

k) The mass flow rate of the igniter was represented by linear functions of time.

l) The burning rate of the propellant was represented by exponential functions of chamber pressure.

m) The gas flow was assumed to be turbulent in the rocket motor chamber, nozzle, and silo reservoir for all heat transfer calculations.

n) The form of the analytical method was applicable to solid-propellant rocket motors only.

4.2 TRADE STUDIES

Several theoretical trade studies were conducted early in the HiBEX program to establish the desired silo configurations and to determine the effect of the silo launch on the vehicle performance.

4.2.1 Effect of Silo Volume

To establish the proper silo size for the desired maximum silo pressures, a study was conducted to determine the effect of silo volume on maximum silo pressure. Both closed-breech and vented silos were investigated. Vent areas were varied from 1 sq ft to 50 sq ft. The results of this study are presented in Figure 6. For the smaller silo volumes, the maximum silo pressure is a strong function of the volume; also, the effect of silo venting on the maximum silo pressures achieved during launch is much more pronounced for small silo volumes.

Silo volume also has a significant effect upon other thermodynamic and performance parameters during launch. Based on the assumption of detached flow in the launch tube (see Section 5.1), the more significant effects are:

a) The maximum average gas temperature obtained in the silo just prior to emergence is substantially higher for the smaller silos. This is demonstrated in Figure 7 where average gas temperature histories are shown for several silo volumes. Silo volumes of 3200 cu ft and 850 cu ft resulted in average gas temperatures of 4500° F and 6000° R, respectively.

b) Silo volume has a similar effect upon the theoretical convective and radiant silo wall heating rates, as shown in Figures 8 and 9. The maximum convective heating rates are almost twice as high for a silo volume of 850 cu ft than they are for a silo volume of 3200 cu ft. The maximum radiant heating rates for the smaller volume are more than three times as high as for the larger silo volume.

c) Silo volume also has an effect upon the vehicle performance during launch if the rocket exhaust flow is detached in the launch tube. These effects are demonstrated in Figures 10 through 12.

The vehicle velocity as the vehicle emerges from the silo is increased by about 13 percent when the silo volume is lowered from 3200 cu ft to 850 cu ft.

The vehicle acceleration as the vehicle emerges from the silo is increased by about 33 percent for the same reduction in silo volume.

The resulting vehicle thrust is increased by about 33 percent for the same reduction in silo volume.

If the flow is attached to the launch tube walls during the entire launch period, the effect of silo volume on vehicle performance is greatly reduced. This was the case for the D-2 and D-3 launches during a large portion of the launch period, as discussed in Sections 5.1 and 5.2.

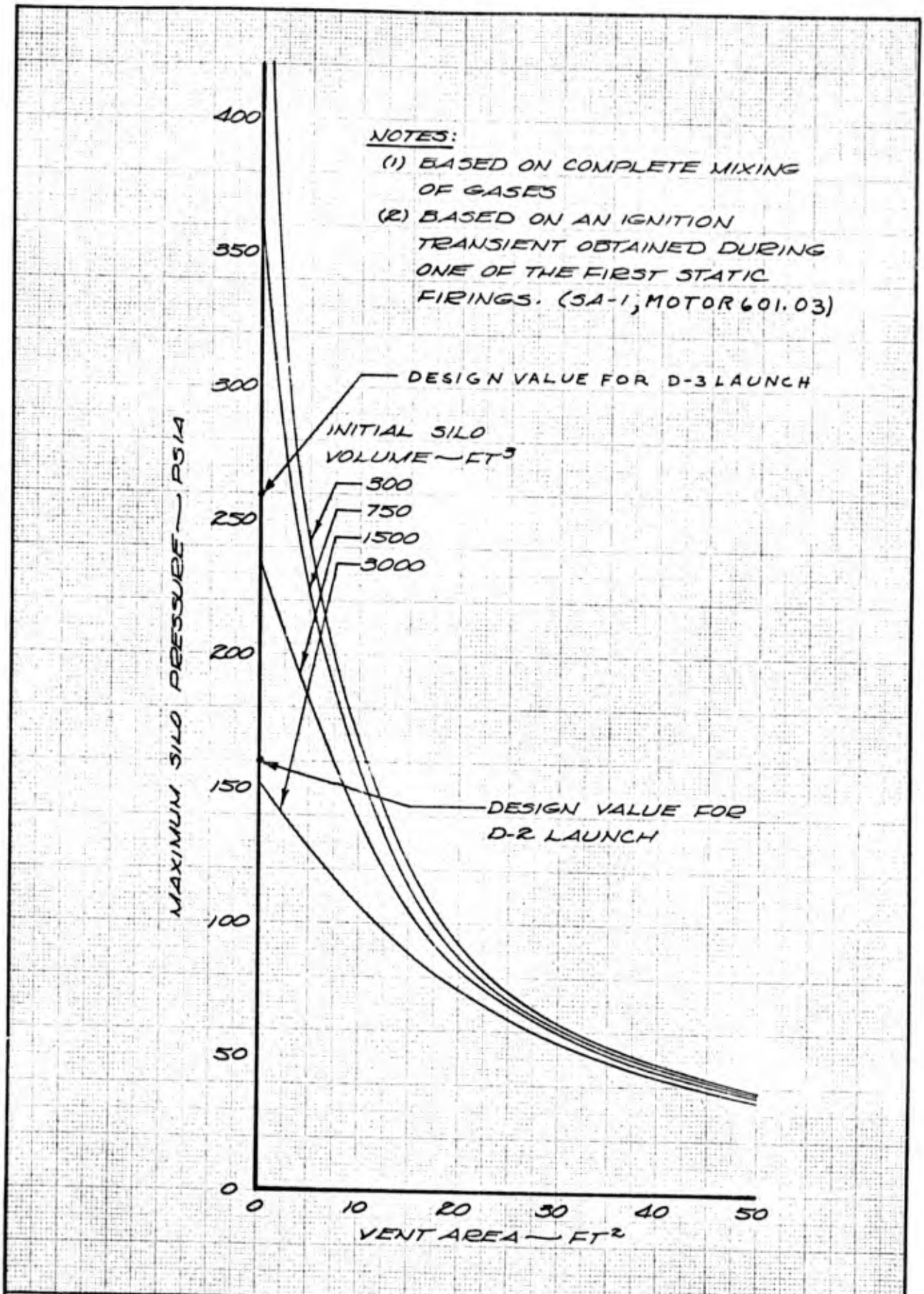

CALC			REVISED	DATE	FIGURE 6 EFFECT OF SILO VOLUME AND VENT AREA ON MAXIMUM SILO PRESSURE	
CHECK						
APR						D2-99603-1
APR						
					THE BOEING COMPANY	PAGE 27

TD 461 C-R4

CLOSED BREECH

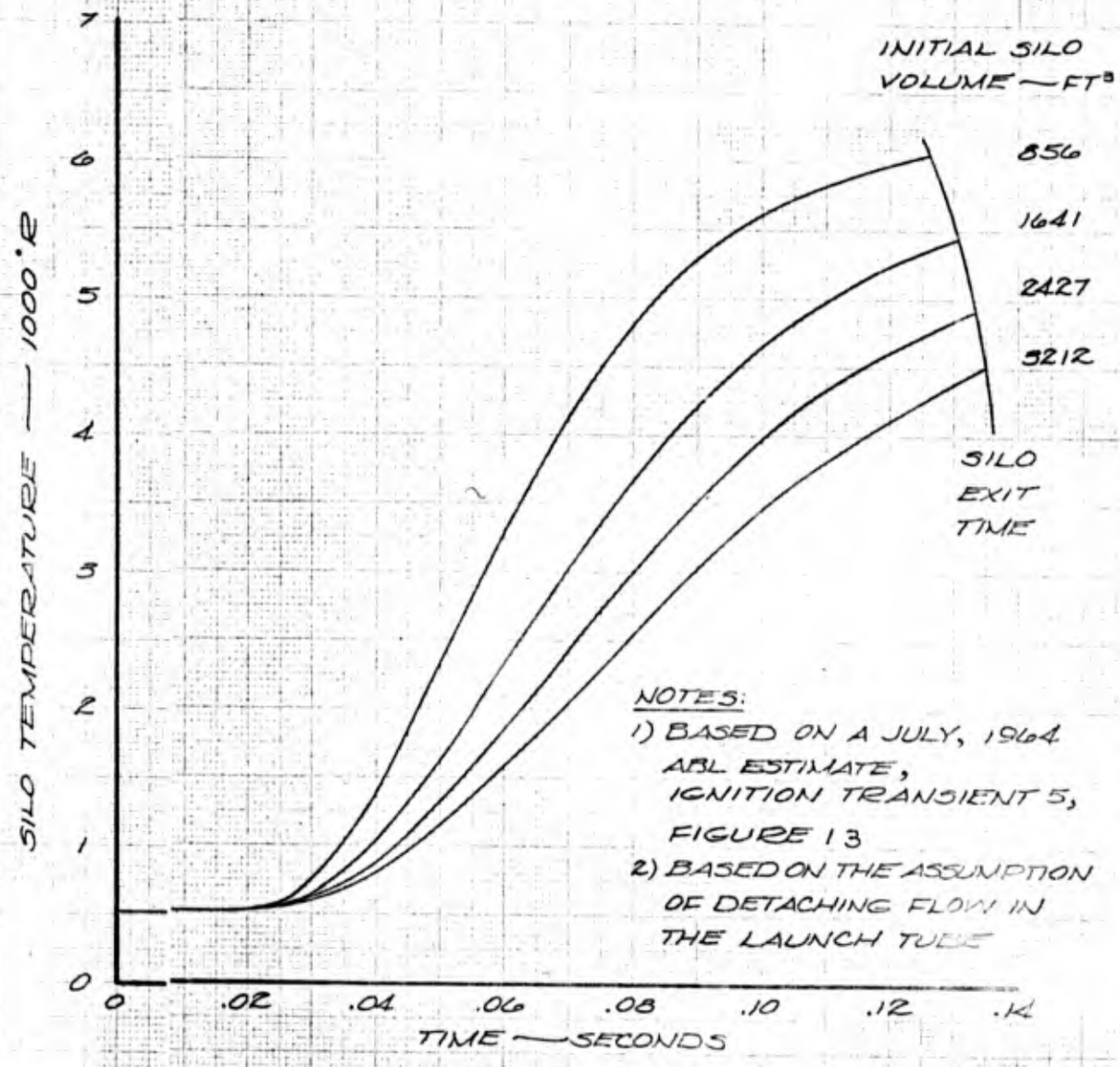

NOTES:

1) BASED ON A JULY, 1964 ABL ESTIMATE, IGNITION TRANSIENT 5, FIGURE 13
2) BASED ON THE ASSUMPTION OF DETACHING FLOW IN THE LAUNCH TUBE

CALC			REVISED	DATE	FIGURE 7 THEORETICAL SILO GAS TEMPERATURE DURING LAUNCH	
CHECK						
APR						D2-99603-1
APR					THE BOEING COMPANY	PAGE 18

TD 461 C-R4

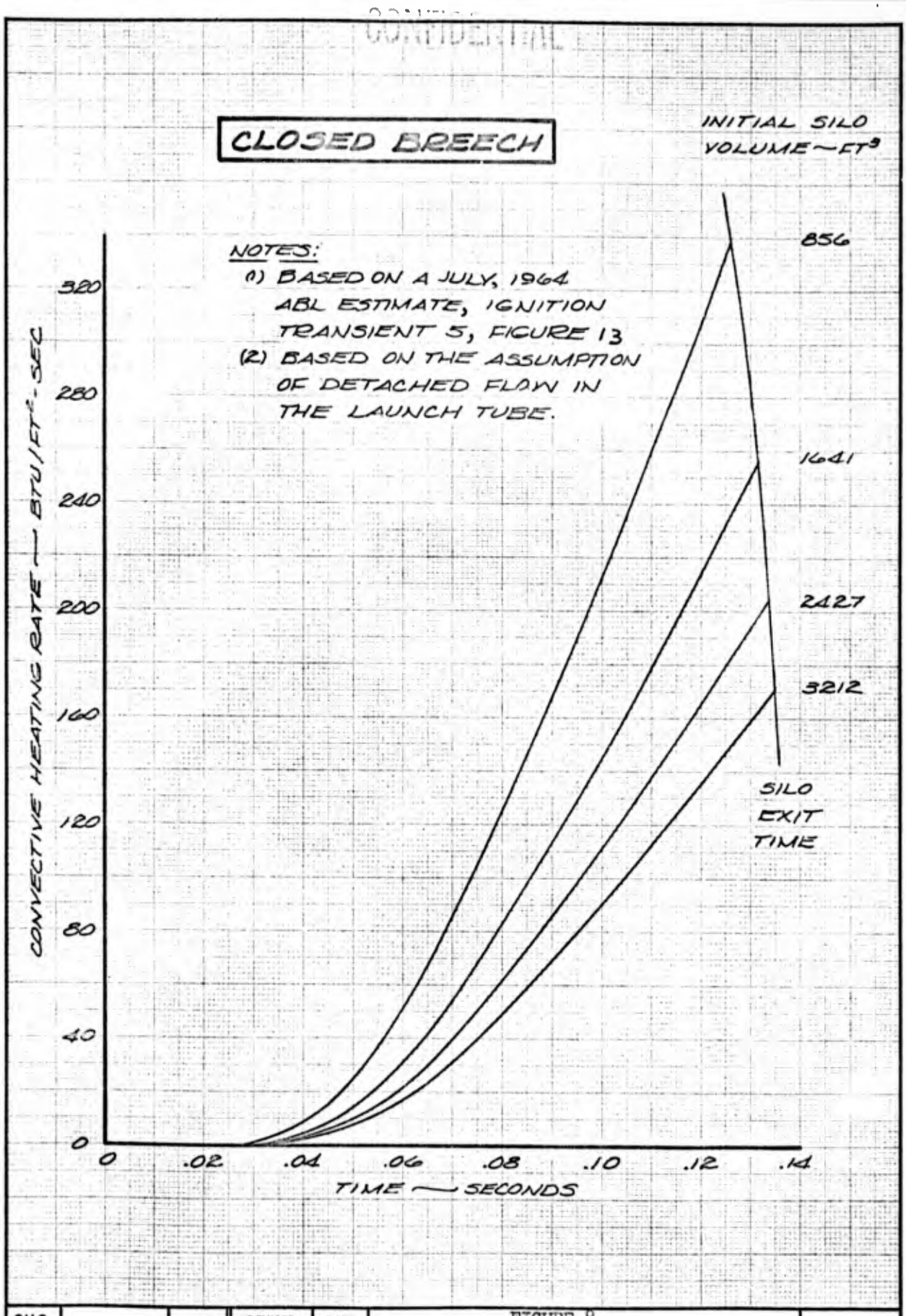

CALC			REVISED	DATE
CHECK				
APR				
APR				

FIGURE 8
CONVECTIVE HEATING RATES TO SILO WALLS DURING LAUNCH

D2-99603-1

THE BOEING COMPANY

PAGE 29

US 4013 8000

K&E ALBANENE TRACING PAPER 71896

CLOSED BREECH

NOTES
1) BASED ON A JULY, 1964 ABL ESTIMATE, IGNITION TRANSIENT 5, FIGURE 13
2) BASED ON THE ASSUMPTION OF DETACHED FLOW IN THE LAUNCH TUBE

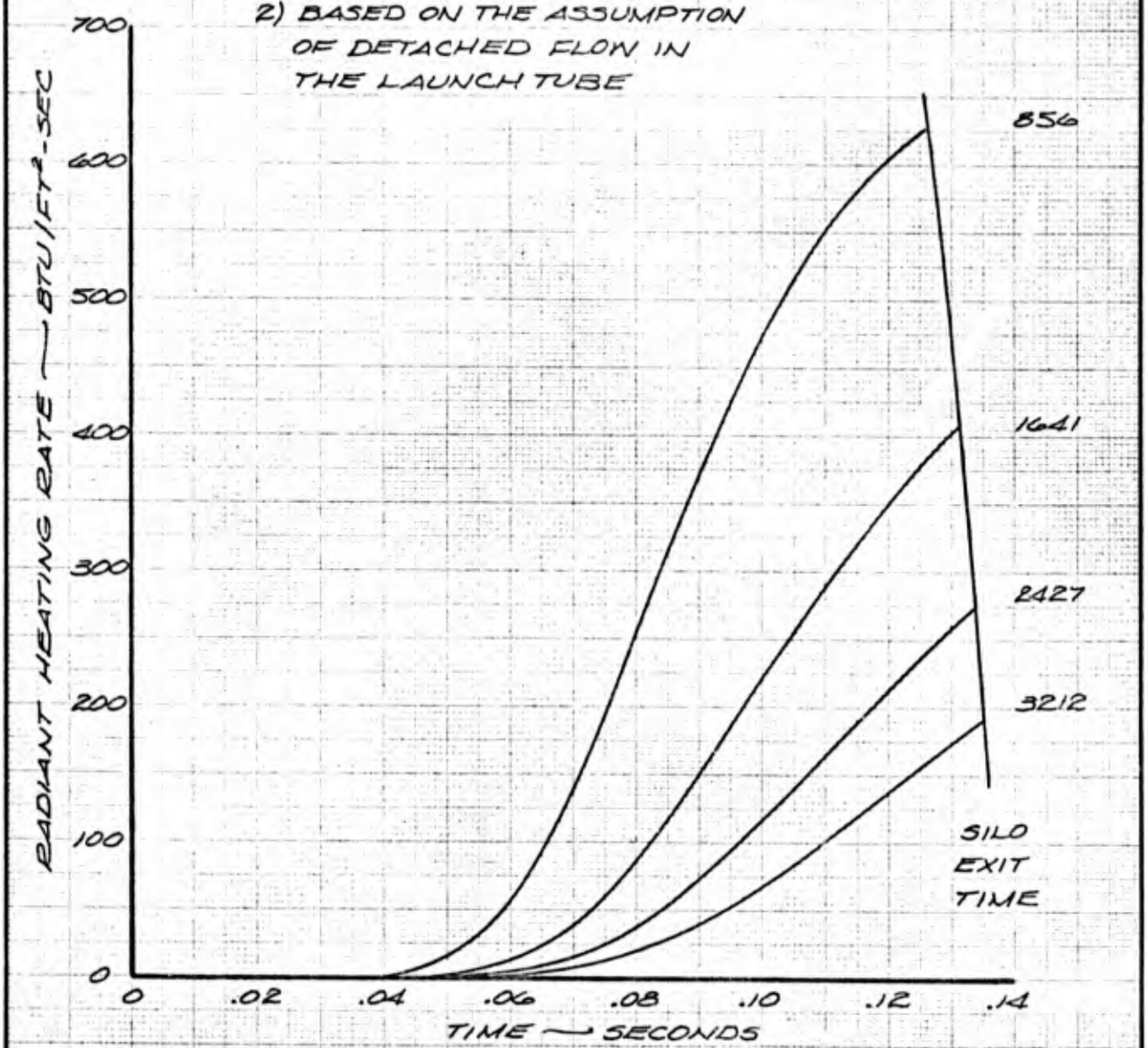

CALC			REVISED	DATE	FIGURE 9 RADIANT HEATING RATES TO SILO WALLS DURING LAUNCH
CHECK					
APR					D2-99603-1
APR					THE BOEING COMPANY
					PAGE 30

US 4013 8000

K&E ALBANENE TRACING PAPER 71896

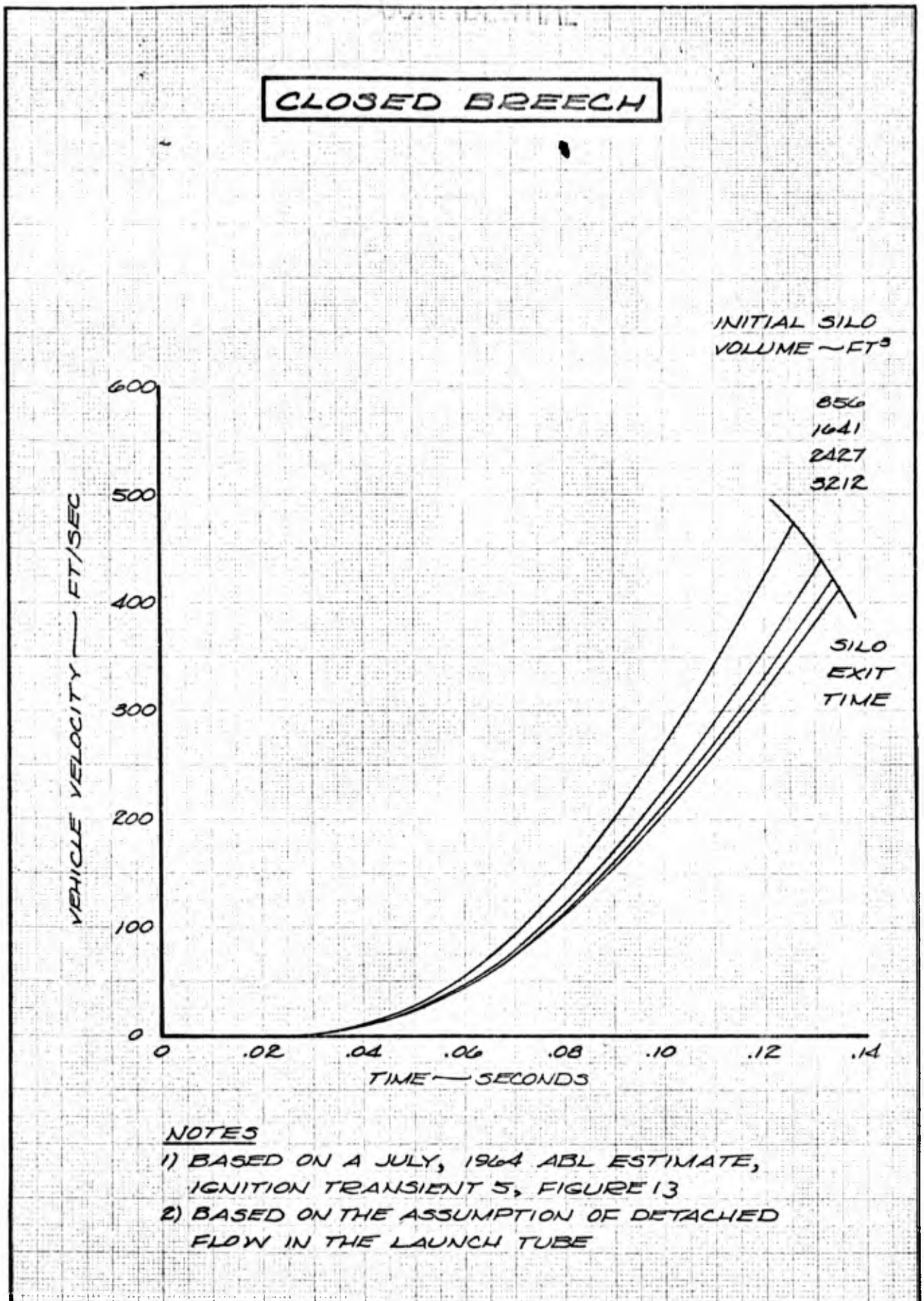

NOTES

1) BASED ON A JULY, 1964 ABL ESTIMATE, IGNITION TRANSIENT 5, FIGURE 13
2) BASED ON THE ASSUMPTION OF DETACHED FLOW IN THE LAUNCH TUBE

CALC			REVISED	DATE	FIGURE 10 THEORETICAL VEHICLE VELOCITY HISTORY DURING SILO LAUNCH	
CHECK						
APR						D2-99603-1
APR					THE BOEING COMPANY	PAGE 31

TD 461 C-R4

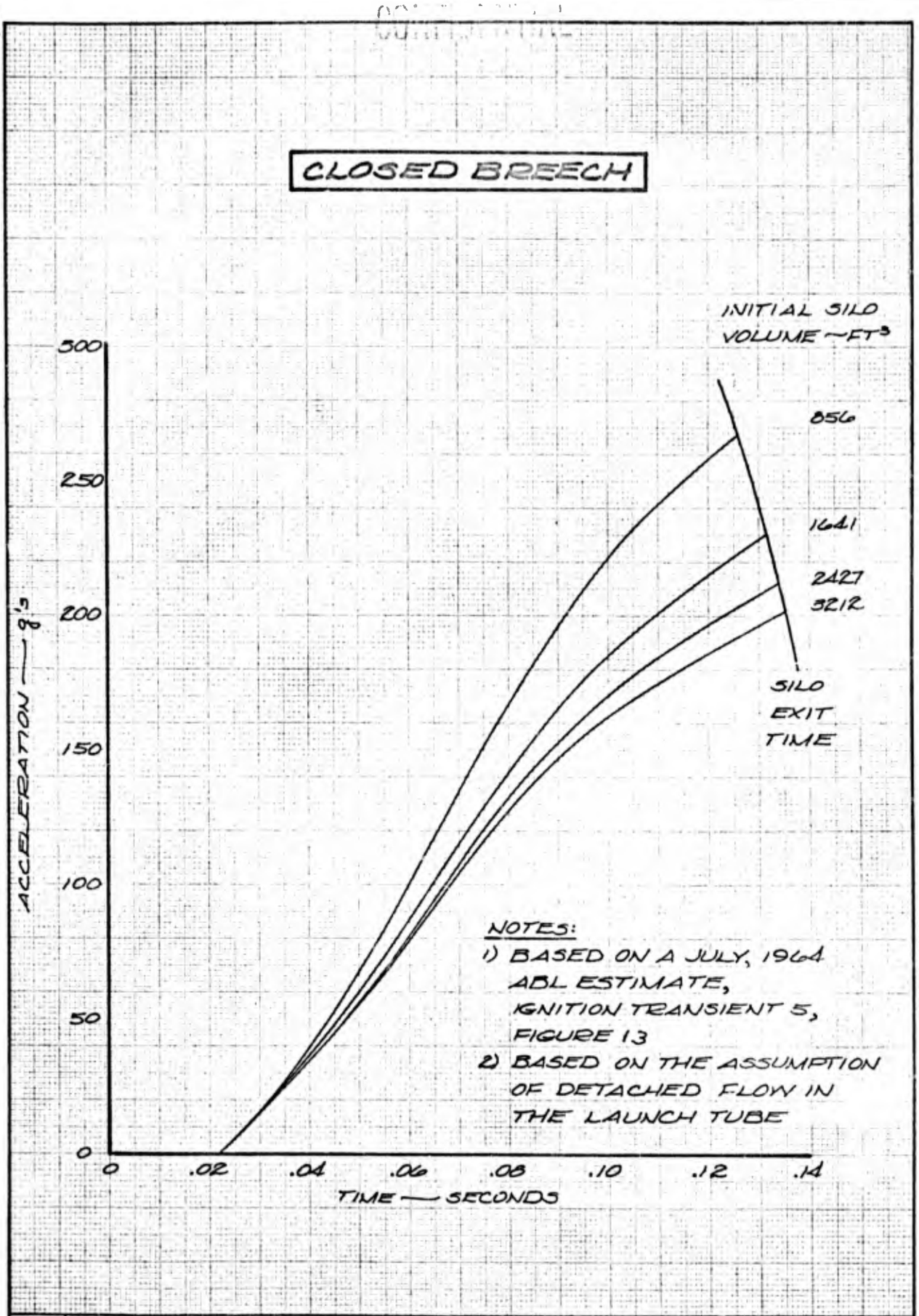

CALC			REVISED	DATE	FIGURE 11 THEORETICAL VEHICLE ACCELERATION HISTORY DURING LAUNCH	
CHECK						
APR						D2-99603-1
APR					THE BOEING COMPANY	PAGE 32

TD 461 C-R4

CLOSED BREECH

NOTES:
1) BASED ON A JULY, 1964 ABL ESTIMATE, IGNITION TRANSIENT 5, FIGURE 13
2) BASED ON THE ASSUMPTION OF DETACHED FLOW IN THE LAUNCH TUBE.

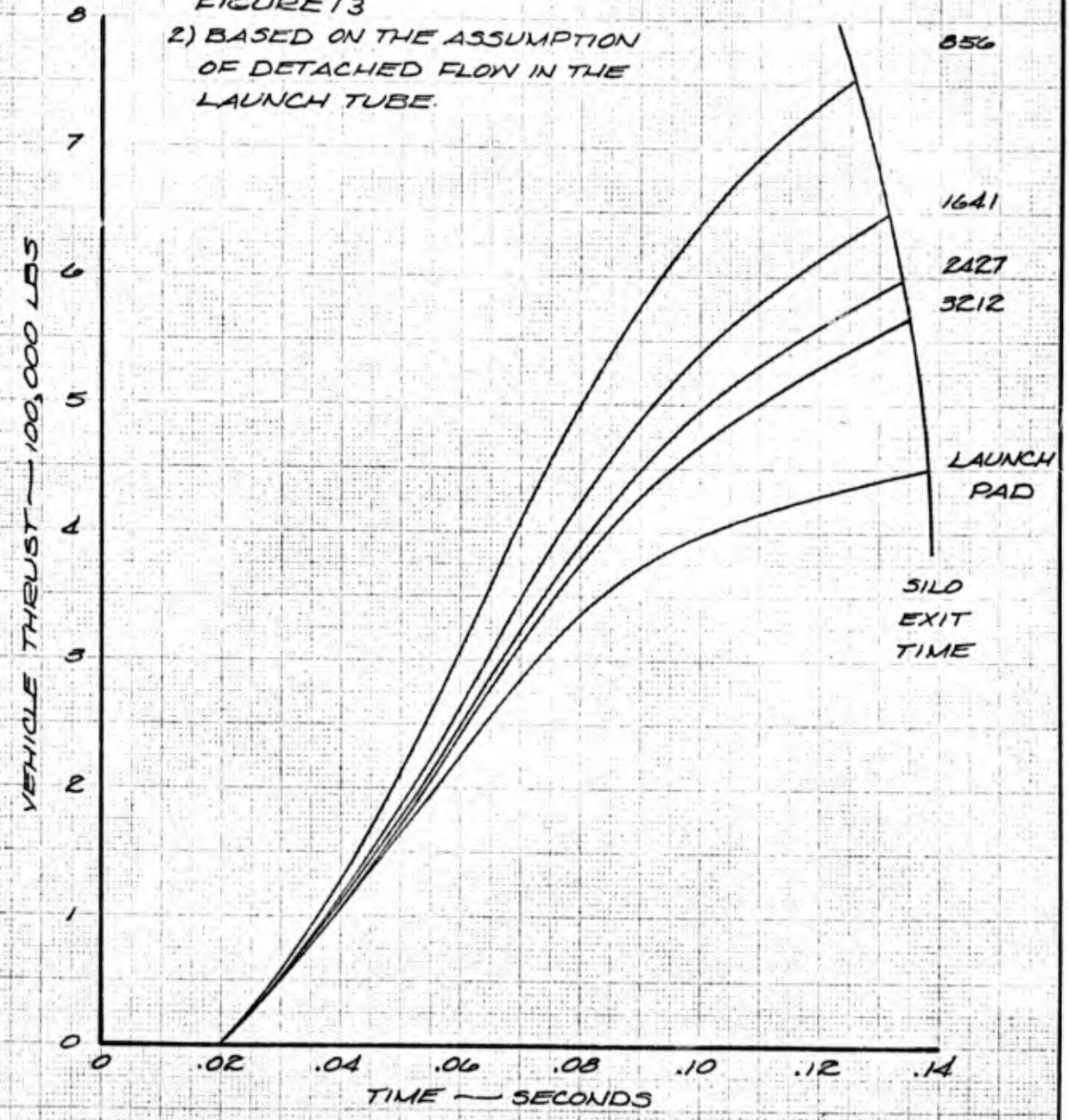

CALC			REVISED	DATE	FIGURE 12 THEORETICAL VEHICLE THRUST HISTORY — LAUNCH PAD vs SILO
CHECK					
APR					
APR					
					THE BOEING COMPANY

D2-99603-1
PAGE 33

TD 461 C-R4

4.2.2 Effect of Rocket Motor Ignition Transient

The effect of the rocket motor ignition transient on silo pressure was also examined analytically during the early phases of the program. Five ignition transients were analyzed, each for a series of silo volumes. The ignition transients studied ranged from very fast, rising to full chamber pressure in 0.080 sec, to very slow, rising to the full chamber pressure in 0.126 sec. The resulting maximum silo pressures are shown in Figure 13.

The type of ignition transient had a relatively small effect on the maximum silo pressure achieved during launch. The reason for this is that the vehicle stayed in the silo longer for the slower ignition transients. This allowed the silo pressure to rise for a longer period of time before the vehicle emerged from the silo.

4.2.3 Vehicle Guide (Sabot) Selection

During launch from the silo, a system was required to guide the vehicle in the launch tube and to seal the launch tube to retain silo pressure and thus prevent rocket motor exhaust gas flow around the vehicle.

The original HiBEX program included Phase C (2) vehicles which did not have a flight control system. A lateral cg offset was utilized to insure down range flight to meet range safety requirements. This cg offset was on the order of 0.40 in. The large cg offset combined with other possible vehicle angular disturbance effects such as thrust misalignment and unsymmetrical distribution of base pressure in the vicinity of the nozzle exit plane produced a high vehicle pitching moment. This moment was reacted by the guide system. From this it became apparent that the system design would require very stiff reactions and would benefit from a minimum base area.

Figure 14 compares advantages and disadvantages of the three types of guide systems which were studied during preliminary design. Types I and II were similar in that they provided lateral reaction at the exit plane and forward of the exit plane. These systems required shear pins or columns to react axial forces on the guides. These were necessary to avoid high unit loadings on the vehicle caused by the wedging action between the cylindrical launch tube and the conical vehicle. If the pins were attached to the vehicle, they became protuberances exposed to high aerodynamic heating effects and contributed to unpredictable aerodynamic flow characteristics. Pins attached to the guide resulted in undesirable holes in the vehicle which were also detrimental from heating and aerodynamic standpoints. The columns did tend to relieve this problem somewhat, but were heavy due to high inertia forces. The conical shape of the vehicle required that these types of systems be segmented to separate from the vehicle, and, due to their location, the possibility of collision with the vehicle existed at guide separation. Neither type I nor II provided moment reaction capability during travel through the full length of the launch tube, and they were subject to fit problems due to the radial and longitudinal expansion of the motor case. They also tended to interfere with, or were subjected to, the roll control exhaust.

4.2.2 Effect of Rocket Motor Ignition Transient

The effect of the rocket motor ignition transient on silo pressure was also examined analytically during the early phases of the program. Five ignition transients were analyzed, each for a series of silo volumes. The ignition transients studied ranged from very fast, rising to full chamber pressure in 0.080 sec, to very slow, rising to the full chamber pressure in 0.126 sec. The resulting maximum silo pressures are shown in Figure 13.

The type of ignition transient had a relatively small effect on the maximum silo pressure achieved during launch. The reason for this is that the vehicle stayed in the silo longer for the slower ignition transients. This allowed the silo pressure to rise for a longer period of time before the vehicle emerged from the silo.

4.2.3 Vehicle Guide (Sabot) Selection

During launch from the silo, a system was required to guide the vehicle in the launch tube and to seal the launch tube to retain silo pressure and thus prevent rocket motor exhaust gas flow around the vehicle.

The original HiBEX program included Phase C (2) vehicles which did not have a flight control system. A lateral cg offset was utilized to insure down range flight to meet range safety requirements. This cg offset was on the order of 0.40 in. The large cg offset combined with other possible vehicle angular disturbance effects such as thrust misalignment and unsymmetrical distribution of base pressure in the vicinity of the nozzle exit plane produced a high vehicle pitching moment. This moment was reacted by the guide system. From this it became apparent that the system design would require very stiff reactions and would benefit from a minimum base area.

Figure 14 compares advantages and disadvantages of the three types of guide systems which were studied during preliminary design. Types I and II were similar in that they provided lateral reaction at the exit plane and forward of the exit plane. These systems required shear pins or columns to react axial forces on the guides. These were necessary to avoid high unit loadings on the vehicle caused by the wedging action between the cylindrical launch tube and the conical vehicle. If the pins were attached to the vehicle, they became protuberances exposed to high aerodynamic heating effects and contributed to unpredictable aerodynamic flow characteristics. Pins attached to the guide resulted in undesirable holes in the vehicle which were also detrimental from heating and aerodynamic standpoints. The columns did tend to relieve this problem somewhat, but were heavy due to high inertia forces. The conical shape of the vehicle required that these types of systems be segmented to separate from the vehicle, and, due to their location, the possibility of collision with the vehicle existed at guide separation. Neither type I nor II provided moment reaction capability during travel through the full length of the launch tube, and they were subject to fit problems due to the radial and longitudinal expansion of the motor case. They also tended to interfere with, or were subjected to, the roll control exhaust.

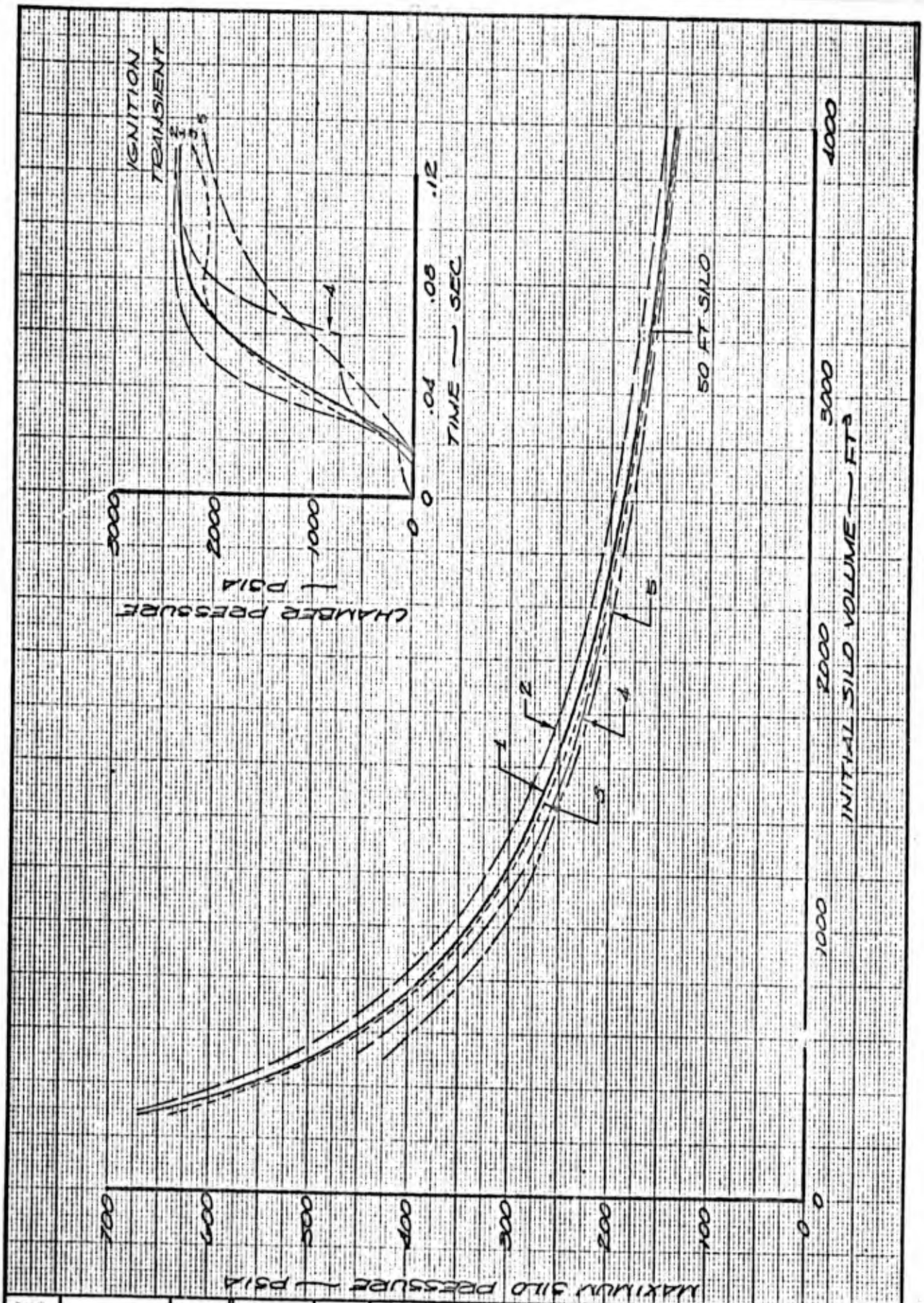

			REVISED	DATE	FIGURE 13 EFFECT OF IGNITION TRANSIENT ON MAXIMUM SILO PRESSURE	
CALC						
CHECK						
APR					D2-99603-1	
APR					THE BOEING COMPANY	PAGE 35

TD 461 C-R4

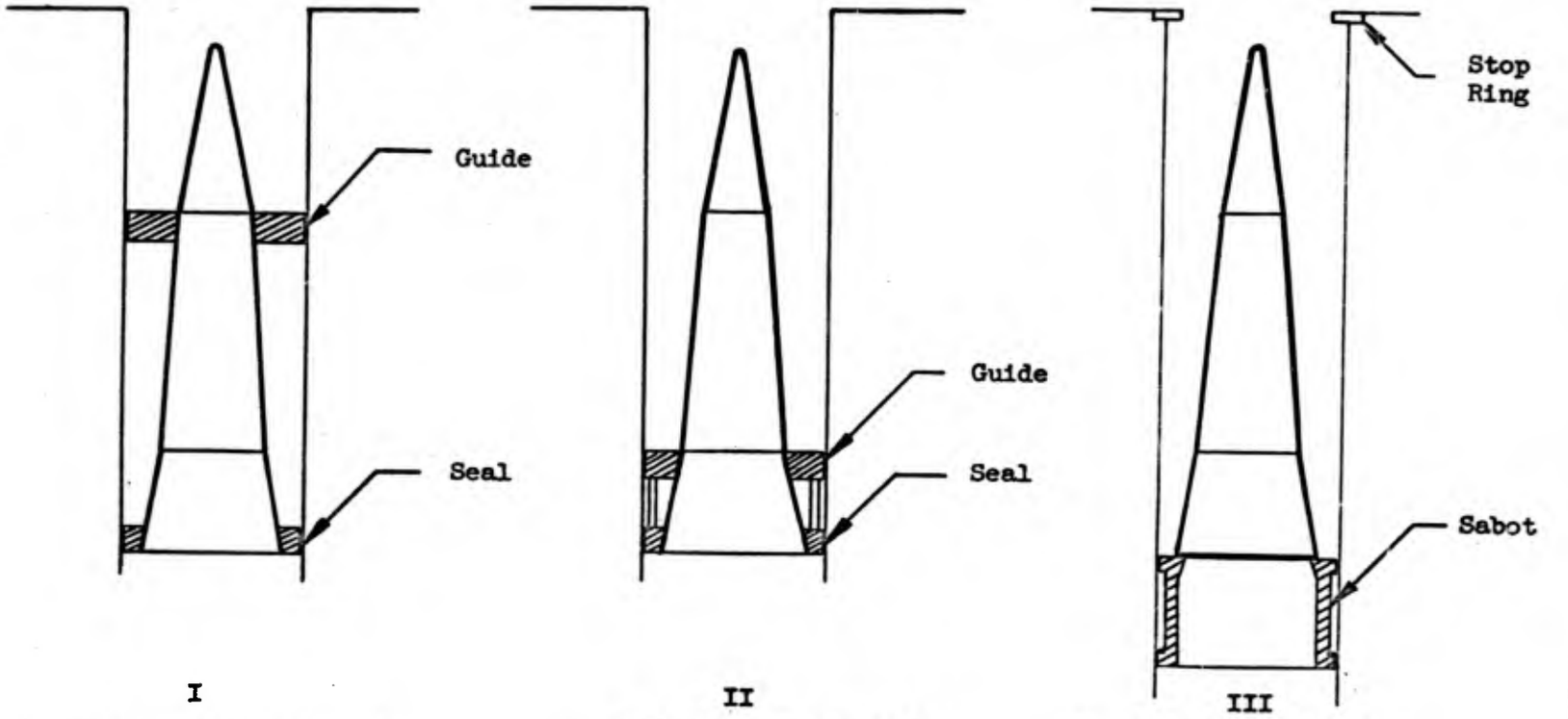

FIGURE 14 - GUIDE SYSTEM COMPARISON

I

1. Low loads on vehicle
2. Lightest
3. Many parts
4. Shear Pins req'd. on skirt & second stage
5. May damage insulation
6. No moment capability after guide exit
7. Clean separation difficult

II

1. High loads on vehicle
2. Heavier
3. Many parts
4. Shear pins req'd. on skirt
5. Interference with R/C exhaust
6. Clean separation difficult

III

1. Low loads on vehicle
2. Heaviest
3. Minimum parts
4. Shear pins or lugs req'd. on skirt
5. No interference with R/C exhaust
6. Clean separation
7. Ablative mat'l. req'd. on sabot skin
8. Required longer launch tube

The type III concept was ultimately selected for use and was more promising in all respects except weight. This was not an extreme disadvantage due to the short silo operation time. A small velocity increase was in fact predicted for the vehicle with the final base area provided. The major advantages of type III (trailing sabot) which were responsible for its selection were:

a) It could be assembled and machined as an integral part to dimensions closely matching the launch tube diameter thereby minimizing angular offset and inertia loads.

b) It did not complicate the vehicle design with shear pins or sockets, latches, etc.

c) It could be cleanly separated from the vehicle with no post-exit collision problem.

d) It did not confine nor was it affected by the roll control system exhaust.

e) It provided the smallest practical base area and therefore the smallest diameter launch tube and the lowest unsymmetrical base pressure loads.

A suitable sabot separation technique was the major problem for the selected guide system. During the initial travel, the vehicle provided the motive force for the sabot. The sabot to skirt tie thus required a tension strength capability for this condition as well as for ground handling. The buildup of silo pressure then eventually produced forces exceeding the sabot inertia force, causing compressive loads on the sabot to vehicle joint. Studies were made of latch, explosive ordnance, and shearable type joints for separation of the sabot. The latch involved many parts, was complicated, and caused concentrated loads. The ordnance type joint was complicated by a separation timing problem. The shearable joint solved both the problems of load distribution and timing. This design involved riveting the sabot and vehicle skirt together at the nozzle exit plane by aluminum rivets in single shear. The riveted joint was capable of withstanding the pitching moment and inertia loads during silo travel, then was sheared by impact with the stop ring at the top of the silo. This provided a simple, passive, cleanly separated, perfectly timed, release of the sabot. Details of the joint design are discussed in Section 4.3.3.

4.3 DESIGN REQUIREMENTS

4.3.1 Vehicle Dynamics

4.3.1.1 Vehicle Silo Alignment

A ± 0.5 deg (3 σ) burnout flight path angular deviation resulting from vehicle-silo alignment was allowed in the total flight path error budget. To obtain the required accuracy, control of the alignment of the gyros, vehicle, and silo relative to range coordinates was required. The following 3 σ launch requirements were imposed in the maneuver and cross range planes relative to the range coordinates:

a)	Gyro vertical launch alignment	± 0.3 deg
b)	Vehicle motor center line	± 0.2 deg
c)	Silo vertical alignment	± 0.1 deg

4.3.1.2 Flight Control Operation in the Silo

The allowable boost burnout flight path error caused by vertical error at exit from the silo was budgeted to be ± 0.5 deg. This burnout error would have resulted from a vehicle vertical axis error of ± 2 deg. Analysis was made of vehicle motion in the silo with, and without, the flight control system in operation. The results are shown in Figure 15. The flight control system caused an unstable moment in the silo, but this was a small effect compared to the vehicle pitching moments which could be caused by asymmetrical vehicle base pressures. As shown in Figure 15, for the more probable base pressure variation (case II), silo guides were required in order to maintain the required vehicle verticality accuracy. A closing bias command was included in the flight control system to sliminate the possibility of TVC injection causing asymmetrical nozzle flow separation while the vehicle was in the silo.

4.3.1.3 Flight Control Operation at Vehicle Emergence From the Silo

The effect of silo launch on the method of initiating vehicle maneuvers was studied, with results shown in Figure 16. Two general methods of maneuver initiation were considered, one based on a preset timer and the second based on distance. The time-based method of initiation of the maneuver was found to be inadequate due to the tolerances in the initial thrust transient. The basic problems were: a) for slow thrust transients, the vehicle could not be allowed to start pitching before sabot separation, b) for fast thrust transients, the vehicle must not have too large a velocity at initiation of the maneuver or the maneuver limit would be exceeded. Figure 16 shows the maximum allowable velocity that would not result in excessive lateral acceleration loads during the maneuver. Figure 16 also shows that the time-based techniques of maneuver initiation caused this maximum allowable velocity to be exceeded. Therefore, it was required that the initial pitchover signal not be initiated by time, but in a more accurate and positive manner, (distance), such as a switch actuated by sabot separation at vehicle exit from the silo. This method was chosen for the HiREX launch.

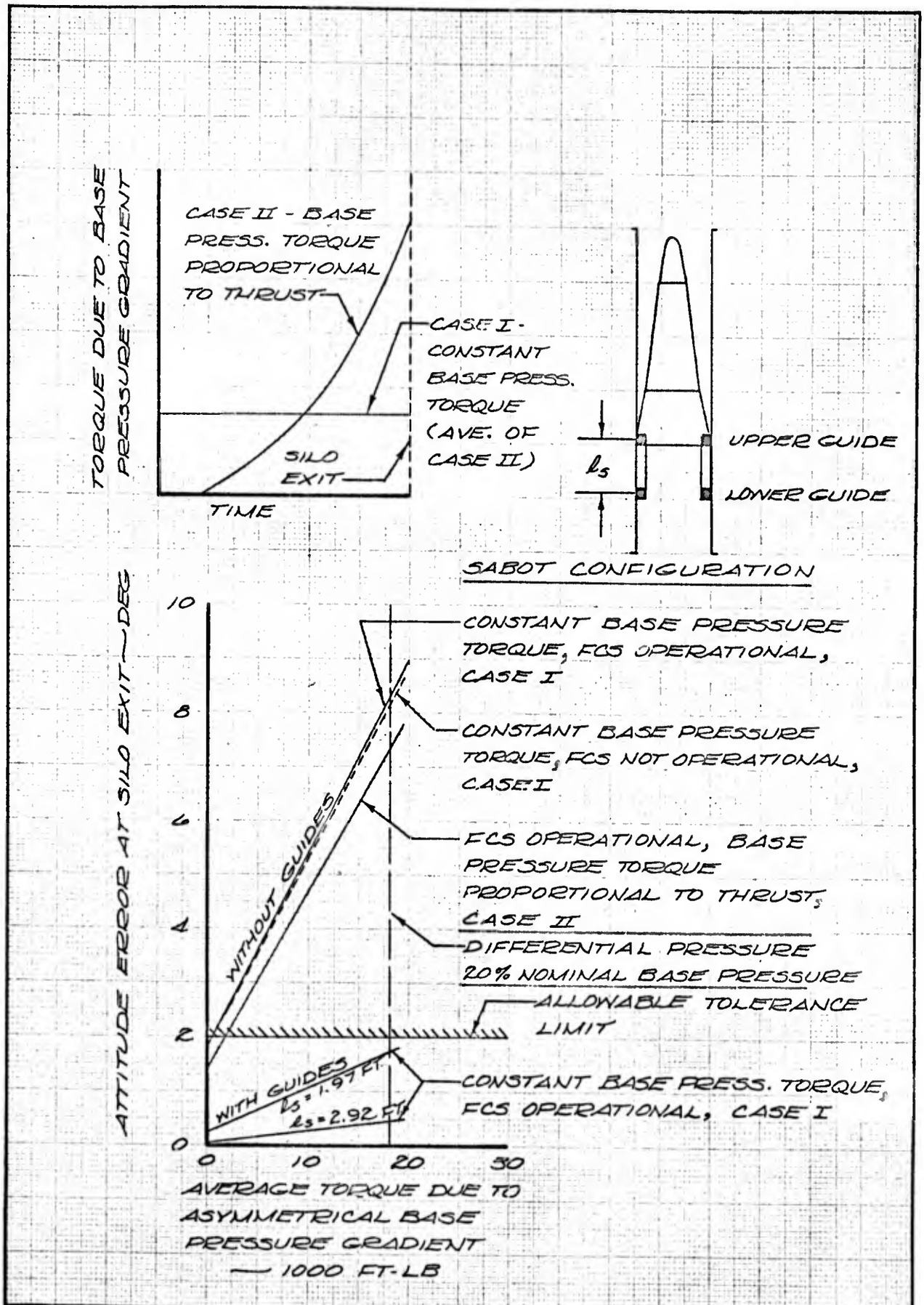

CALC			REVISED	DATE	FIGURE 15 EFFECT OF SILO DIFFERENTIAL PRESSURE ON VEHICLE ATTITUDE ERROR
CHECK					
APR					D2-99603-1
APR					
					THE BOEING COMPANY

PAGE 39

TD 461 C-R4

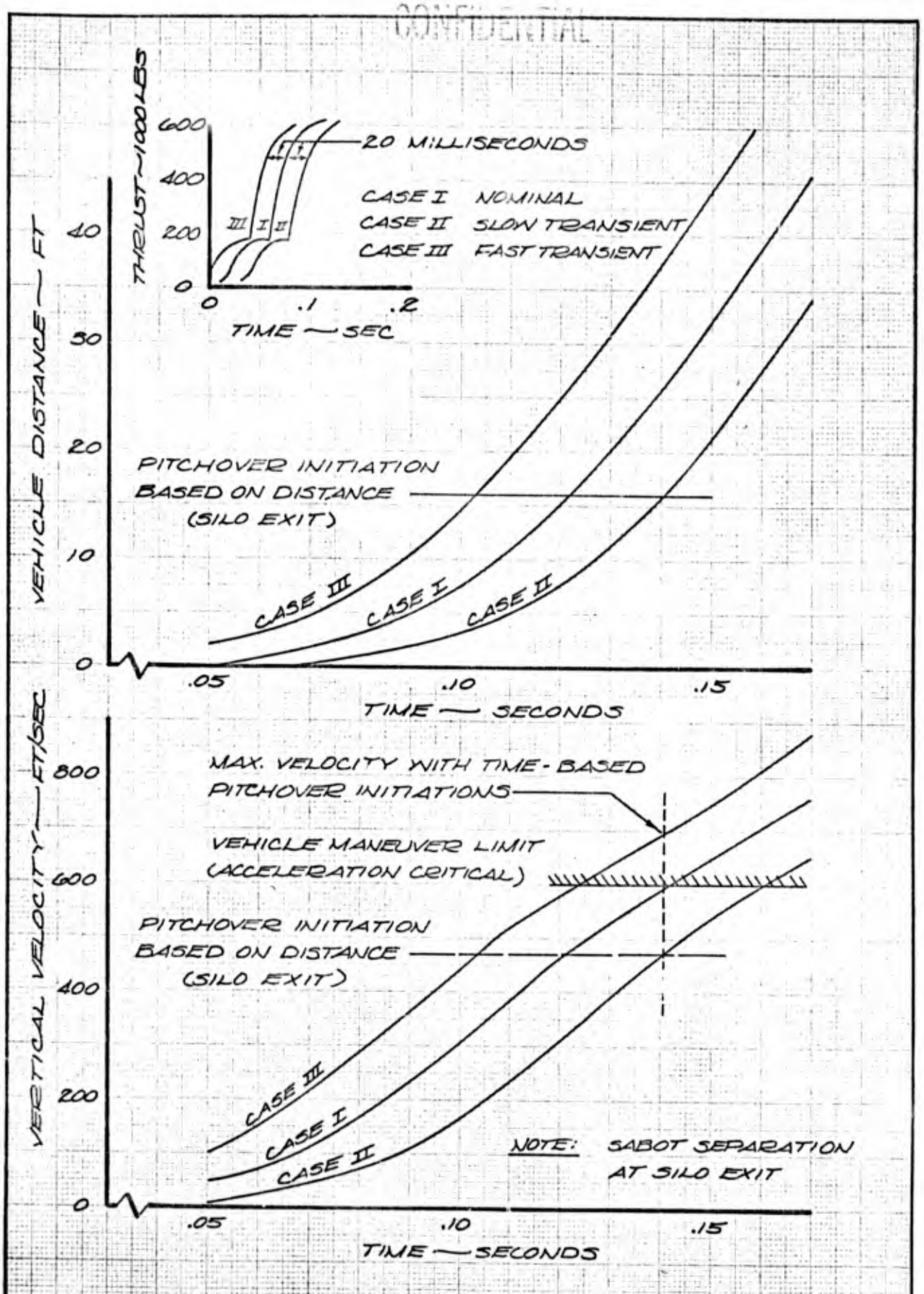

			REVISED	DATE
CALC				
CHECK				
APR				
APR				

FIGURE 16
SILO LAUNCH INTERACTIONS
WITH CONTROL SYSTEM

D2-99603-1

THE BOEING COMPANY

PAGE 40

TD 461 C-R4

4.3.2 Vehicle Loads

4.3.2.1 Structural Heating

Since a closed-breech silo was utilized for HiBEX, the vehicle was isolated from rocket motor exhaust gas flow by the sabot seal. The thermal environment encountered by the vehicle during launch from a silo was therefore not significantly different from that encountered during launch from a surface launcher.

The roll control gas generators were ignited 50 ms prior to ignition of the rocket motor, so that there was a short period during which the hot roll control gases were confined between the skirt and the launch tube. The additional structural heating so produced was found to be slight, and no specific protective measures were necessary.

4.3.2.2 Structural Loads

The sabot configuration selected for the HiBEX silo launch was a trailing cylinder attached to the aft skirt by means of a tension tie. The sabot was separated from the vehicle when the sabot struck a heavy steel stop ring as the vehicle left the silo, thus shearing the rivets between the tension tie and the aft skirt. This concept for the sabot caused the following load conditions:

a) Longitudinal and lateral loads, and internal pressure during travel in the silo determined the structural size of the sabot and the tension and compression requirements of the sabot to aft skirt joint.

b) Internal loads of the sabot at impact with the stop ring required a sabot design that insured the integrity of the sabot until the rivets between the tension tie and aft skirt were completely sheared.

c) An impulse load on the skirt caused by shearing of the rivets which must not exceed the structural capability of the skirt attachment to the rocket motor.

For loads purposes, it was assumed that the lateral motion of the vehicle in the silo did not affect the vertical motion. Therefore, the longitudinal trajectory parameters could be taken from independent analysis and used as inputs for the loads equations. Both maximum and minimum pressure launches were considered in order to give maximum compression and tension loads.

The lateral reactions of the sabot were determined by solving the dynamic lateral equations of motion. The solutions were checked by reducing the dynamic equations to their static form. Lateral bending loads were determined from the lateral reactions during vehicle travel in the silo and at exit. Axial loading of the vehicle aft skirt and sabot was determined by summing the axial pressure, inertia, and friction forces active during launch. Axial loading of the aft skirt at sabot separation was determined by analysis of a mathematical model of the skirt which included a mass to represent the roll control equipment mounted on the skirt.

The sign convention and coordinate system used to derive the equations of motion are shown in Figure 17. The results of the structural loads analyses are presented in subsequent paragraphs.

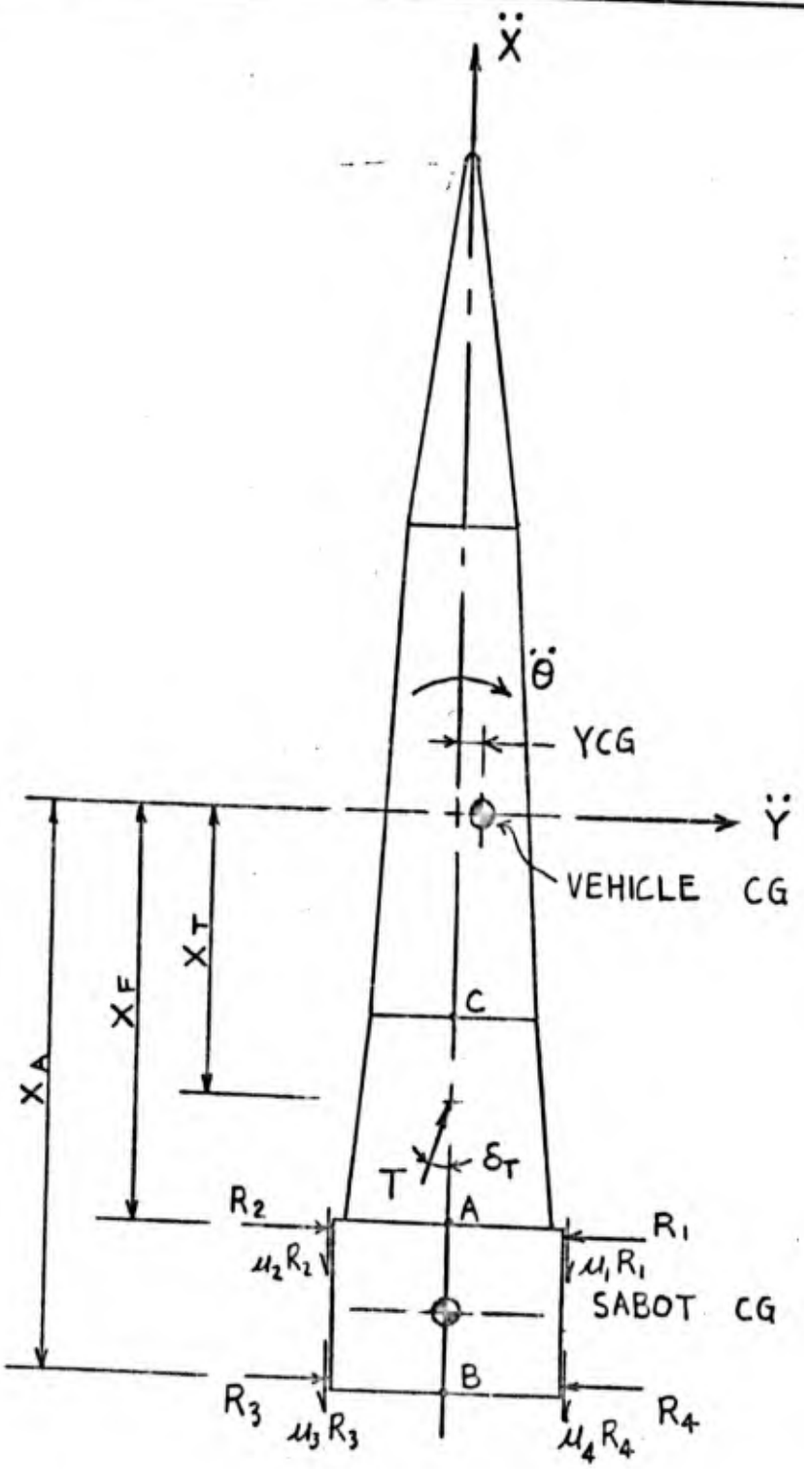

	INITIALS	DATE	REV BY INITIALS	DATE	TITLE	MODEL
CALC	RJL	1·27·65			SILO LAUNCH LOADS STUDY COORDINATE SYSTEM	
CHECK						
APPD						
APPD						

FIGURE 17

U3 4038 8000 REV. 12-62

2-5142.2

Fig. 10

REV SYM _____

a) Dynamic Lateral Equations of Motion

The lateral reactions of the sabot were determined by solving the general dynamic lateral equations of motion:

$$I\ddot{\theta} = T'; \; m\ddot{Y} = F$$

where:

I = Moment of inertia of sabot and vehicle about the center of gravity

$\ddot{\theta}$ = Angular acceleration

T' = Moments about the center of gravity

m = Mass of the vehicle and sabot

$\ddot{Y}$ = Lateral acceleration of the center of gravity

F = Lateral forces acting on the vehicle

The launch tube was considered to be infinitely stiff and the spring rate of the sabot rings varied as a non-linear function of deflection. It was also assumed that the vehicle was rigid compared to the flexibility of the sabot rings; the lateral equations of motion were then:

$$I\ddot{\theta} = R_1 x_F + R_4 x_A + \mu_1 R_1 r + \mu_4 R_4 r - R_2 x_F - R_3 x_A - \mu_2 R_2 r - \mu_3 R_3 r + Y_{CG} m\ddot{x} + C_P p$$

$$m\ddot{Y} = R_2 + R_3 - R_1 - R_4 + T\theta - C_T T$$

Also,

$$\delta_1 = -\delta_{o1} + Y - x_F \theta$$

$$\delta_2 = -\delta_{o2} - Y + x_F \theta$$

$$\delta_3 = -\delta_{o3} - Y + x_A \theta$$

$$\delta_4 = -\delta_{o4} + Y - x_A \theta$$

Where the symbols not previously defined are:

δ = Lateral deflection of the sabot centerline at the reaction point

R = A non-linear function of δ, based upon the stiffness of the sabot ring bearing against the silo insert

μ = Coefficient of friction of the sabot bearing surfaces

r = Radius of the sabot

T = Thrust

δ_o = Initial clearance between sabot and launch tube

YCG = Lateral center of gravity offset from the thrust line

C_p = Coefficient to account for unsymmetrical pressures acting on the base of the vehicle and sabot

C_T = Angular misalignment of the thrust

p = Silo overpressure acting at the base of the sabot

Subscripts

1, 2, 3, 4 = Sabot reaction points

The relationship between R and δ was determined by assuming that the sabot rings bore against an infinitely stiff launch tube. As the contact between the rings and the launch tube increased, the spring rate of the sabot rings increased. The shear deflection of the sabot was incorporated into the spring rate of the aft ring. The resulting force versus deflection curve for each ring is shown in the upper part of Figure 18 for nominal spring rates.

The above equations were solved to obtain histories of lateral motion and sabot reactions as the vehicle was launched from the silo. A typical solution for the sabot reactions is shown in Figure 19.

In order to check the solution, the dynamic equations of motion were reduced to their static form (i.e. $\ddot{\theta} = 0$; $\ddot{y} = 0$). The resulting equations were solved with various values for the sabot ring stiffness (spring rates). The lateral reactions were determined from both the dynamic solution and the static solution. A comparison of the two solutions is given in the lower part of Figure 18, which shows that the static solution gave higher values for the spring rates considered. Further study determined that the dynamic solution was transient and had not attained the maximum reaction by the time the sabot reached the top of the silo. If the dynamic solution was permitted to run beyond the silo exit point, a peak value of about twice the static value was found as shown by the points in the lower part of Figure 18. This dynamic magnification factor of two was reasonable if the frequency of the sabot and the vehicle was low compared to the forcing function (the ignition transient).

An additional check of the equations of motion was made by determining the frequency of the vehicle and sabot. The expression for the frequency was:

$$(2\pi f)^2 = \frac{1}{2}(a+c) \pm \sqrt{\frac{1}{4}(a-c)^2 + \frac{mb^2}{I} + \frac{bT}{I}}$$

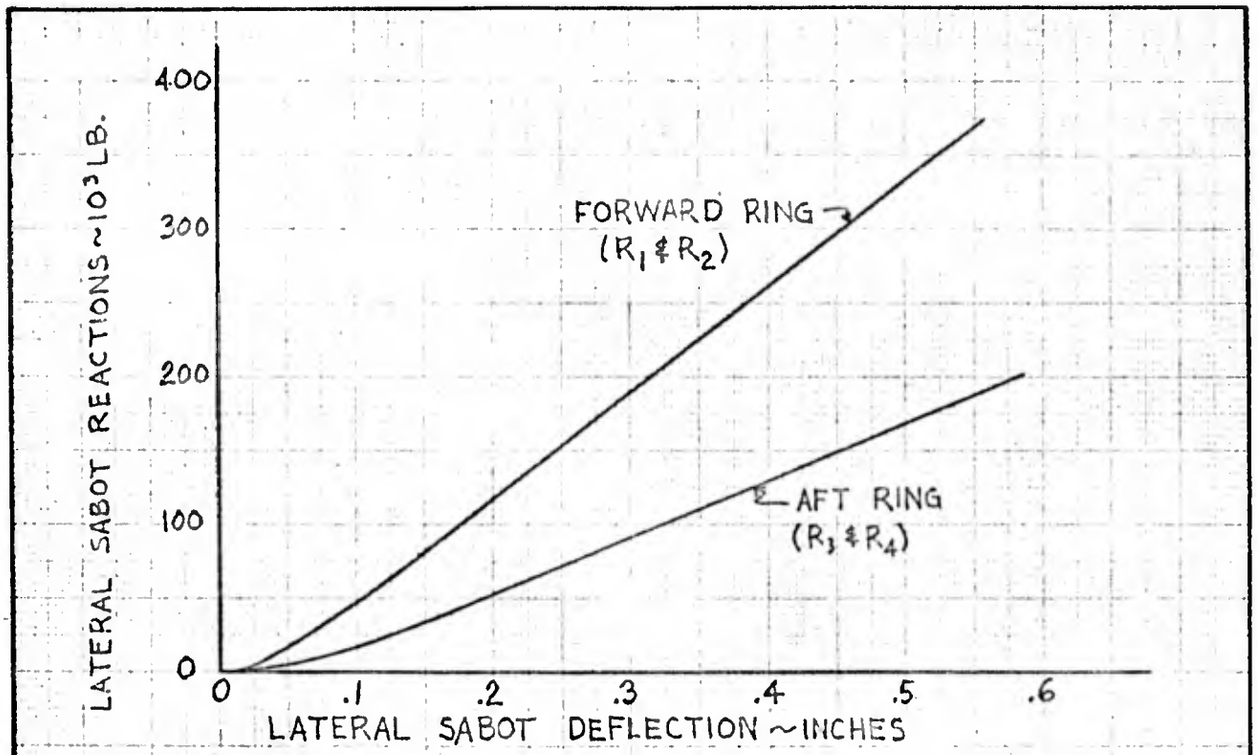

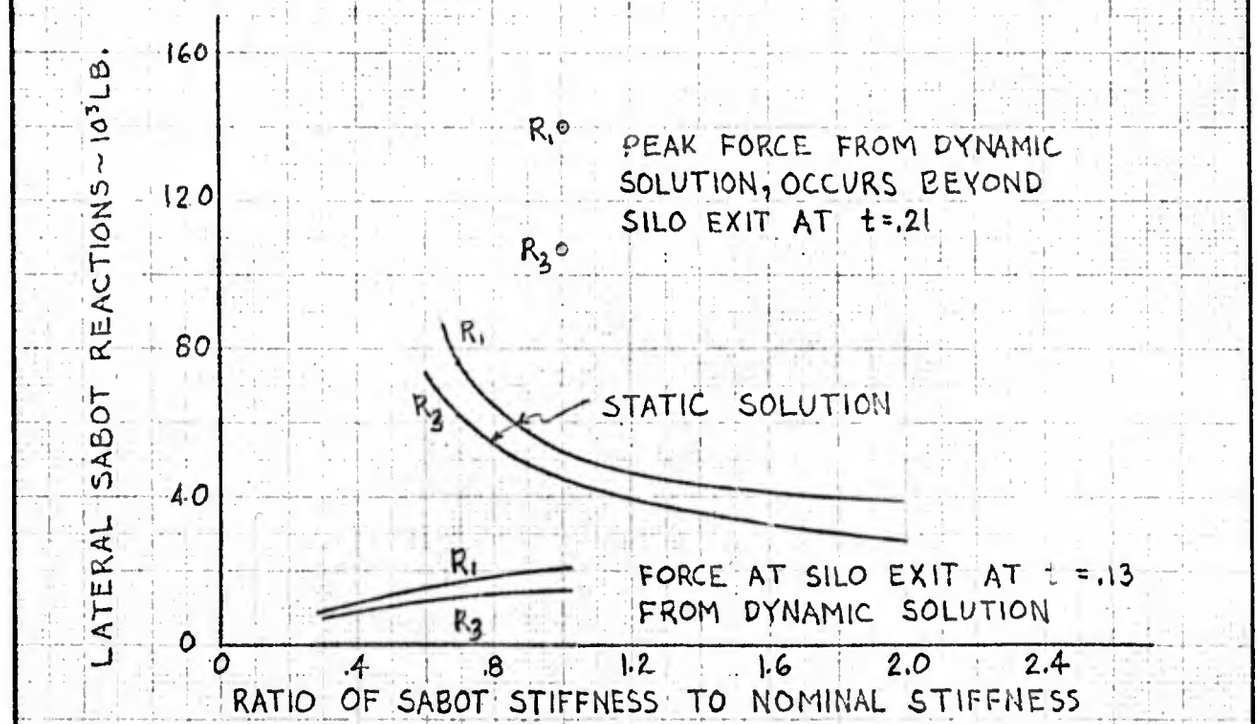

	INITIALS	DATE	REV BY INITIALS	DATE	TITLE	MODEL
CALC	RJL	1·8·65			SABOT STIFFNESS AND SABOT REACTIONS I	
CHECK						
APPD.						
APPD.						

FIGURE 18

U3 4013 8000 REV. 12-64

REV LTR_____

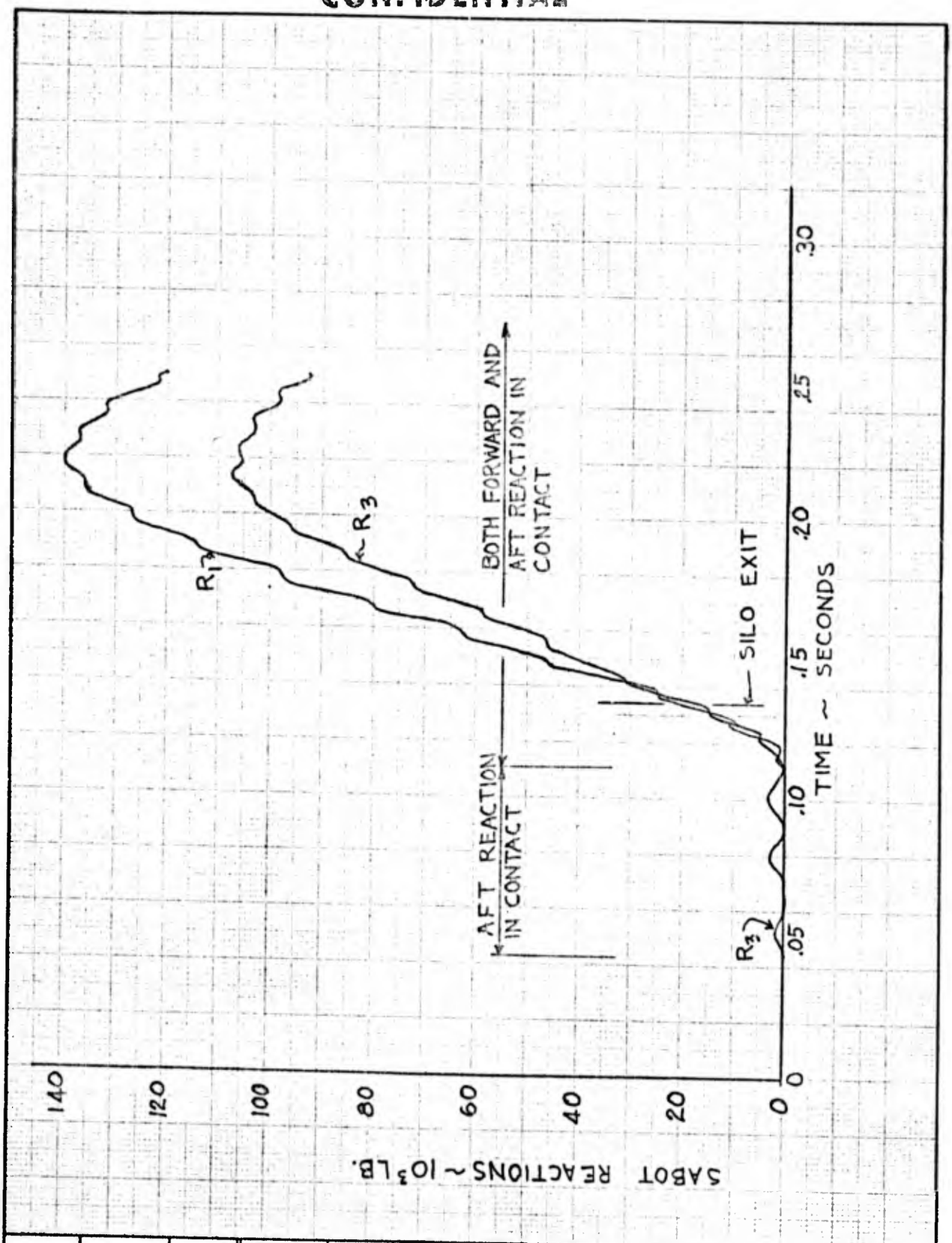

	INITIALS	DATE	REV BY INITIALS	DATE	TITLE	MODEL
CALC	RJL	1-26-65			SABOT REACTION ... HISTORIES FOR A TYPICAL SILO LAUNCH	
CHECK						
APPD.						
APPD.						

FIGURE 19

U3 4013 8000 REV. 12-64

REV LTR_____

Where the symbols not previously defined are:

$a = \frac{(K_1 x_F^2 + K_3 x_A^2}{I}$

$b = \frac{(K_3 x_A - K_1 x_F}{m}$

$c = \frac{(K_1 + K_3}{m}$

f = Frequency of the vehicle/sabot in the silo

K = Equivalent spring rate for sabot reactions

The solution of the frequency equation can be compared to the frequencies which are apparent in the dynamic solution shown in Figure 19. In this solution the vehicle initially had just the aft reaction (R_3) in light contact due to clearance between the sabot and launch tube. With the appropriate spring constant for R_3, the frequency equation gave a single value of f_1=37.8 cps. This value approximately agreed with that of the dynamic solution. At a later time in the analysis, both forward and aft (R_1 and R_3) reactions were in contact and the frequency equation yielded f_1=3.57 cps and f_2=94.6 cps. The high frequency was readily checked in the dynamic solution. The low frequency is apparent in the dynamic solution, however, it was difficult to obtain a good check on its magnitude. These frequencies throw some light on the dynamic magnification factor discussed previously. The low frequency degree of freedom had a relatively large period compared to the ignition transient. Thus a dynamic magnification factor of two would be expected in response to lateral driving forces which had histories corresponding to the ignition transient.

b) Lateral Bending Loads

The lateral bending moments were determined from the general equation:

$M_A = F\,\ell$

where:

M_A = Bending moment about point A

F = Lateral force

ℓ = Moment arm

Referring to Figure 17 the detailed equation for lateral bending moment was of the form:

$$M_A = -(C_{p\,sabot})\,p_b + \mu r(R_2 + R_3 - R_1 - R_4) + \ell_3 (R_3 - R_4) + \ell_1 (R_2 - R_1) - m_A(\ddot{Y} - \bar{l}_s \ddot{\theta})\,\ell_3 + I_3 \ddot{\theta} - Y_{CG} m_A \ddot{x} + \ell_3 \theta m_A \ddot{x}$$

Where the symbols not previously defined are:

r = radius of the sabot reaction rings

ℓ_3 = distance from point "A" to aft reaction

ℓ_1 = distance from point "A" to forward reaction

$\bar{\ell}_s$ = distance from total vehicle c.g. to sabot c.g.

ℓ_s = distance from point "A" to sabot c.g.

I_s = moment of inertia of sabot about a normal line through point "A"

YCG = assumed lateral c.g. offset

Values for the above parameters were taken from the silo launch analysis and the lateral motion analysis at the silo exit. High magnitudes from the static solution or the peak dynamic solution would occur after the vehicle had traveled about 1-3/4 vehicle lengths farther. Reasonable sabot reactions for the load calculation were obtained from the dynamic solutions with the Phase D vehicle characteristics. The loads results are shown in summary form in Table I.

c) Axial Loads

The axial loads were determined by summing the axial pressure, inertia and friction forces active during launch. The general equation was:

$$P_A = p_b A_s + m_A \ddot{X} + \mu R$$

where:

P_A = Axial load at point A

p_b = Pressure acting on the base

A_s = Base area at point A

m_A = Mass aft of point A

$\ddot{X}$ = Axial acceleration

μR = Friction force

The detailed equations were of the following form:

$$P_A = p_b A_s + m_A \ddot{X} + \mu_1 R_1 + \mu_2 R_2 + \mu_3 R_3 + \mu_4 R_4 + F_D$$

TABLE I
LIMIT SILO LAUNCH LOADS

Load Parameter	Load Condition		
	Detached Flow		Attached Flow
	Max. Compression Silo Overpressure = 235 psia(Nominal)	Maximum Tension Silo Overpressure = 100 psia (Nominal)	Maximum Tension Not Dependent on Silo Overpressure
Bending Moment:			
On Joint M_A	+ 235,000 in-lb	+ 158,200 in-lb	+ 29,700 in-lb
On Skirt M_A	+ 189,000 in-lb	-	-
M_B	- 48,600 in-lb	-	-
M_C	+ 99,000 in-lb	-	-
Axial Load:			
On Joint P_A	- 23,200 lb	+ 30,700 lb	+ 29,300 lb
On Skirt P_A	- 68,800 lb	-	-
P_B	- 75,200 lb	-	-
P_C	- 40,000 lb	-	-
Lateral Reactions:			
R_1	20,400 lb	-	-
R_3	14,600 lb	-	-

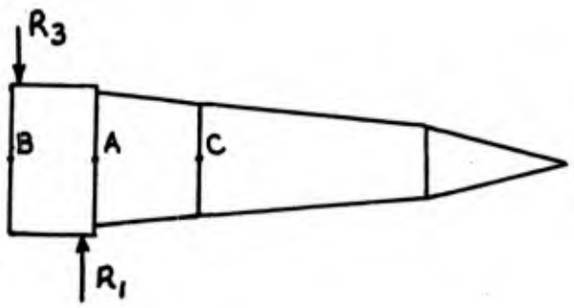

Assumptions:
D vehicle c.g. offset = 0.1"
Sabot to launch tube clearance = 0.1" (on the diameter)
Fwd. sabot ring stiffness = 570,000 lb/in (maximum)
Aft sabot ring stiffness = 310,000 lb/in (maximum)
Sabot weight = 200 lb.

USE FOR TYPEWRITTEN MATERIAL ONLY

Where the coordinates are shown in Figure 17 and the symbols not previously defined are:

μ = coefficient of friction of the sabot reaction rings at points 1, 2, 3, 4.

R = lateral reaction forces at points 1, 2, 3, 4.

F_D = surface drag due to flow

In applying the axial loads equation, it was significant whether the flow in the launch tube was detached or attached. Detached flow would result in high compressive loads at vehicle exit from the silo when the back pressure was at a maximum. The tension load under detached flow conditions was the result of the interaction between back pressure and acceleration; the maximum tension load occurred for the minimum silo pressure launch at a time prior to silo exit. For a launch with attached flow conditions, the sabot base does not feel the silo pressure, therefore, the maximum tension load would occur at vehicle exit when the greatest acceleration occurs. The static analysis for detached flow conditions with minimum silo pressures yielded the maximum tension loads; the dynamic analysis yielded lower loads. A loads summary is given in Table I. Loads calculated for a silo launch with attached flow conditions are also given in Table I. These loads were obviously less than the design tension condition, therefore, the given design loads were sufficient for either detached or attached flow conditions.

d) Sabot Loads at Separation

Figure 20 shows the stop-ring at the top of the launch tube, the top of the sabot, and the tension tie to the aft skirt of the vehicle. The longitudinal response of the aft skirt to the sabot separation loads was determined by means of the model shown in Figure 21.

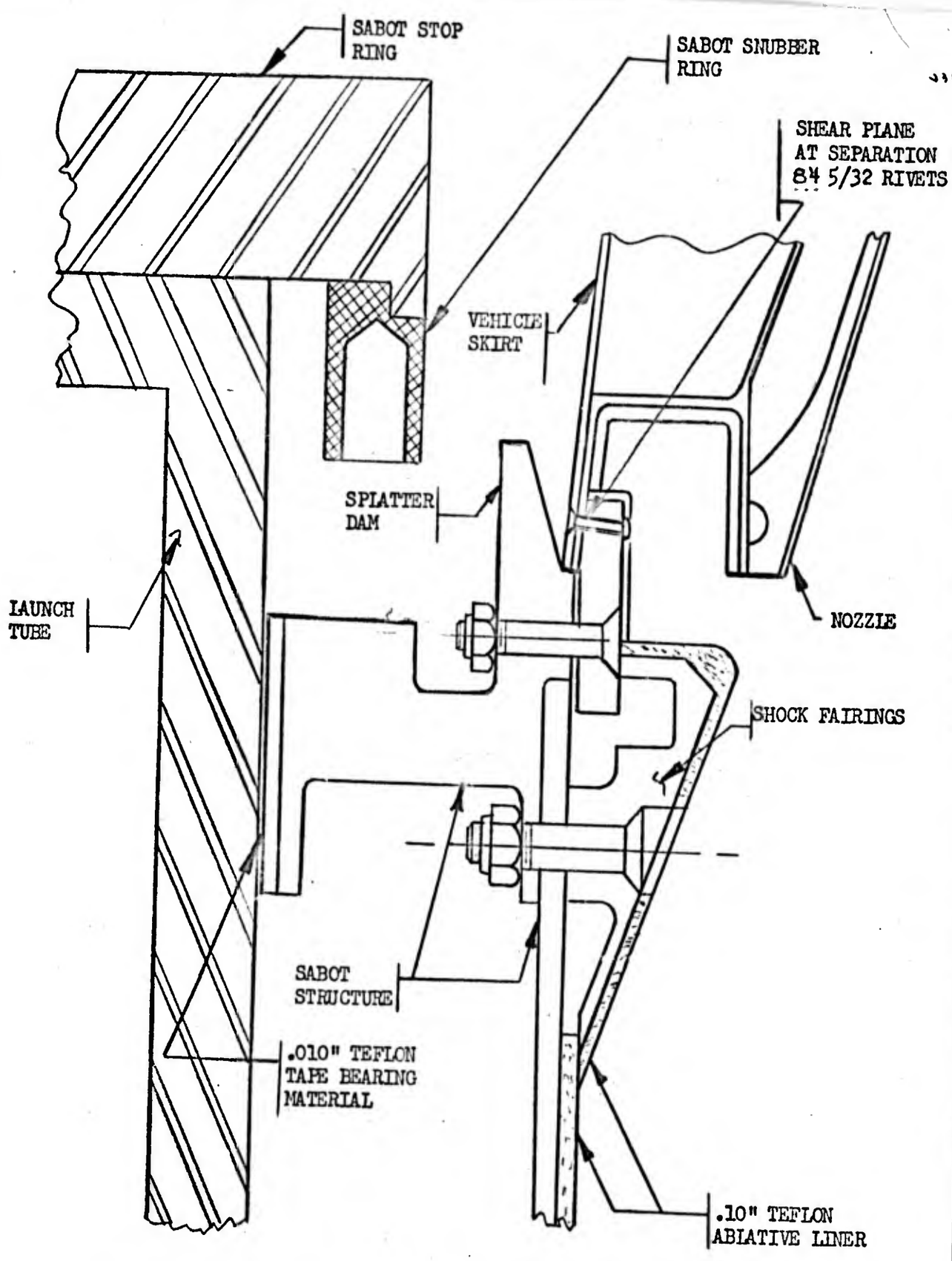

SABOT TO SKIRT ATTACHMENT DETAIL

FIGURE / 20

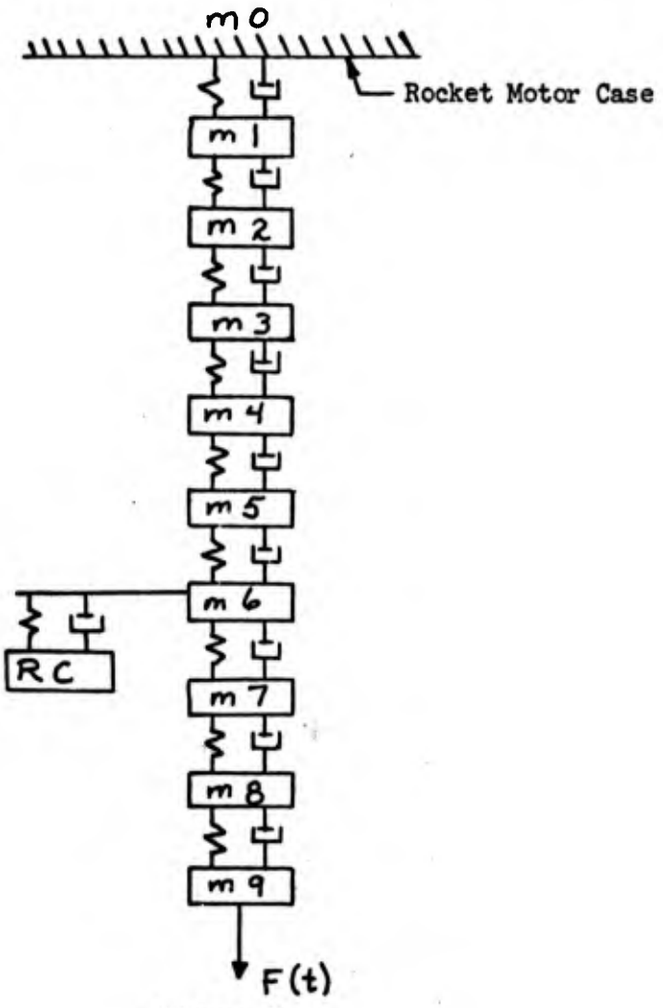

Figure 21

Skirt Mass-Spring Model

The skirt shell was divided into nine equal length mass lumps (m_n) and to this was added a mass spring representing the skirt-mounted portion of the roll control system. A tensile impulsive force, F(t), representing the shearing of the sabot to skirt joint, was applied to the aft mass. The resulting force wave in the shell is shown in Figure 22 along with the force applied at the aft end of the skirt. This figure shows the attenuation of the load as it entered the structure and travelled forward. The wave rebounded from the skirt to motor attachment and reinforced itself, doubling its magnitude at that point. However, the load at the skirt to motor attachment was still only 60% of the load applied at the aft end.

Another loading condition existed when the skirt to sabot joint, (point "A" in Table I) had a compression load resulting from the high silo pressure launch. The magnitude of this load was determined by $P'_A = 2\pi r \left(\frac{P_A}{2\pi r} \pm \frac{M_A}{\pi r^2}\right)$. When

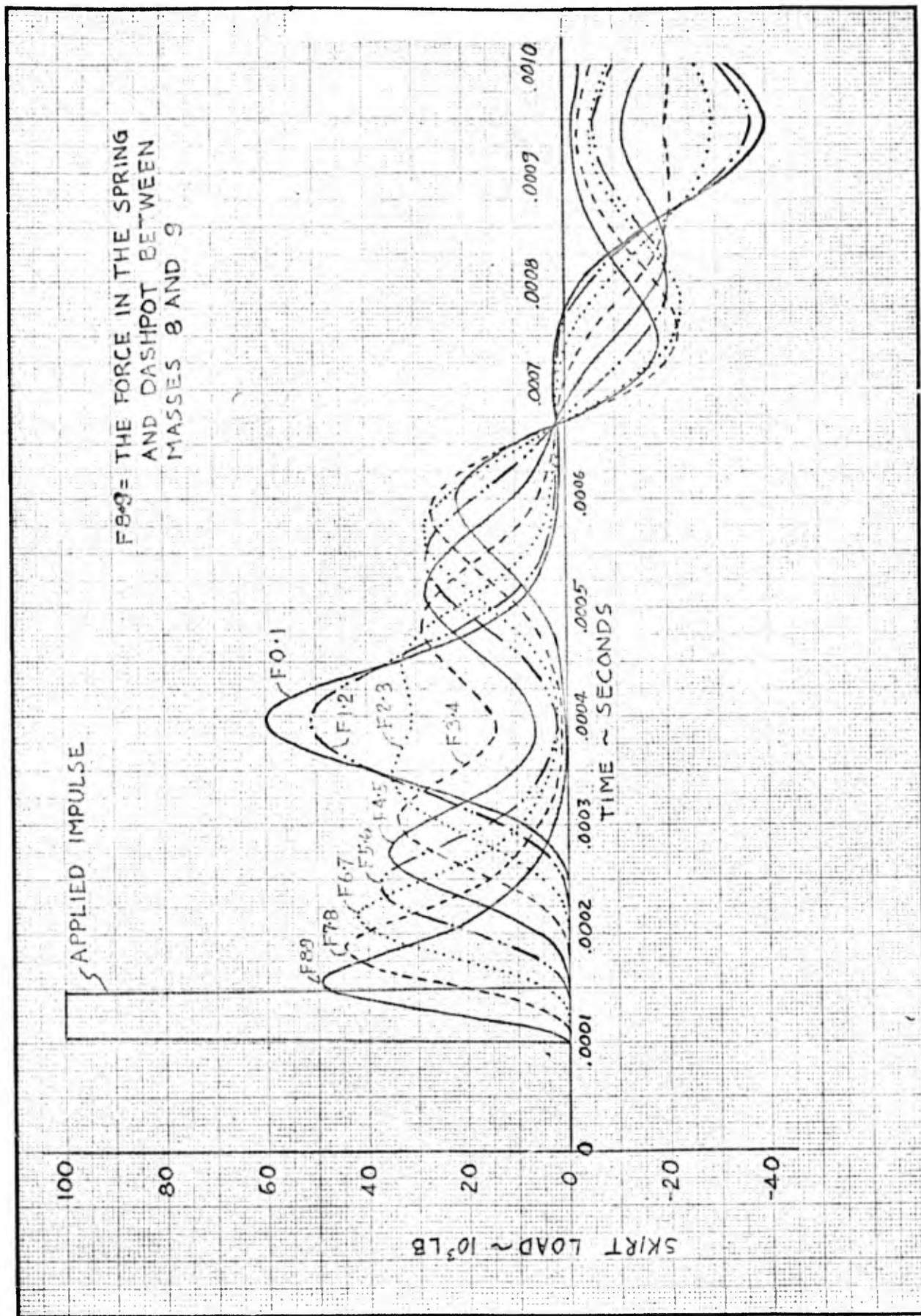

CALC	RJL	1-29-65	REVISED	DATE
CHECK				
APR				
APR				

SKIRT RESPONSE TO IMPULSE LOAD AT SABOT IMPACT FIGURE 22

1

D2-99603-1

THE BOEING COMPANY

PAGE 53

US 4013 8000

K•E ALBANENE® TRACING PAPER 71288

the sabot hit the stop the compressive load was removed as a step function. The resulting load time history in the skirt structure is shown in Figure 23. These curves show that the load in the skirt started at the compression level, reduced to zero, and overshot by approximately 100%. This meant that the skirt-to-motor case joint felt a tension load equal in magnitude to the compression load acting at point "A" prior to sabot impact. Another response of significance was the acceleration imparted to the roll control system. The solution indicated that the acceleration level was plus or minus 530 g for every 100,000 pounds of compression preload. This acceleration was added to any other steady state acceleration or vibration occurring at the same instant.

This analysis showed that there were no structural problems caused by the impulse loading since the dynamic load was not greater than the load prior to sabot impact. It was estimated that the roll control on the "D" vehicle would feel an acceleration due to impact of 290 g plus the nominal steady state acceleration of 210 g.

As the top sabot ring impacted the stop ring, the rivets between the tension tie and the aft skirt were sheared. This required the tension tie bolts to be strong enough to shear the rivets and decelerate the tension tie. By placing a sabot snubber ring of soft aluminum (ultimate bearing = 20,000 psi) on the sabot stop ring, the severity of the impact was reduced. The force applied by the sabot was:

$$P_{crush} = d_{Block}\, \pi\, DS_B$$

$$= 0.75\, \pi\, 42 \times 20{,}000 = 2 \times 10^6 \text{ lb.}$$

Where:

P_{crush} = axial load applied by sabot

d_{Block} = width of snubber

D = diameter of snubber ring

S_B = ultimate bearing strength of snubber ring

Then assuming, for the short time period involved, that a third of the sabot was being stopped:

$$\frac{W_s}{3} \ddot{X}_s = P_{crush}$$

$$\ddot{X}_s = \frac{2 \times 10^6}{60} = 33{,}300\, g$$

Where:

W_s = weight of sabot

$\ddot{X}_s$ = axial acceleration of the sabot

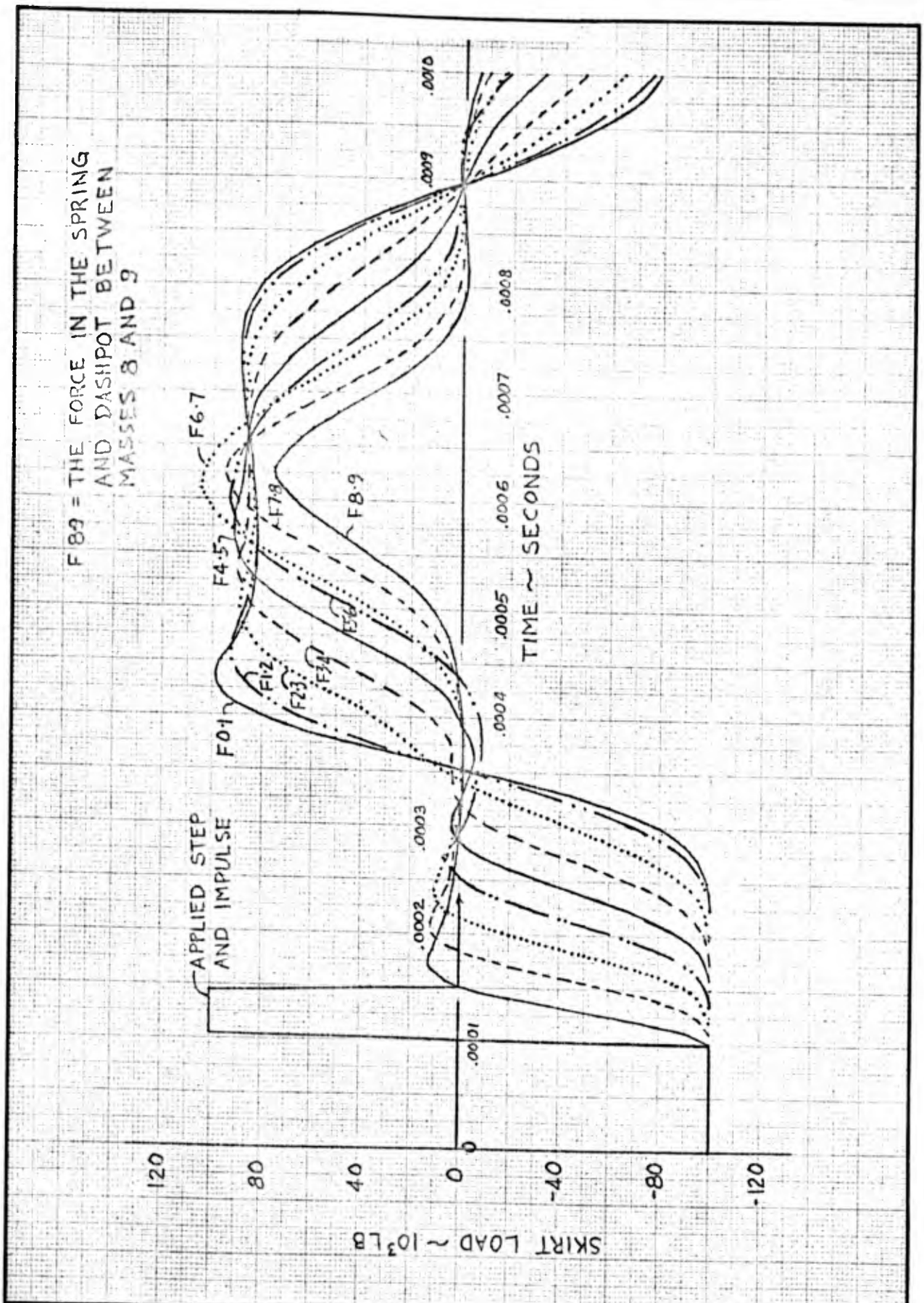

CALC	RJL	1-29-65	REVISED	DATE
CHECK				
APR				
APR				

SKIRT RESPONSE TO STEP PLUS IMPULSE LOAD AT SABOT IMPACT FIGURE 23 D2-99603-1

THE BOEING COMPANY

PAGE 55

US 4013 8000

K+E ALBANENE® TRACING PAPER 71836

The tension tie bolts must then have the following strength:

$$T_B = \ddot{X}_s W_{Tension\ Tie} + P_{Rivets}$$
$$= 33,300 \times 6 + 100,000 \approx 300,000\ lb$$

Where:

T_B = required strength of tension tie bolts

P_{rivets} = ultimate shear strength of skirt to tension tie rivets

$W_{Tension\ Tie}$ = weight of the tension tie

It was essential that a large gap be left between the tension tie and other sabot structure (such as the nozzle fairing) which might otherwise bear against the tension tie during the deceleration.

To determine the height of the sabot snubber ring the acceleration of the stop ring, also, was found:

$$W_p \ddot{X}_p \approx P_{crush}$$
$$\ddot{X}_p = \frac{2 \times 10^6}{322} = 6200\ g$$

Where:

W_p = weight of the stop ring

$\ddot{X}_p$ = axial acceleration of the stop ring

The vehicle was assumed to have zero acceleration. Then these accelerations were double integrated to obtain displacement as shown on Figure 24. This figure shows that the height of the snubber ring required was 0.6 in. Repeating the analysis assuming the full weight of the sabot being stopped showed a ring height of 1.2 in. required. By varying the crushing strength of the ring the following tension tie bolt requirements were determined:

S_B	T_{Bolts}
20,000 psi	300,000 lb.
30,000 psi	400,000 lb.
50,000 psi	600,000 lb.

Due to uncertainties involved in the analysis (such as the portion of the sabot being stopped), it was decided to use a 20,000 psi aluminum snubber ring 1.0 in. high by 0.75 in. wide. The tension tie bolts were designed to 400,000 lb.

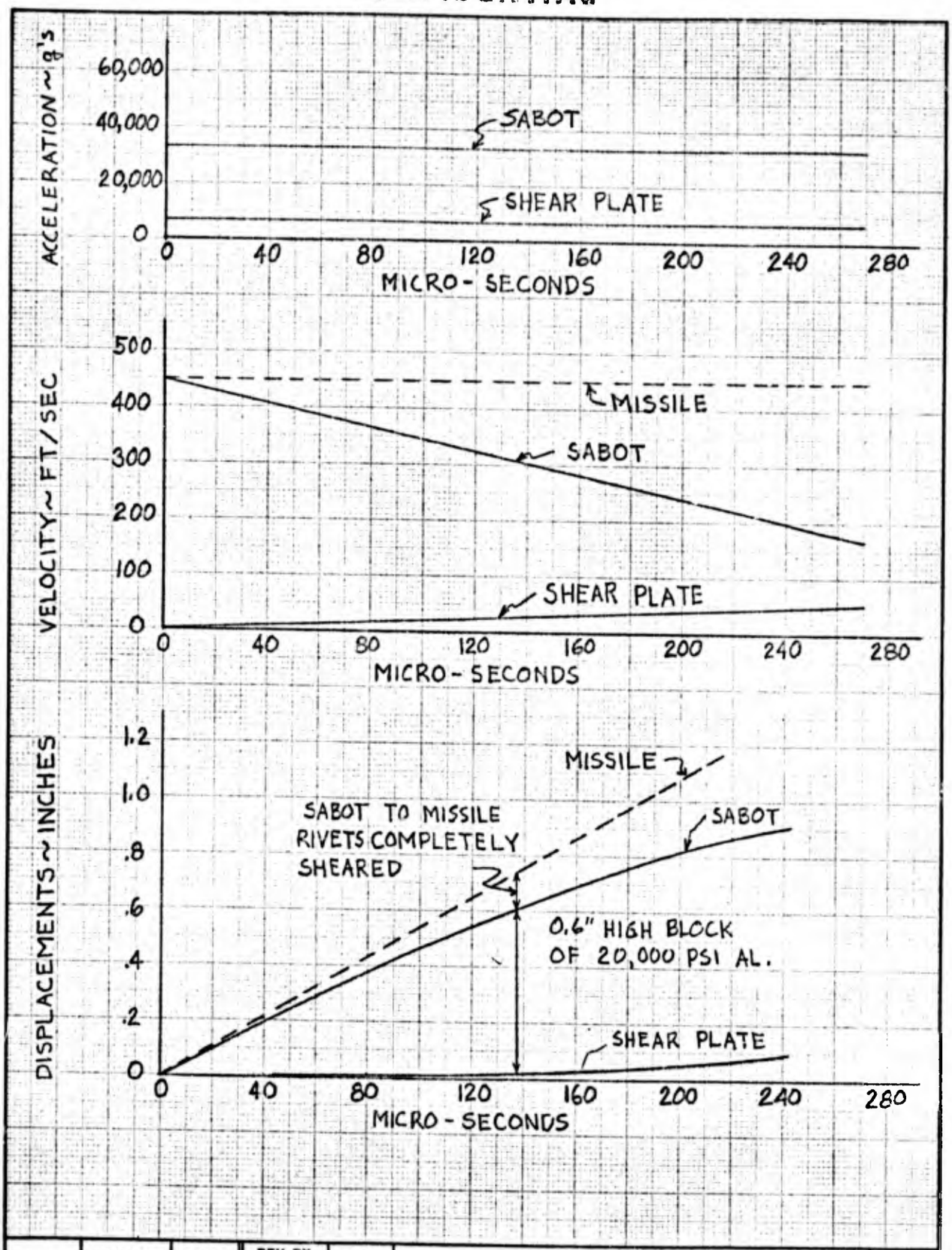

	INITIALS	DATE	REV BY INITIALS	DATE	TITLE	MODEL
CALC	RJL	11-24-64			SABOT IMPACT EFFECTS	
CHECK						
APPD.						
APPD.						

FIGURE 24

U3 4013 8000 REV. 12-64

REV LTR

BOEING NO. D2-99603-1

SH.

4.3.2.3 Nozzle Loads

With separated flow existing in the launch tube the silo pressure could also cause separation of the flow from the nozzle walls. This resulted in pressure distribution shown in the lower part of Figure 25 for the nozzle design loads. Summation of the pressure forces plus inertia loads resulted in the following nozzle axial load equation:

$$P_{NOZ} = -\sum_{Throat}^{Sep.} p_i A_i - p_b A_{sep.} + W_{Nozzle} \ddot{X}$$

where the terms are defined above or as follows:

P_{NOZ} = nozzle axial load

p_i = normal nozzle pressure

A_i = projected area of the nozzle back to the separation plane

p_b = pressure acting on the base

A_{sep} = separated area of the nozzle

W_{Nozzle} = weight of the nozzle

$\ddot{X}$ = longitudinal acceleration

Nozzle axial load obtained from the above equation is shown in the upper part of Figure 25.

4.3.2.4 Vibration

A marked increase in the vibration level of the vehicle second stage was expected for the open silo launch configuration. This increase over the pad launch configurations was predicted in anticipation of the envelopment of the vehicle by the high pressure silo blast wave. The design vibration environment for the closed breech silo conservatively retained the allowance for envelopment of the missile by the high pressure wave discharged from the silo after launch. However, the launch results discussed in Section 5.3 indicated that the silo discharge pressure wave did not affect the vehicle. A more complete discussion of vibration may be found in "HiBEX Vibration Environment", D2-99572-1[7].

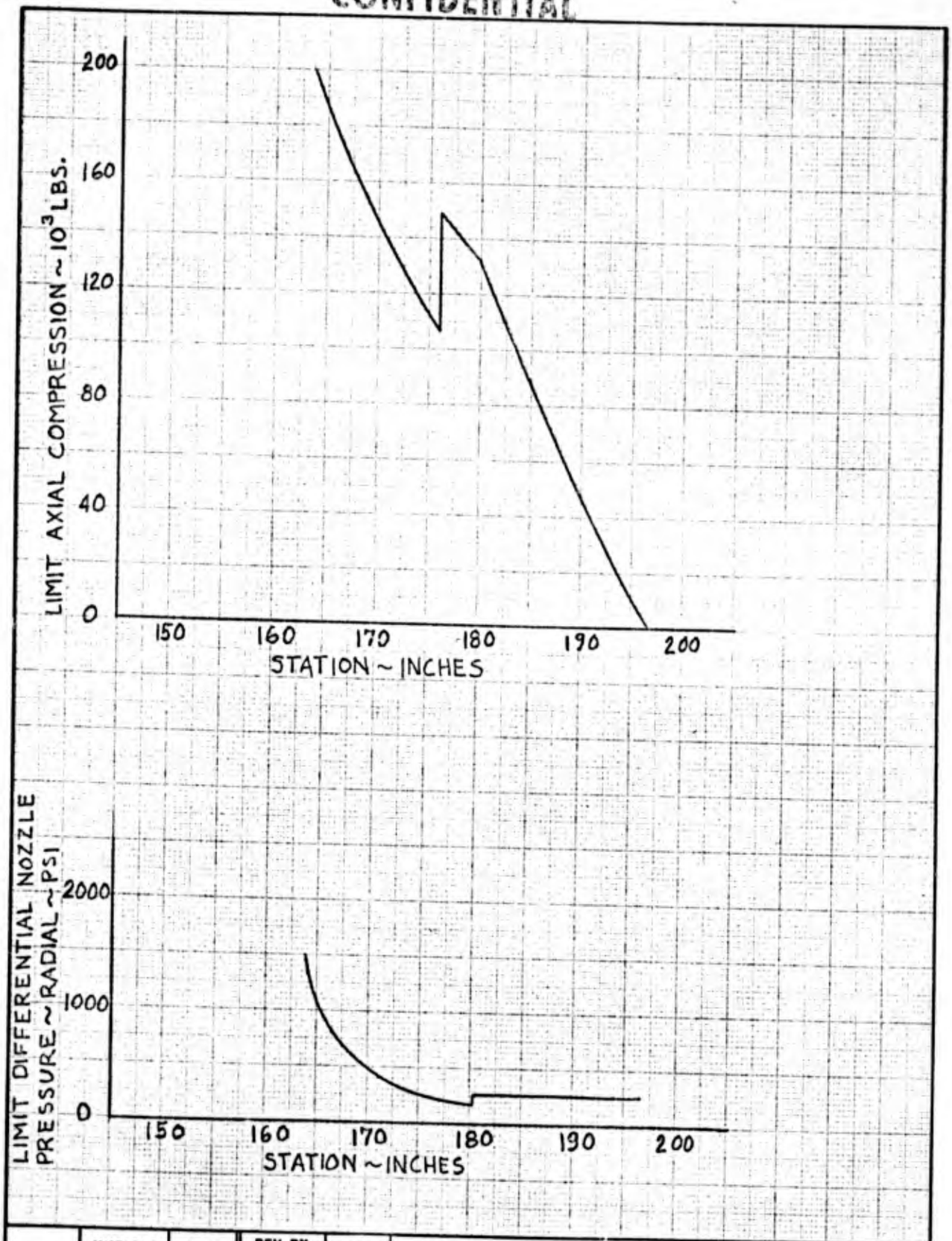

	INITIALS	DATE	REV BY INITIALS	DATE	TITLE	MODEL
CALC	RJL				SILO LAUNCH NOZZLE LOADS	
CHECK						
APPD.						
APPD.					FIGURE 25	

U3 4013 8000 REV. 12-64

REV LTR_____

4.3.3 Sabot Design

Prior to launch, the sabot supported the vehicle, allowed free rotation of the vehicle for azimuth adjustments, and provided the necessary hardware for quick disconnect umbilicals at both the base and top surface of the sabot (See Figure 26).

4.3.3.1 Sabot Structural Requirements

Structural design requirements for the sabot were as follows:

1. The sabot must withstand the loads specified in Section 4.3.2.
2. The sabot must provide for handling equipment attachment for vehicle emplacement in the silo.
3. The sabot must support the vehicle prior to and during launch and provide for positive separation from the vehicle at exit from the silo without damage to the vehicle.

a) Structural Description:

The sabot structure consisted of circumferential rings at stations 196.57 and 221.57, 10 longitudinal intercostals uniformly spaced around the circumference, and an insulated 7075-T6 aluminum alloy inner shell. The rings and intercostals were fabricated from 7075-T6 aluminum plate and extrusion respectively. A wedge shaped fairing was installed inside the sabot shell to provide flow transition from the nozzle contour to the cylindrical sabot inner shell. Both the shell and fairing were insulated against heat from the rocket exhaust by teflon sheet bonded to the exposed surfaces. The base ring was insulated by a cork ring bonded in place. The sabot was attached to the aft section skirt base by a tension tie ring bolted to the sabot upper ring, and riveted to the skirt.

A close fit was maintained between the sabot and the launch tube to minimize the exhaust gas leakage and silo loads, and maintain the desired launch angle. The nominal launch tube inside diameter was 44.500 in., and sabot nominal diameter clearance was 0.075 in.

Teflon tape 0.010 in. thick was bonded to the ring surfaces contacting the silo wall to reduce friction drag load.

b) Design Criteria:

The following criteria were observed in the sabot design:

1. Limit design loads during launch were increased by a factor of safety of 1.5 to obtain ultimate design loads, (excluding the sabot/skirt joint loads.)

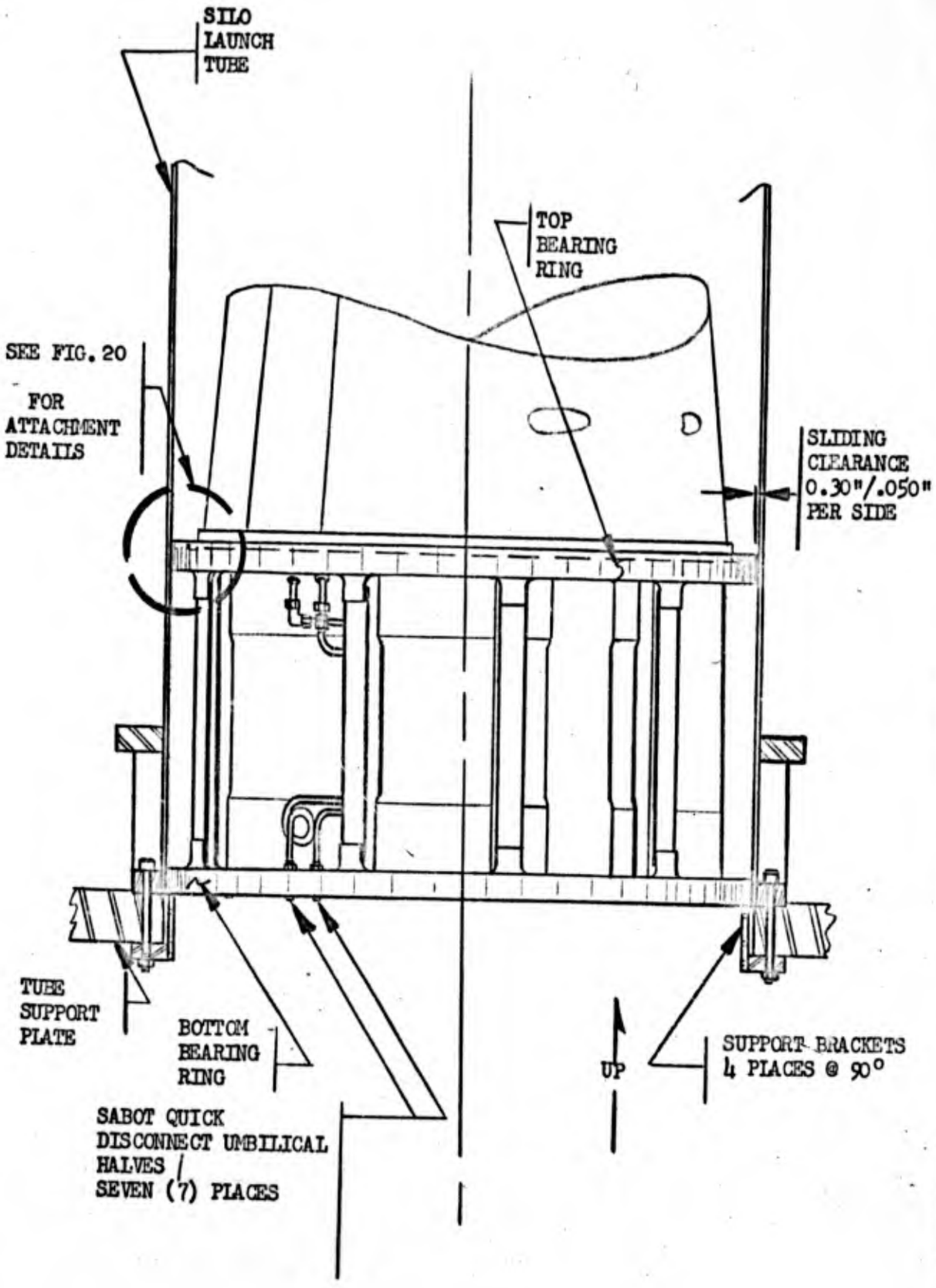

FIGURE 26 - SABOT DESIGN

2. The proof tested st[illegible]gth of the aft rocket motor case extension joint was 116,000 lb. The maximum sabot separation tension force, minus skirt inertia, must not exceed this value.

3. The factor of safety for the sabot/skirt joint was 1.25.

4. Ground handling load factor of safety was 5.0.

5. The sabot components must not break up at impact before the sabot/skirt joint rivets sheared.

6. Structural strength margin of safety of components must be ≥ 0 at design ultimate load.

c) Analysis and Design:

Final design analysis of the sabot structural components considered an internal sabot working pressure of 400 psig although dynamic loads analyses were based on a nominal pressure of 235 psia which was increased by factors to account for above nominal performance, including motor thrust variation. The structure was insulated from heat from the rocket exhaust so that no degradation in structural strength would occur from temperature effects.

The shell was analyzed for both internal pressure and the combination of bending moment and axial load during launch. Data on the elastic stability of shell under combined loads were obtained from Boeing Document D2-3617[8], and the analysis considered combined stresses as follows:

$$R_B + R_c = 1.0$$

where R = Ratio of applied to allowable stress;
subscript B refers to bending stress and
subscript c refers to compression stress.

The shell was found to be critical for the design ultimate internal pressure of 600 psig. A longitudinal splice provided circumferential strength continuity. The shell thickness was increased locally at the ring attachment for discontinuity stresses.

The rings were analyzed for the reaction loads imposed by the sabot resistance to vehicle overturning moments. The design considered the reaction load to be applied to the ring in a cosine distribution. The ring section was then designed to withstand the resulting combined internal moment, axial, and shear loads based on closed ring analysis[10].

Intercostals were spaced uniformly around the circumference between the rings to resist the twisting of the circular rings caused by drag loads and non-uniform base pressure distribution. Design analysis combined the load induced by bending due to internal pressure deformation of the shell with an equivalent axial compression load due to the over-all bending of the sabot and pressure forces on the base.

The wedge shaped fairing was designed by tension loads due to internal sabot pressure and attachment requirements to insure that it would not break up prematurely due to high deceleration forces developed at impact of the sabot with the stop ring. The fairing was attached with 55, 5/16 in. diameter, 160,000 psi heat treated steel bolts. The tension tie was bolted to the upper sabot ring with 84, 1/4 in. diameter, 160,000 psi heat treated steel bolts. Other sabot structural components had butt fit compression load carrying surfaces bearing against the upper sabot ring to prevent premature failure and flying parts.

The sabot/skirt joint design data are shown in Figure 27 and details of the joint are shown in Figure 20. The important requirements of the joint were:

1. It must provide sufficient strength to carry the combined loads imposed by the vehicle disturbances as it traveled up the launch tube.

2. It must have an axial tension failing strength below the proof tested axial tension strength of the rocket motor aft skirt joint minus skirt inertia load.

Figure 27 illustrates graphically the compliance of the joint design with these requirements. Rivet single shear strength used for development of Figure 27 are shown in Figure 28. The figure shows the cumulative probability of rivet failure as a function of rivet strength, and the values used for the joint design based on a statistical analysis.

4.3.3.2 Sabot Thermal Requirements

The following thermal requirements applied:

1. A thermal ablative liner over the inner surface of the sabot must limit the temperature rise in the sabot structure to 100°F or less.

2. The sabot material bearing against the launch tube must be compatible with the environment caused by the roll control and rocket motor exhaust during emergence from the silo.

3. The sabot configuration must effectively seal the launch tube during launch.

4. The sabot configuration must provide a smooth fairing from the rocket motor nozzle through the cylindrical section of the sabot to the exit plane of the sabot.

5. The sabot structure must not interfere with the roll control system exhaust.

The thin aluminum skin of the sabot required protection from the rocket motor exhaust gases. Teflon was chosen because it was relatively flexible and easy to apply, and tough. Charring ablators were felt to offer no improvement because the char would be removed by the high velocity gas flow and particle impingement.

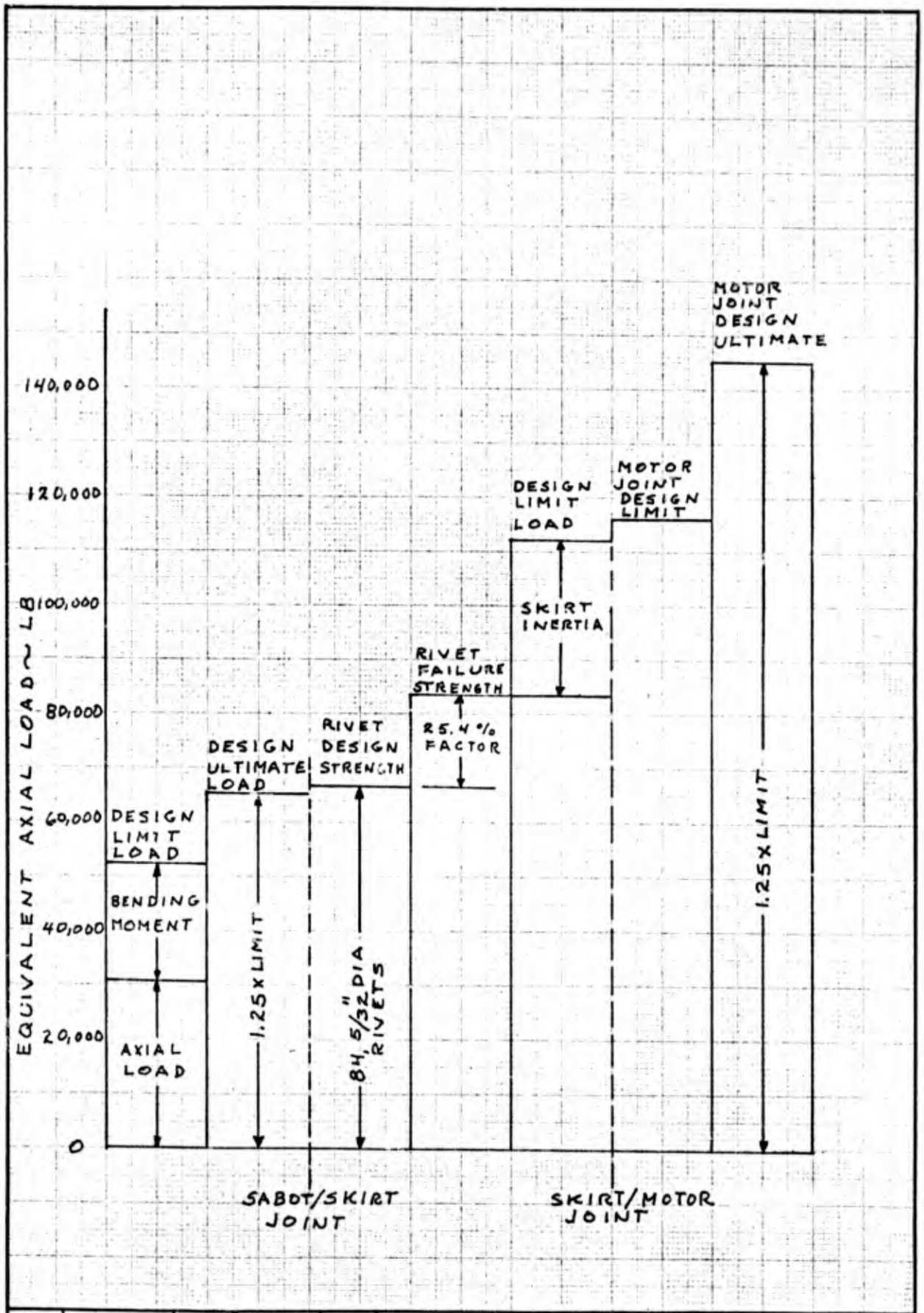

CALC			REVISED	DATE
CHECK				
APR				
APR				

FIGURE 27
PHASE D VEHICLE
SABOT/SKIRT JOINT DESIGN CRITERIA

D2-99603-1

THE BOEING COMPANY

TD 461 C-R4

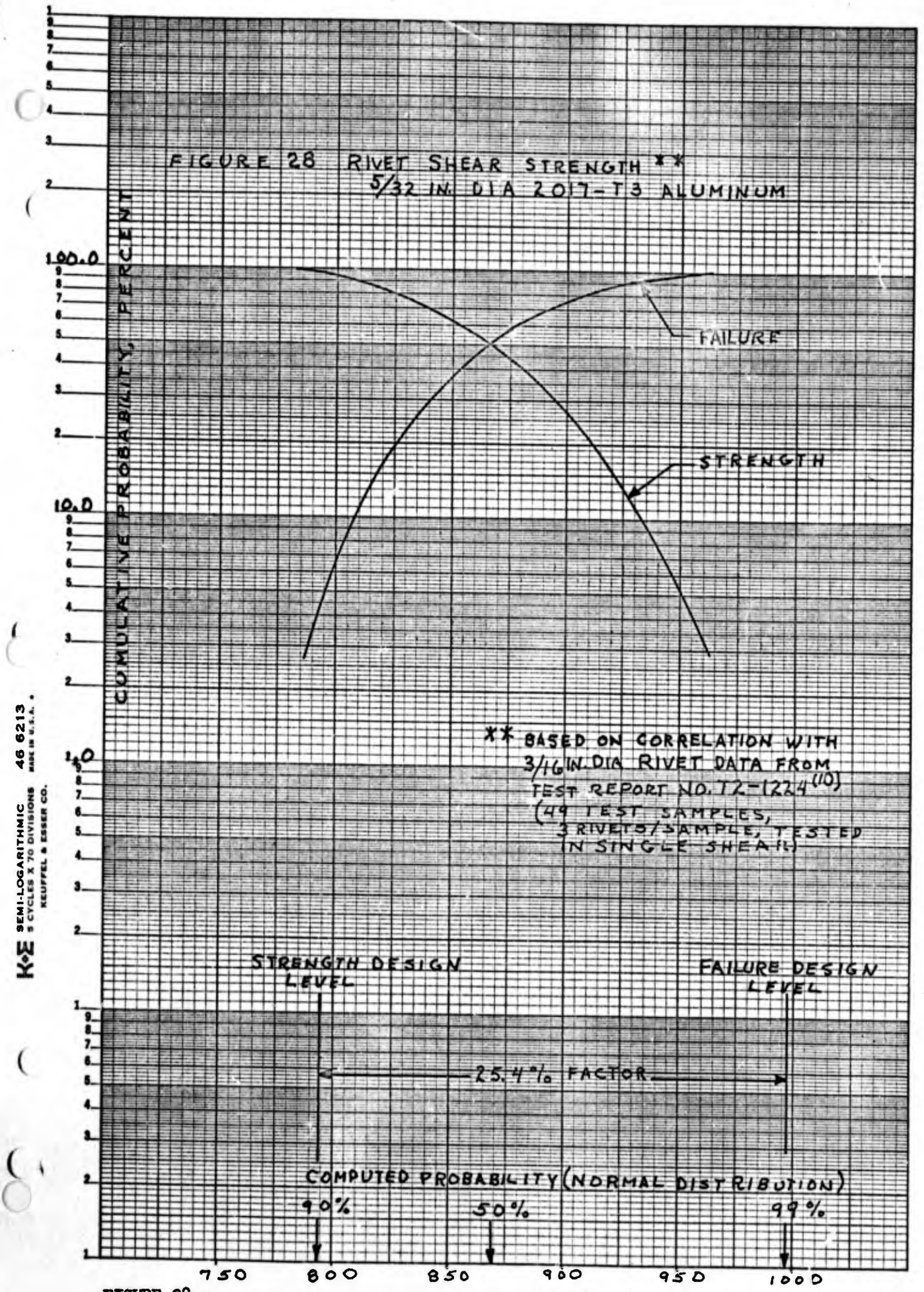
FIGURE 28 RIVET SHEAR STRENGTH **
5/32 IN. DIA 2017-T3 ALUMINUM
CUMULATIVE PROBABILITY, PERCENT
100.0
10.0
1.0
FAILURE
STRENGTH
** BASED ON CORRELATION WITH 3/16 IN. DIA RIVET DATA FROM TEST REPORT NO. TZ-1224 (10) (49 TEST SAMPLES, 3 RIVETS/SAMPLE, TESTED IN SINGLE SHEAR)
STRENGTH DESIGN LEVEL
FAILURE DESIGN LEVEL
25.4 % FACTOR
COMPUTED PROBABILITY (NORMAL DISTRIBUTION)
90 %
50 %
99 %
750
800
850
900
950
1000
RIVET STRENGTH, LB/RIVET (SINGLE SHEAR)
K&E SEMI-LOGARITHMIC 46 6213
5 CYCLES X 70 DIVISIONS
KEUFFEL & ESSER CO.

FIGURE 28 -

Investigation of ablation material thickness required was undertaken during sabot design. A theoretical estimate of the convective and radiant heating rates on the inner surface of the sabot is presented in Figure 29. The effect of impinging hot metallic oxide particles on the ablating surface was unknown, and tests of cold particle impingement on an ablating surface in the Boeing Hypersonic Wind Tunnel were inconclusive. Considerable abrasion was observed in these tests, however, and it was felt that ablation rates would be severely increased over those calculated on the conventional basis of hot gas flow. Furthermore, it was necessary in the analysis to modify the ablator material properties to account for the effect of the exhaust flow properties, which were different from those of air, on the effective heat of ablation for the material. Finally, it was known that the Teflon was not opaque to radiant heating, so that a relatively thick layer would be necessary to avoid delamination of the Teflon/aluminum bond. A 0.1 in. thickness of Teflon was employed which provided a safety factor of about 4.0.

4.3.4 Silo Configuration

The silo configuration was required to be adaptable to open silo, closed breech and vented silo launches, and to various plenum volumes.

4.3.4.1 Constraints on Silo Pressure Imposed by Vehicle Structural Capability

Analysis indicated that separated rocket motor exhaust gas flow conditions might exist in the launch tube, sabot, and rocket motor nozzle. These conditions would have resulted in compressive loading of the sabot and vehicle aft skirt and in radial loading of the nozzle exit cone.

The compressive load capability of the aft skirt limited the silo maximum operating pressure to 260 psia. The aft skin bay on the vehicle aft skirt was critical from compressive loads at this pressure. Therefore an increase in silo pressure would have required an increase in the strength of this bay, and possibly other bays as well.

The nozzle used for the silo launches was near the critical design point at the exit cone for the liner limitation of 1.23 percent circumferential elongation which occurred at 290 psia. The proof test requirement for the nozzle exit cone was 260 psia, however, the liner did not sustain damage during the nozzle structural test to a pressure of 342 psia. Silo conditions which resulted in separated flow in the nozzle giving pressures in excess of 260 psia would have jeopardized the vehicle as designed.

4.3.4.2 Silo Size Determination

The closed-breech launches required silo plenum volumes to be variable from 3200 cu ft to 1600 cu ft. Low pressure silo dimensions of 10 ft diameter and 50 ft deep were established as satisfactory for the 3200 cu ft volume during the Task I study(2). The 10 ft diameter also provided work space around

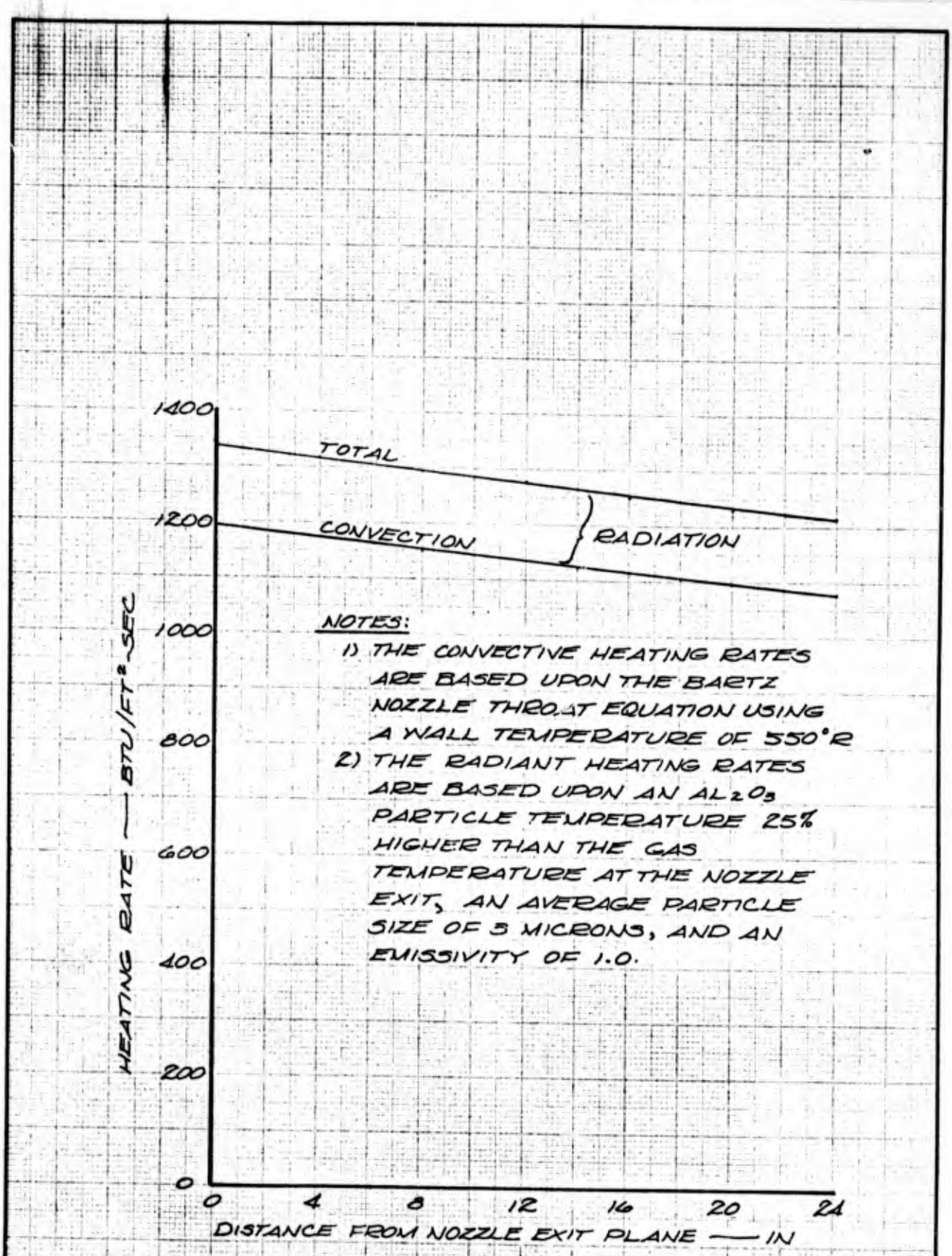

NOTES:

1) THE CONVECTIVE HEATING RATES ARE BASED UPON THE BARTZ NOZZLE THROAT EQUATION USING A WALL TEMPERATURE OF 550°R
2) THE RADIANT HEATING RATES ARE BASED UPON AN AL_2O_3 PARTICLE TEMPERATURE 25% HIGHER THAN THE GAS TEMPERATURE AT THE NOZZLE EXIT, AN AVERAGE PARTICLE SIZE OF 3 MICRONS, AND AN EMISSIVITY OF 1.0.

CALC			REVISED	DATE	HEATING RATE DISTRIBUTIONS ALONG INNER SURFACE OF SABOT FIGURE 29
CHECK					
APR					
APR					
					THE BOEING COMPANY

D2-99603-1

TD 461 C-R4

the launch tube for service and testing. The smaller silo plenum volume was achieved by partially filling the silo with sand and covering the sand with a concrete floor faced with steel. This assembly was anchored by tie rods to the original floor to prevent rebound (see Figure 30).

4.3.4.3 Launch Tube

The launch tube was 44.5 in. inside diameter and 18 ft long which placed the nose of the vehicle just below ground level. A machined and honed inner surface was necessary to be compatible with sabot requirements outlined in Section 4.3.3. The tube was fabricated from 1 in. thick A36 steel plate, and was nominally 0.75 in. thick after machining. As shown in Figure 31, bolting flanges were provided on the outside of the launch tube to attach the moat cover, sabot stop ring, pressure diaphragm, and base plate. The tube was designed to withstand a maximum operating differential pressure of 400 psi on the outside or inside surface. The launch tube bottom flange was required to react a tension load of 2,800,000 lb derived by combining one-third of the 400 psi pressure diaphragm load with the impact load generated by sabot separation at the top flange. Removable hatches, flush with the inner surface, were required as an integral part of the tube in order to accomplish servicing, handling, and testing after the vehicle was emplaced in the tube. The inner surface was heavily coated with molybdenum disulfide for lubrication and protection from oxidation and motor exhaust deposits.

The launch tube bore was required to be straight within 0.030 in., round within 0.016 in., and to be aligned with 0.1 deg of the vertical. The inner surface finish was required to be 32 microinches rms.

4.3.4.4 Pressure Diaphragm and Base Brackets

The pressure diaphragm and base plate brackets made up the primary support members between the silo wall and the launch tube (See Figure 32). The annulus around the tube was made pressure tight by a diaphragm composed of eight sections. A silo pressure of 400 psi would induce a 3,900,000 lb force on the diaphragm.

The launch tube flange load was reacted by the four base plate brackets that were anchored to the silo wall, as shown in Figure 32. All components were fabricated from structural A-36 steel with plate thickness varying from 1 in. to 4 in. Structural design criteria provided for no yield at maximum operating loads (limit loads) and no failure at ultimate loads (2.0 X limit).

4.3.4.5 Vented Silo Requirements

The planned vented silo required exhaust orifices sized to bleed the silo pressure down to a maximum of approximately 160 psia for a plenum volume that would produce a maximum pressure of 235 psia during a closed-breech launch.

Theoretical venting orifice size varied from 6 to 10 sq ft. The hardware was designed with minimum sized orifices that could be altered as indicated by the data from the initial closed-breech launches.

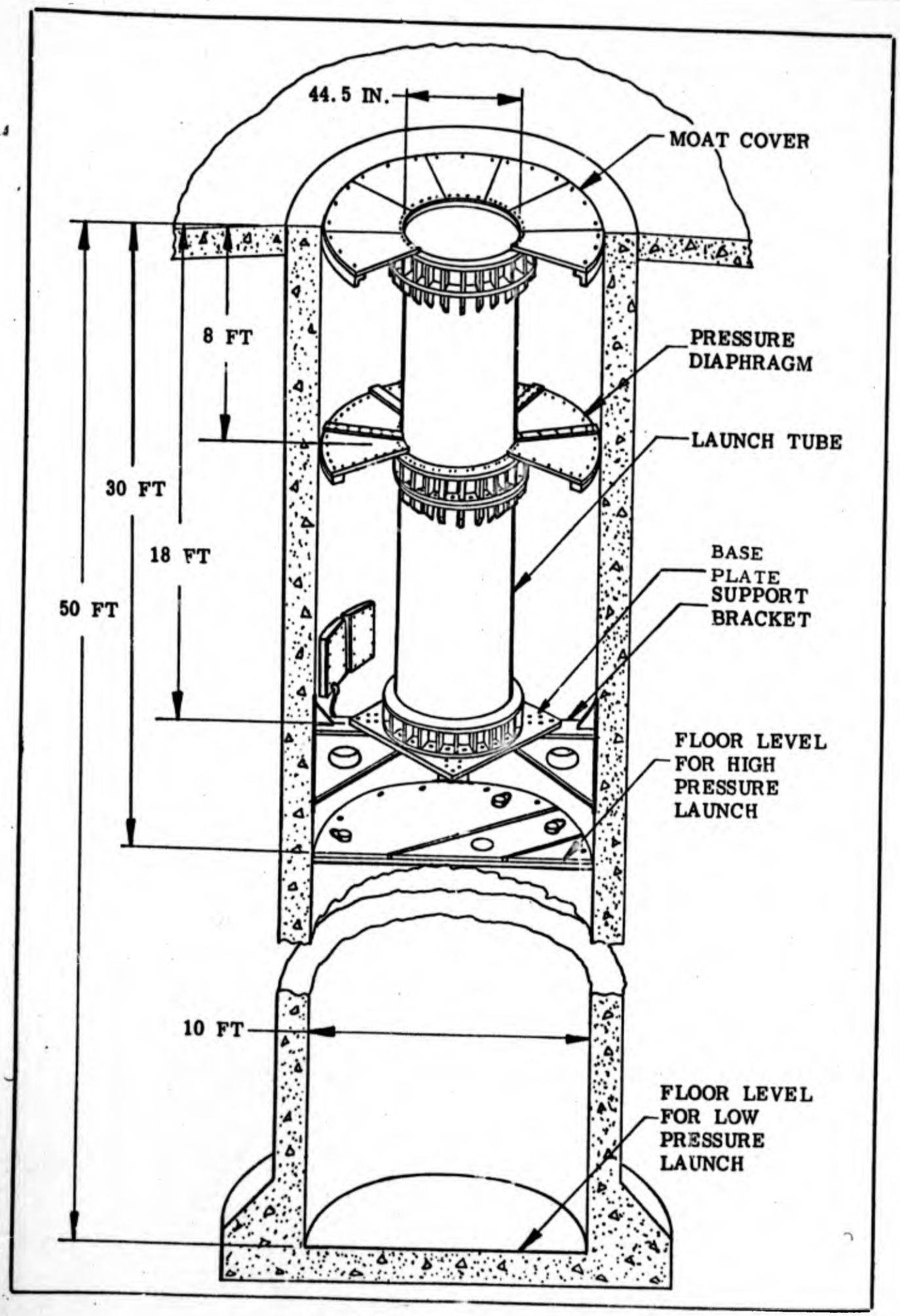

FIGURE 30 - HIBEX SILO

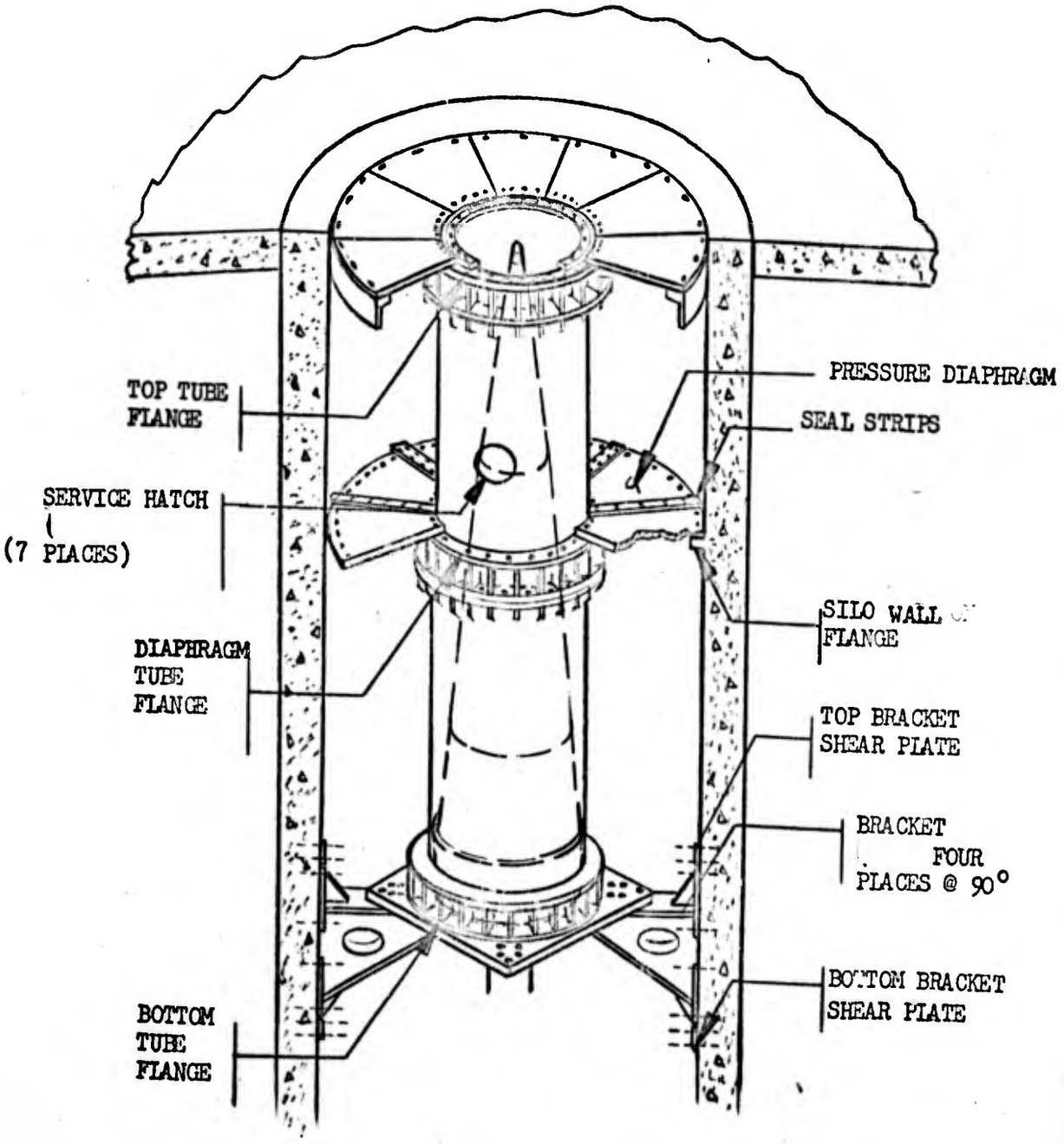

FIGURE 31 - SILO PRESSURE DIAPHRAGM & BASE BRACKETS

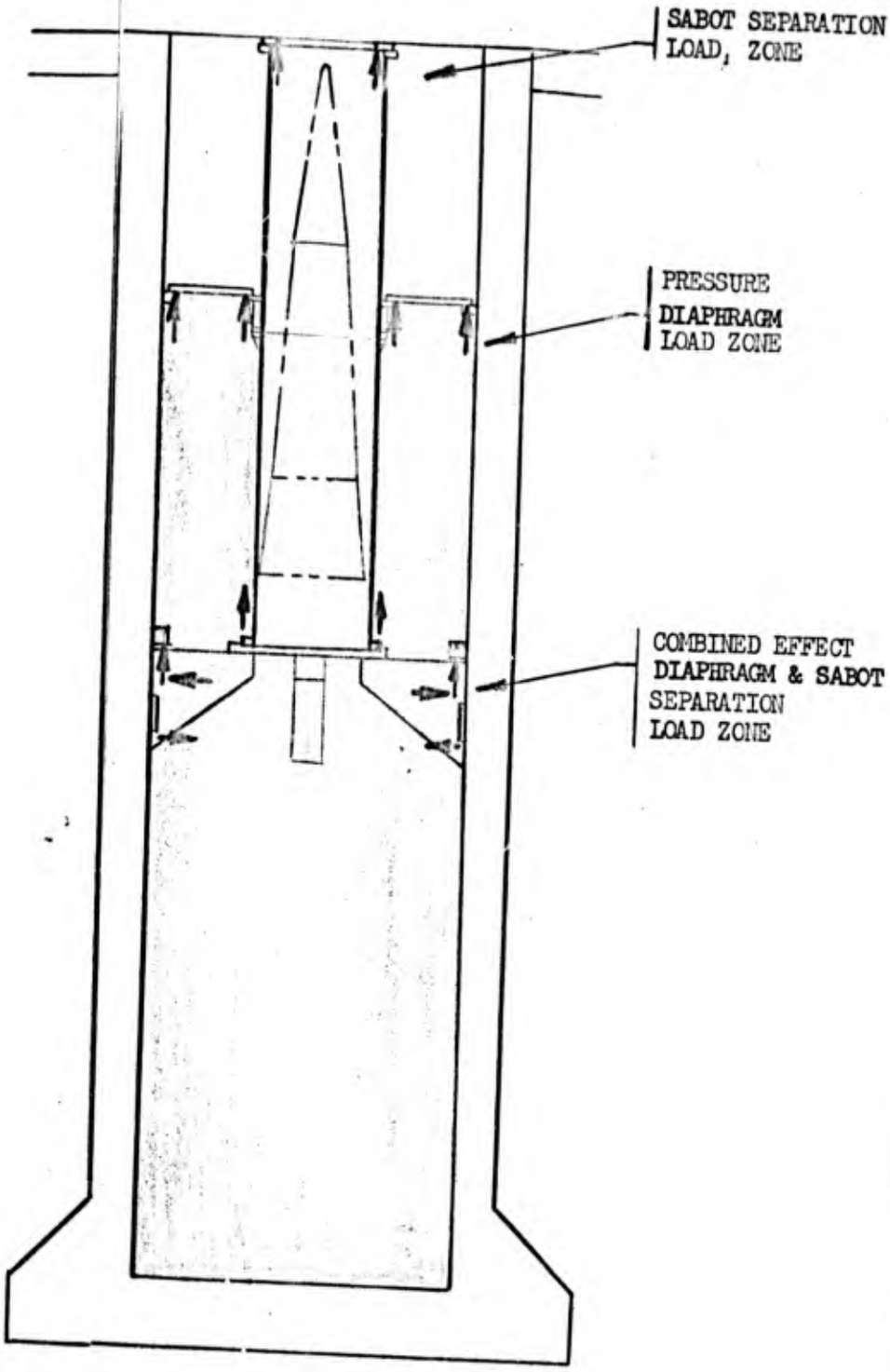

FIGURE 32 - SILO LOAD SCHEMATIC

= PRESSURIZED PLENUM

= LOAD REACTING POINTS

Vented exhaust gases from the diaphragm orifices were directed 30 deg outward, by louvers through the moat cover segments. The minimum louver area was 1.5 times the orifice area. (See Figure 33)

4.3.4.6 Supplemental Requirements

A removable work platform was required at approximately the -23 ft level to gain access to the sabot umbilical fittings and lower launch tube service hatches after vehicle emplacement in the silo. Removable wall ladders were bolted to the silo wall throughout the entire silo depth. Ladders were staggered 180 deg to provide for personnel safety. All ladders were equipped with safety belt attachments for use by test personnel.

Quick-disconnect fittings for all umbilical servicing at the sabot base were housed in fabricated steel enclosures. This insured against flying parts that could damage the silo instrumentation. The enclosures were designed to resist 600 psi blast pressures resulting from exhaust plume impingement.

All tubing and wiring was securely clamped to silo structure and routed in protected areas between the vehicle and the umbilical service box built into the silo wall. This equipment was required to remain secured during launch.

Covering and fairing of the 8 ft deep moat formed by the launch tube, silo wall and pressure diaphragm was required at ground level to eliminate unsymmetrical exhaust plume deflection onto the vehicle after it emerged from the silo. Moat cover sections were made from 2 in. thick A36 structural steel plates to resist a load varying from 150 psi at the tube lip to 50 psi at the silo wall. The cover consisted of twelve segments to simplify handling during silo refurbishment. One segment was fabricated from aluminum and hinged for use as a personnel access hatch.

Instrumentation outlets and mounting facilities were required throughout the silo plenum to support all possible silo launch configurations. Twenty-one instrument mounting boxes were built flush with the silo wall. Boxes were equally spaced along the East-West wall, the pressure diaphragm, and the silo floor. The instrument mounting plates required close tolerance control with the instrument box for pressure sealing and fairing requirements. See Figure 34 for typical box detail.

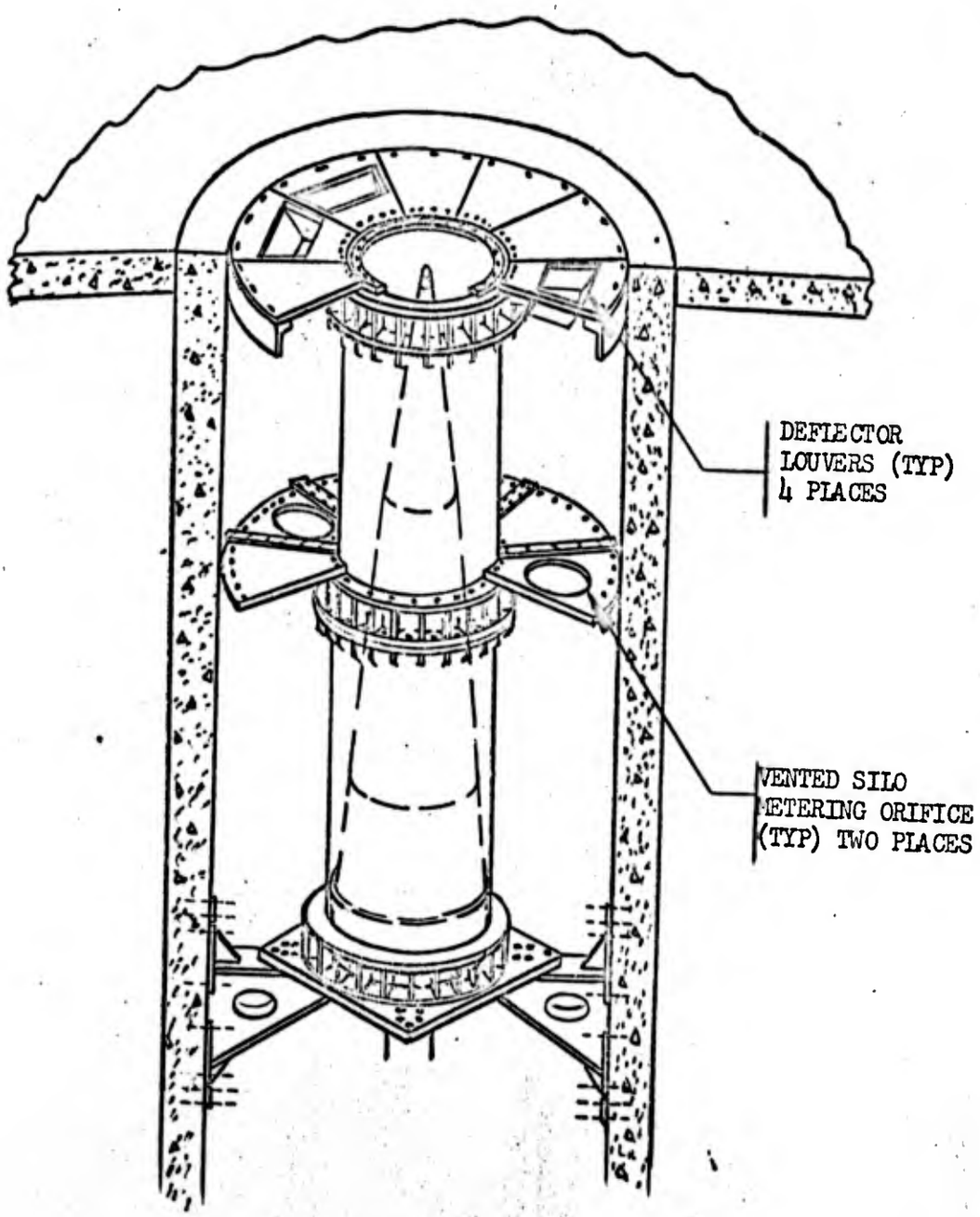

VENTED SILO ARRANGEMENT

FIGURE 33

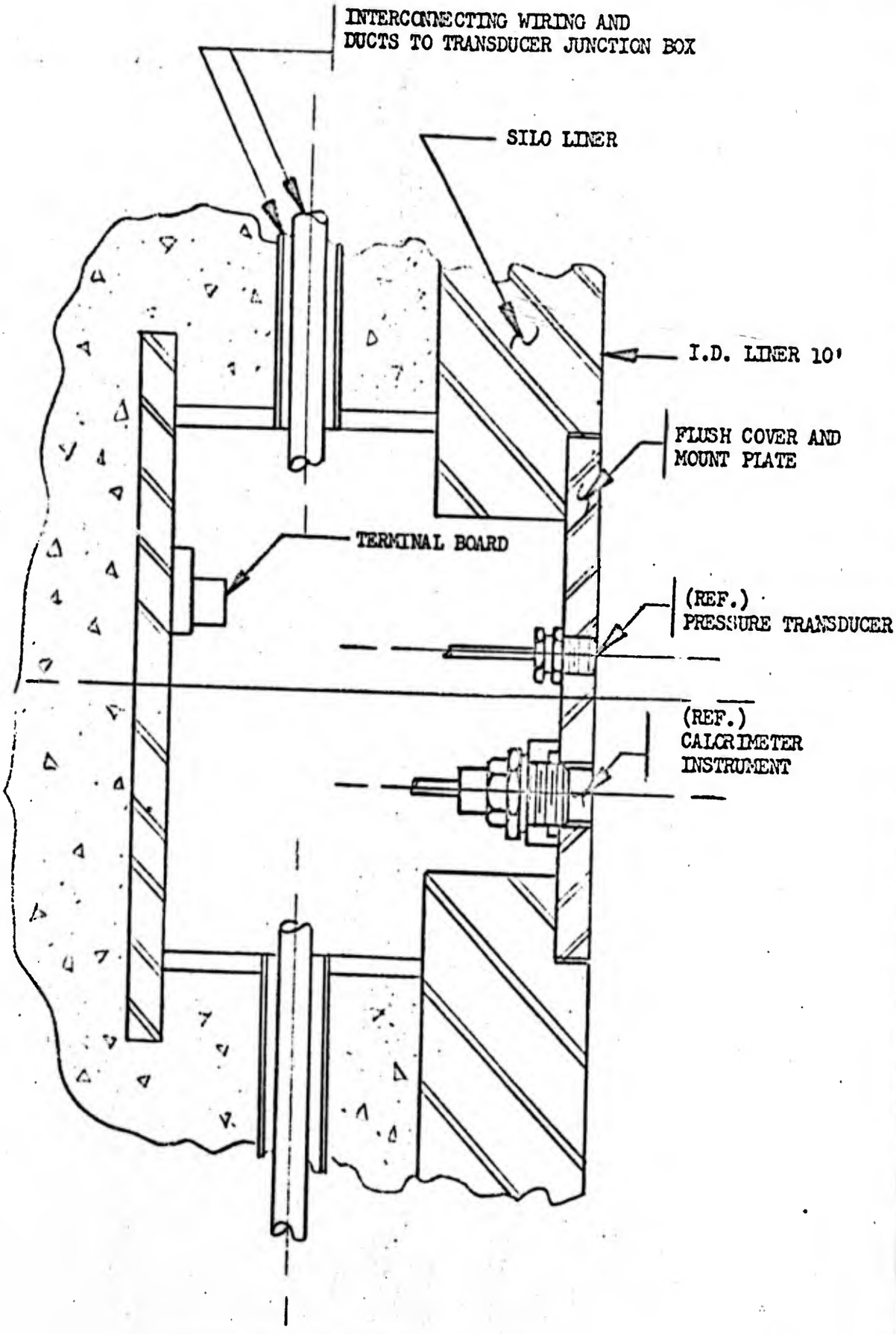

TYPICAL SILO INSTRUMENT INSTALLATION

FIGURE 34

4.4 SILO LAUNCH INSTRUMENTATION

4.4.1 Heating Rates

During a closed breech silo launch, the rocket motor exhaust gas is sealed off by the sabot and trapped below the vehicle in the plenum. The silo walls are subjected to both radiant and convective heating. To obtain both radiant and total heating rate data for comparison with theoretical calculations, rapid response low and high range heating rate instruments were developed.

Two ranges of total heating rate measurements were required. A high range, 0 to 4500 BTU/ft^2-sec, was required for areas near the silo floor. A low range, 0 to 320 BTU/ft^2-sec, was required for areas high on the silo wall and on the lower surface of the pressure diaphragm. The required measurement range for radiation was 0 to 320 BTU/ft^2-sec. The radiometers were nitrogen-purged to help prevent oxide deposits from coating the window. Details of the instrument design, construction and calibration may be found in Boeing Document D2-99590-1, reference (9). The heating rate instrumentation installed in the silo is shown in Figures 35 and 36 for the D-2, and D-3 launches, respectively. A silo heating rate instrumentation list is presented in Table II.

4.4.2 Pressures

Silo pressures to be measured in the closed breech launcher were: 1) silo floor total pressure, 2) silo wall static pressure, and 3) launch tube static pressure for determination of flow separation. Silo volume was adjusted by moving the silo floor between tests to yield the approximate desired silo pressure; this required some instrument relocation. For two test volumes used, the plenum pressure instrumentation was scaled for 160 psia and 260 psia.

Microsystem pressure transducers, which utilize a small, thin diaphragm with piezoresistive strain elements, were used to measure the silo pressure. The pressure instrumentation installed in the silo and launch tube is shown in Figures 35 and 36 for the D-2 and D-3 launches, respectively. A silo pressure instrumentation list is contained in Table III.

4.4.3 Vehicle Performance

If the rocket motor exhaust gas flow separates from the launch tube, pressure near the silo static acts on the base of the sabot. If separated flow occurs on the sabot shock fairing or in part of the rocket nozzle, those pressures will similarly be increased. This pressure can produce a significant increase in the vehicle acceleration in the launch tube.

There were no measurements specifically designed to measure vehicle performance in the silo. However, measurements were made with the airborne linear accelerometer. Sabot separation was a good check point for distance travelled and was used to check the double integrated accelerometer data.

D-2 SILO CONFIGURATION

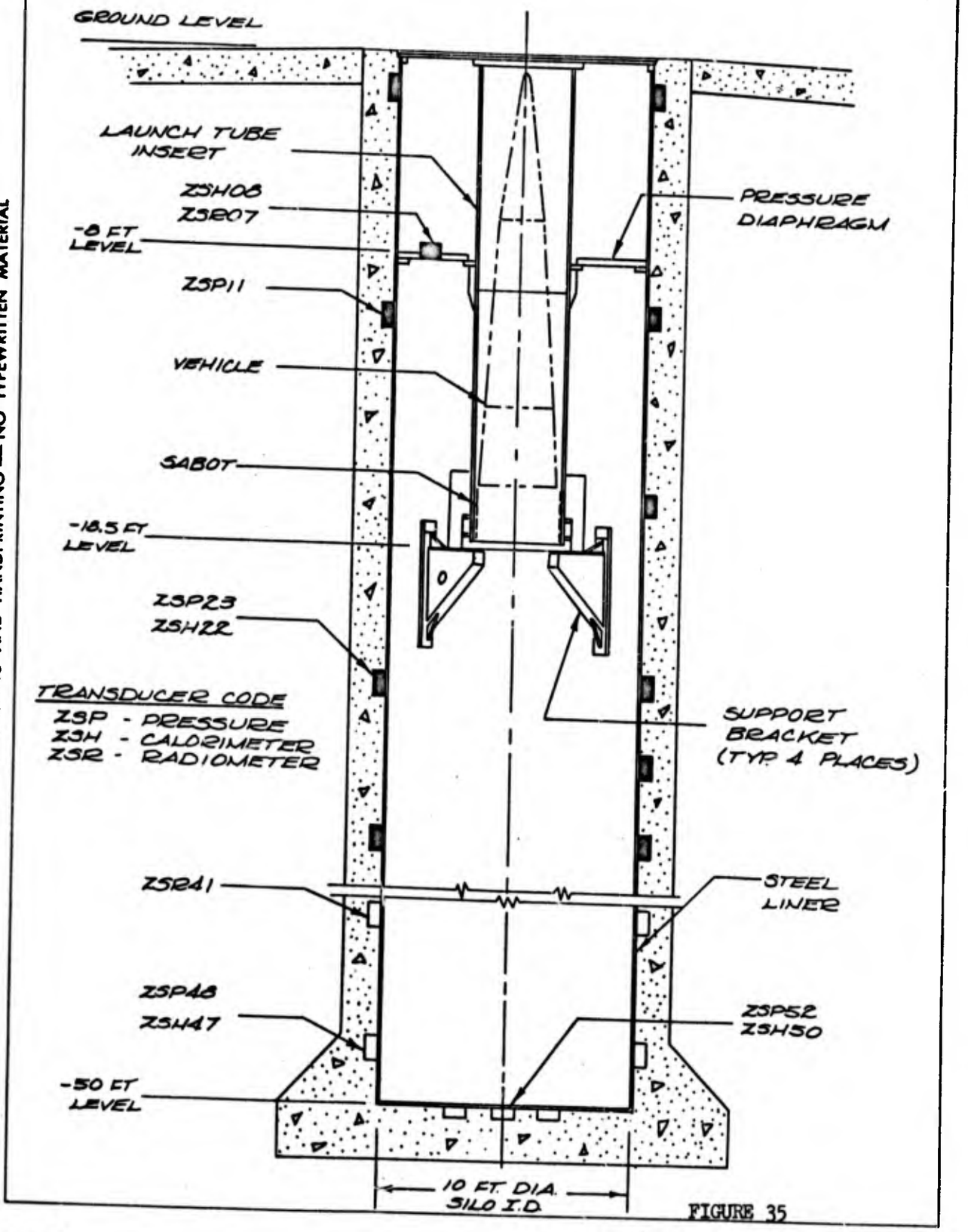

FIGURE 35

USE FOR DRAWING AND HANDPRINTING — NO TYPEWRITTEN MATERIAL

REV LTR _____

U3 4288 2001 ORIG. 5-65

BOEING NO. D2-99603-1

SH

D-3 SILO CONFIGURATION

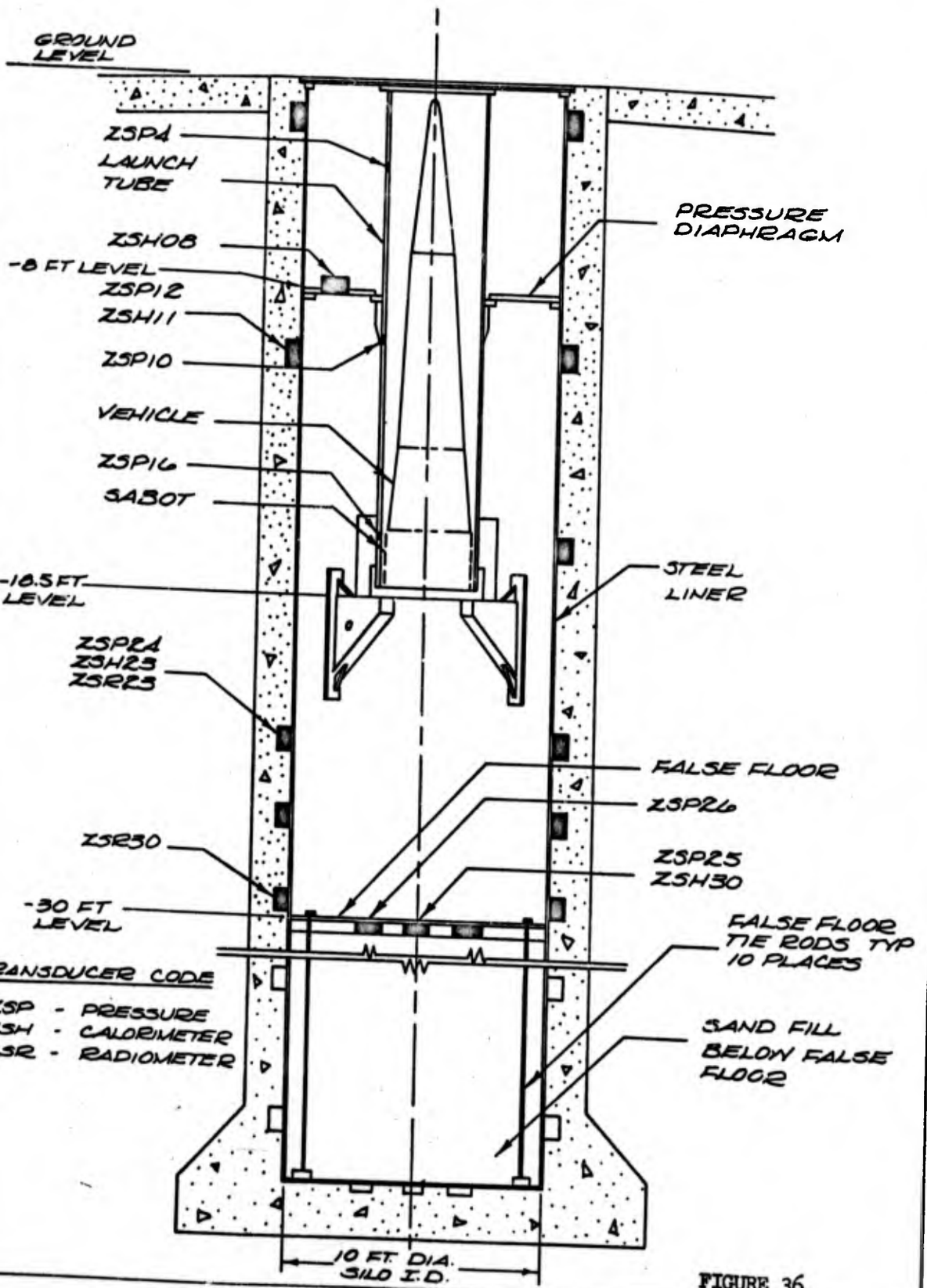

FIGURE 36

USE FOR DRAWING AND HANDPRINTING — NO TYPEWRITTEN MATERIAL

REV LTR _____

U3 4288 2001 ORIG. 5-65

BOEING NO. D2-99603-1

SH 77

TABLE II

SILO HEATING RATE INSTRUMENTATION

VEHICLE	INSTRUMENT	INSTRUMENT RANGE (BTU/SQ FT-SEC)	LOCATION	
			LEVEL* (FT)	DISTANCE FROM CENTER OF SILO (FT)
D-2	Calorimeter	0-4500	47	5.0
	Calorimeter	0-4500	50	0.0
	Calorimeter	0-320	8	3.4
	Calorimeter	0-320	23	5.0
	Radiometer	0-320	8	3.4
	Radiometer	0-320	41	5.0
D-3	Calorimeter	0-4500	23	5.0
	Calorimeter	0-4500	30	0.0
	Calorimeter	0-320	8	3.4
	Calorimeter	0-320	11	5.0
	Radiometer	0-320	23	5.0
	Radiometer	0-320	29	5.0

* Below surface of ground

TABLE III

SILO PRESSURE INSTRUMENTATION

VEHICLE	INSTRUMENT	INSTRUMENT RANGE (PSIA)	LOCATION	
			LEVEL (FT)	DISTANCE FROM CENTER OF SILO (FT)
D-2	Silo Plenum	0-160	11	5.0
	Silo Plenum	0-160	23	5.0
	Silo Plenum	0-160	47	5.0
	Silo Plenum	0-160	50	0.0
D-3	Launch Tube	0-300	3	1.8
	Launch Tube	0-300	9	1.8
	Launch Tube	0-300	15	1.8
	Silo Plenum	0-300	11	5.0
	Silo Plenum	0-300	23	5.0
	Silo Plenum	0-900	30	0.0
	Silo Plenum	0-300	30	2.5

USE FOR TYPEWRITTEN MATERIAL ONLY

4.4.4 Sabot Performance

4.4.4.1 Exhaust Flow Separation

Two pressure transducers at 180 deg spacings were installed in the sabot base ring to determine the magnitude of base pressures, thus detecting a separated flow condition in the launch tube and providing an indication of sabot pressure symmetry. In addition, two pressure transducers were located near the exit plane of the rocket motor nozzle to determine flow conditions.

4.4.4.2 Sabot Liner

Available test data on Teflon indicated that a layer 0.025 in. thick was expected to be ablated during launch, however, Teflon sheet 0.10 in. thick was installed to allow uncertainties. The ablation occurring during launch was determined by inspection of recovered sabot fragments.

4.4.5 Silo Structural Performance

The structural steel silo components were designed to conservative allowables and no yielding of silo structure was expected. Measurements of critical launch tube dimensions were made before and after launches to determine structural effects. The short duration of exposure to the thermal environment was expected to result in no damage. Visual inspection of the silo and installed equipment after each launch was utilized for confirmation.

The launch tube was instrumented with strain gages on the D-3 vehicle launch in order to obtain qualitative information on the stress wave response to the diaphragm pressure and sabot impact loads. Strain gages were located as follows:

a) Stop ring (3 circumferential gages, 120 deg spacing)

b) Launch tube (3 longitudinal gages at 3-1/2, 12, and 16 ft distances from the exit plane)

c) Tube support bracket (1 longitudinal gage on the bracket flange)

4.4.6 Vehicle Structure

The only vehicle structure designed by the silo launch conditions was the skirt in the region of the sabot attachment. Strain gages were installed on the aft skirt at 0 deg and 180 deg to provide an indication of the actual lateral motion and also the magnitude of the axial loads. Furthermore, these gages would indicate whether the sabot aft skirt joint failed prematurely and also the magnitude of the skirt response to sabot separation. Instrumentation provided to measure the flight vibration environment also recorded the vibration environment during silo launch.

4.4.7 Acoustic Overpressure

One important objective of the HiBEX program was to determine the ground acoustic overpressure environment in the immediate vicinity of the launch. The silo blast wave effect on surrounding launch area structure could be an important design criterion for future programs employing this type of launcher and vehicle. Overpressure microphones were placed in the launch area to measure dynamic pressure for both the silo and pad launches. Distances of 1300, 800, 300, 100 ft were chosen to provide an assessment of the pressure distribution. Measurements at 60 ft and two at different elevations at 5 ft were also made during the D-3 launch. Figure 37 shows the instrument locations relative to the silo.

The estimation of the ground environment to permit selection of instrumentation was accomplished by conventional methods, but in most cases required large extrapolations to the HiBEX levels. The rocket noise environment was scaled from abundant information on large capacity, low burning rate, long time duration rocket motors. The silo blast wave data were scaled from theory using the silo blast as a potential of high pressure gas escaping, and propagating as an explosive wave. The rocket noise environment was superimposed on the classical blast wave shape. Peak estimated and measured pressures are compared in Section 5.4.

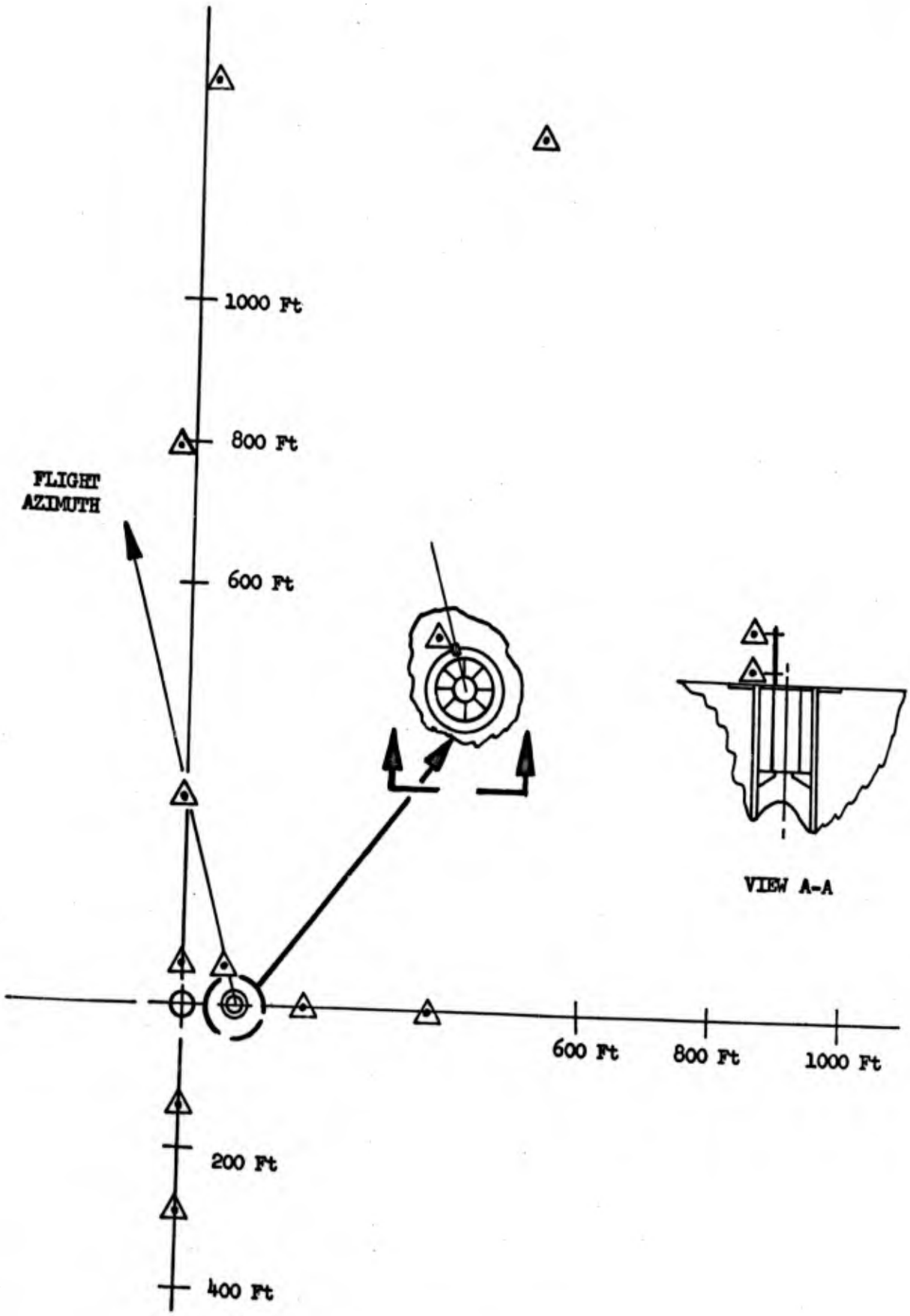

FIGURE 37 - ACOUSTIC OVERPRESSURE TRANSDUCER LOCATIONS

5.0 TEST RESULTS

This section contains a discussion of the data obtained during the silo launch portion of the HiBEX D-2[3] and D-3[4] flights. Measured values of various parameters are compared with theoretical values to evaluate the adequacy of the analytical methods employed in designing the HiBEX vehicle and silo launcher.

5.1 SILO ENVIRONMENT

The silo launch environment was measured during both the D-2 and D-3 launches. Silo total heating rates, radiant heating rates and pressures were measured on the silo walls at several locations during both launches.

5.1.1 Silo Heating Rates

Two heat transfer mechanisms were in operation in the silo during launch. These were forced convection resulting from the flow of hot rocket exhaust gases and radiation from the cloud of solid and/or liquid aluminum oxide and zirconium oxide particles suspended in the exhaust gases. The total heating rate is the sum of these two components and was the value measured by the calorimeters.

The heating rates to the silo and launch tube walls were quite severe. Because the time of exposure was very short, the total heat transferred to the walls was small. Heating rate instrumentation for the HiBEX silo launches was described in paragraph 4.4.1.

In the theoretical model, it was assumed that the exhaust gases and air in the silo would be subjected to an instantaneous complete mixing. This assumption was required in the development of the mathematical model. The results of the D-2 and D-3 launches indicate that complete mixing of gases was not achieved, especially in the annular region between the silo and launch tube walls. This did not have a significant effect upon the pressure distribution within the silo, but it did have an appreciable effect upon the convective and radiant heating rate distributions in the silo. The effect of the incomplete mixing on the total heating rate distribution is shown in Figure 38. An examination of the radiant heat transfer data discussed later also indicates incomplete mixing.

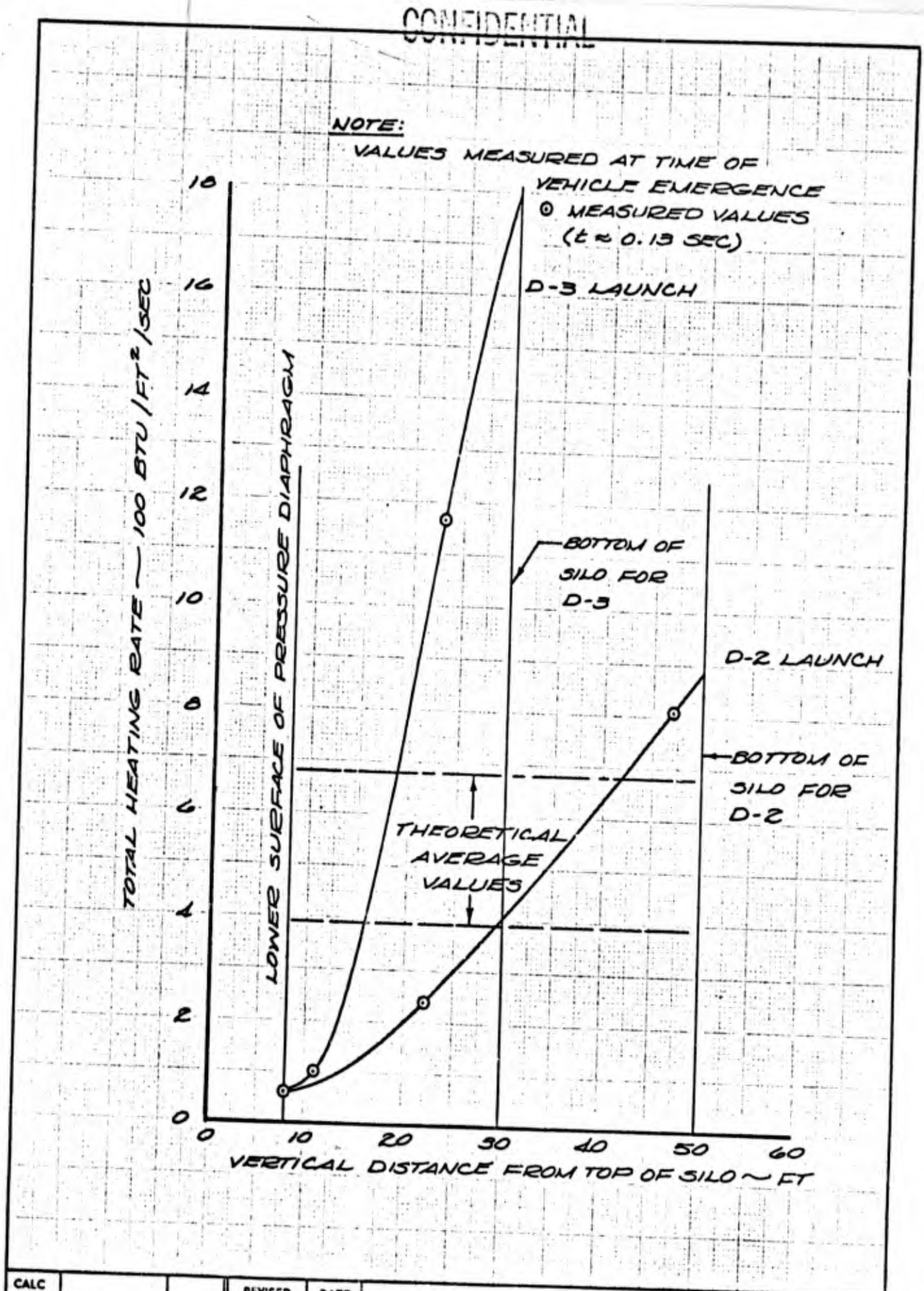

CALC			REVISED	DATE
CHECK				
APR				
APR				

FIGURE 38
TOTAL HEATING RATE DISTRIBUTIONS IN SILO

D2-99603-1

THE BOEING COMPANY

PAGE 83

TD 461 C-R4

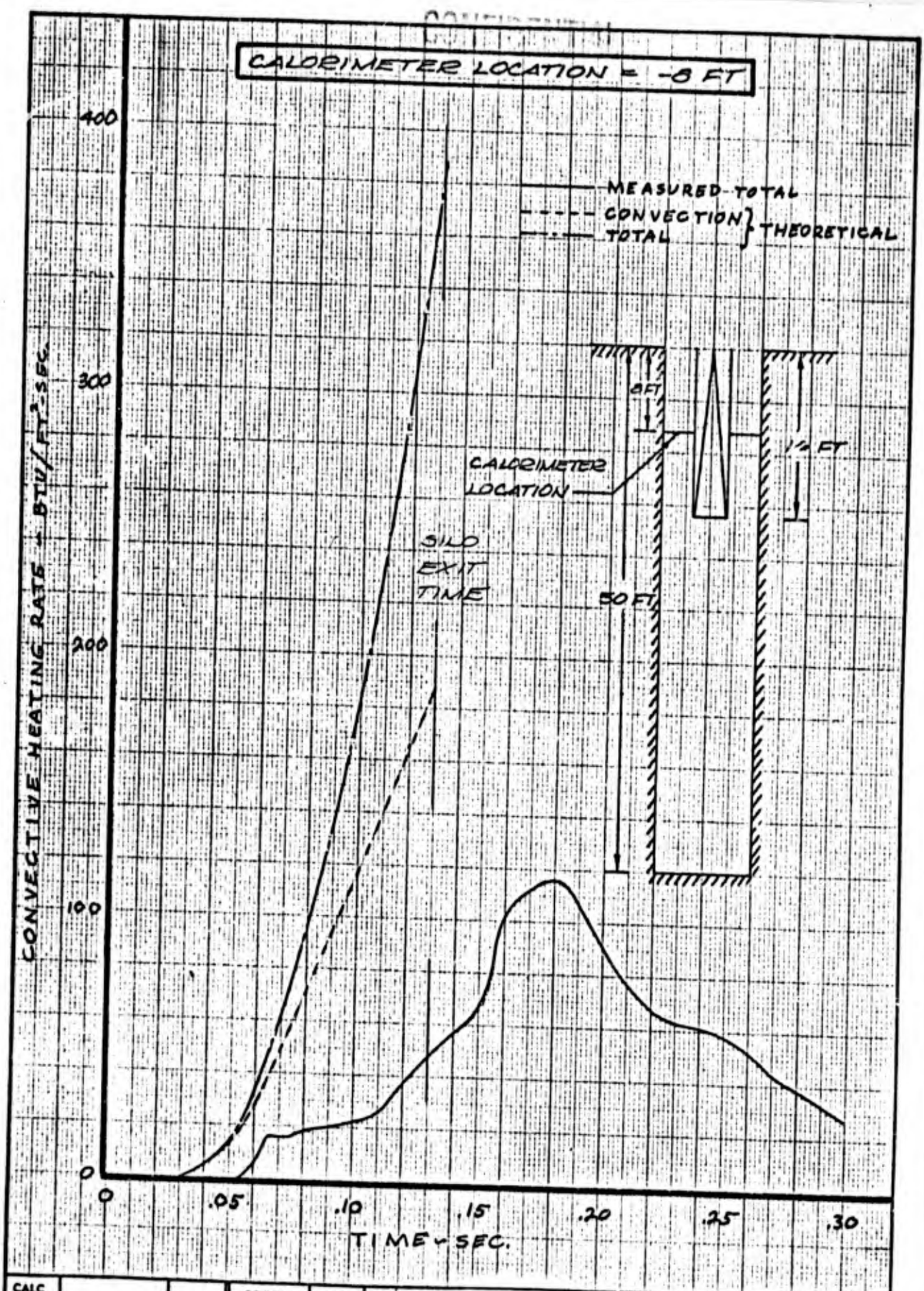

CALC			REVISED	DATE	SILO HEATING RATES DURING LAUNCH D-8. FLIGHT FIGURE 39
CHECK					
APR					
APR					
					THE BOEING COMPANY

D2-99503-1

PAGE 84

TD 461 C-R4

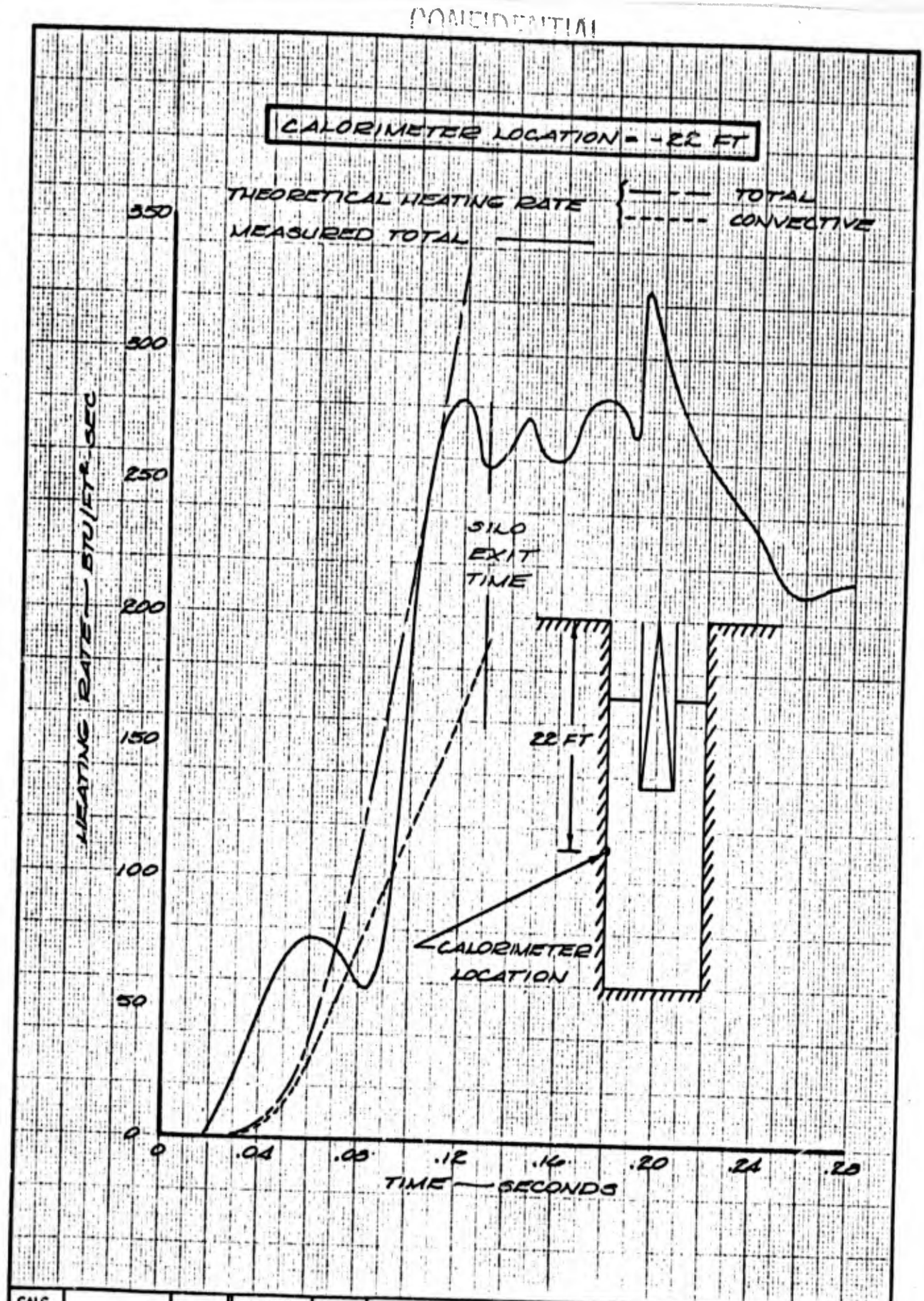

CALC			REVISED	DATE	SILO HEATING RATES DURING LAUNCH D-2 FLIGHT FIGURE 40
CHECK					
APR					
APR					
					THE BOEING COMPANY

D2-99603-1

PAGE 85

TD 441 C-R4

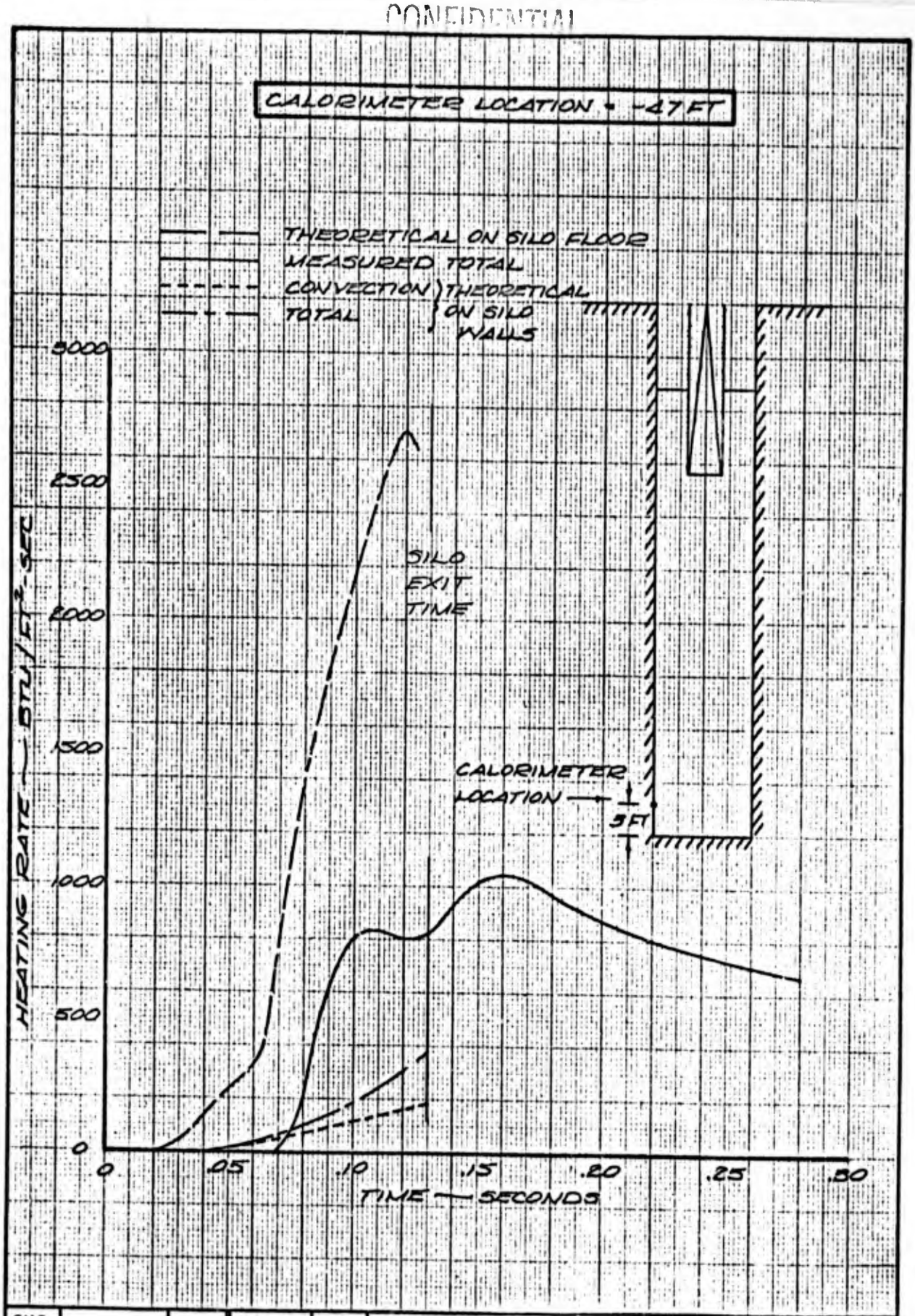

CALC			REVISED	DATE	SILO HEATING RATES DURING LAUNCH D-2 FLIGHT FIGURE 41	
CHECK						
APR						D2-99503-1
APR					THE BOEING COMPANY	PAGE 86

TD 461 C-R4

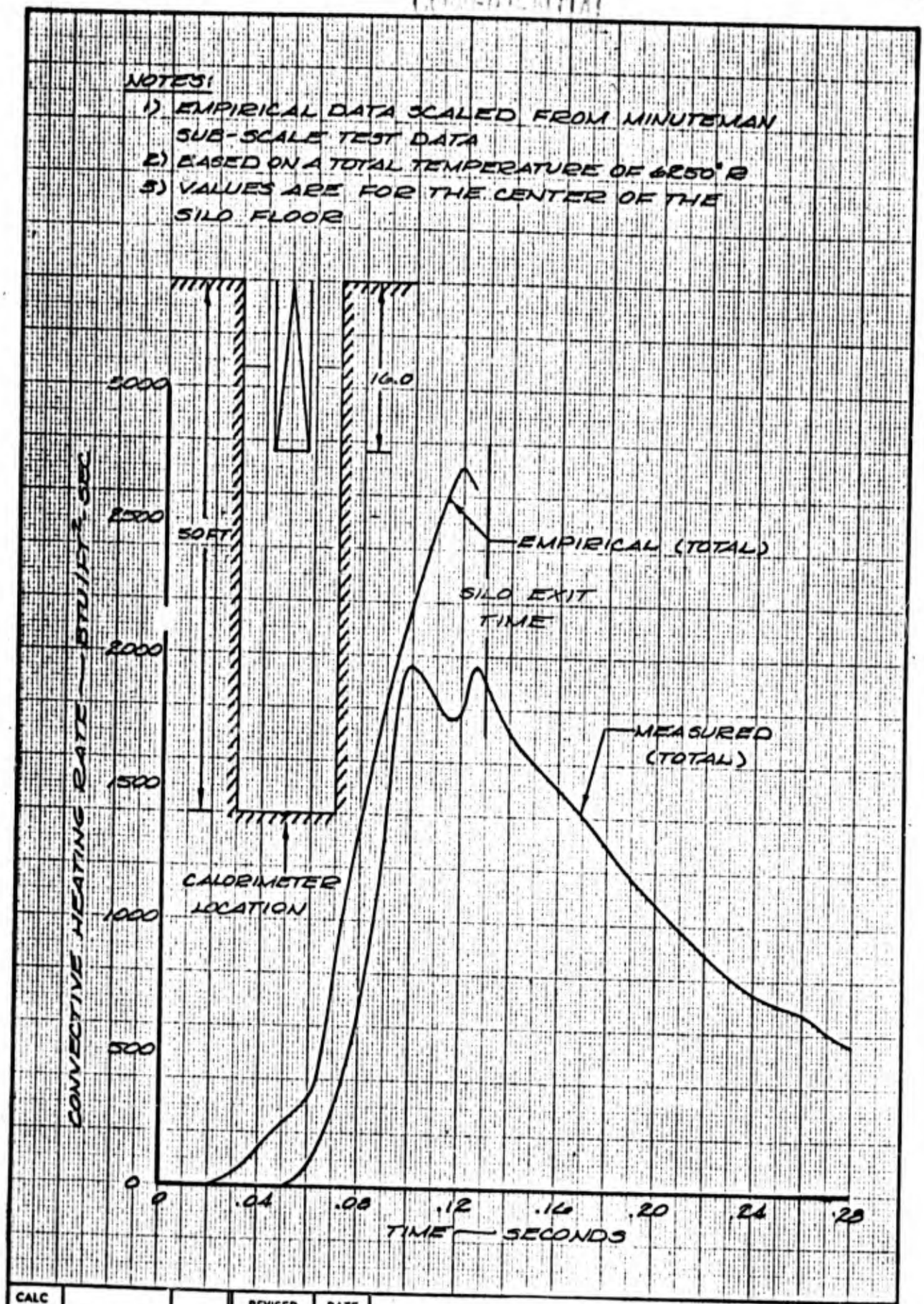

CALC			REVISED	DATE	CONVECTIVE HEATING RATES ON SILO FLOOR DURING LAUNCH D-2 FLIGHT FIGURE 42
CHECK					
APR					
APR					
					THE BOEING COMPANY

D2-99603-1

PAGE 87

TD 461 C-R1

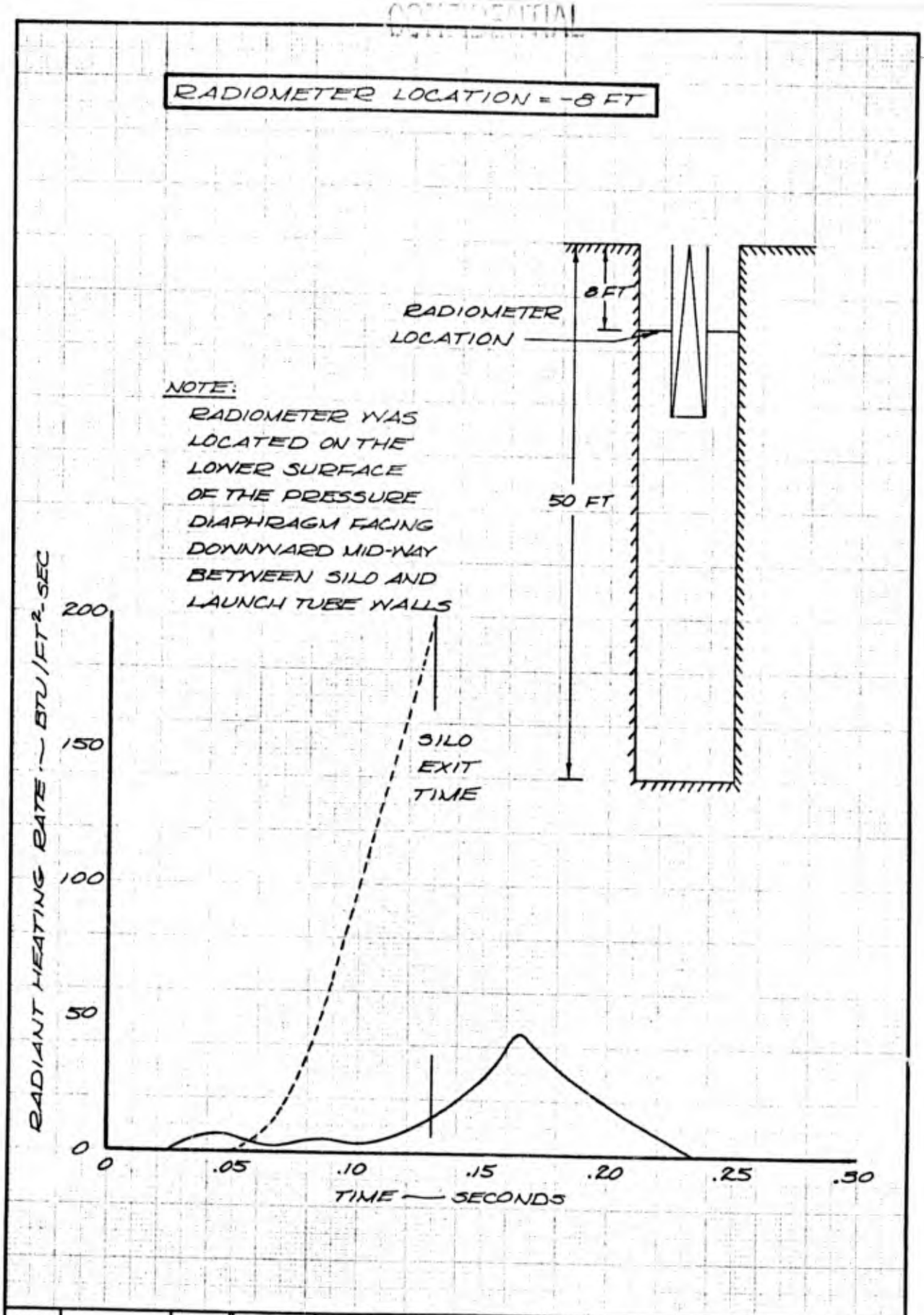

CALC			REVISED	DATE	FIGURE 43 SILO RADIANT HEATING RATES ON PRESSURE DIAPHRAGM DURING LAUNCH, D-2 FLIGHT
CHECK					
APR					D2-99603-1
APR					THE BOEING COMPANY
					PAGE 88

TD 441 C-R4

5.1.1.1 D-2 Launch

The calorimeter at -8 ft was located on the lower surface of the pressure diaphragm midway between the silo and launch tube walls. The total heating rate at this point was substantially lower than the predicted average value in the silo, as shown in Figure 39. This was at least due partly to incomplete mixing of exhaust gases and air in the annular region between the launch tube and the silo since the time available for mixing was so short.

The calorimeter at -22 ft was located on the silo wall 4 ft below the bottom of the launch tube. The close proximity of the launch tube exit and the rocket exhaust gases resulted in total heating rates which were much higher than the measured values on the lower surface of the pressure diaphragm. The measured values at this location were quite close to the theoretical total values. This is shown in Figure 40, where the theoretical convective and total heating rates have both been presented. The dip in the measured total heating rates at 0.08 sec is probably associated with the change in flow that occurred when the rocket exhaust plume became attached to the launch tube.

The measured total heating rate on the silo wall at -47 ft is compared with theoretical values for the silo wall and silo floor in Figure 41. Calculations of the heating rates at this location were not made because of the complex flow pattern where the silo wall meets the floor. It was expected that the heating rates at this location would lie between the silo wall and floor values. The measured values lie much closer to the silo floor values than the wall values while the flow was detached in the launch tube ($0 < t < 0.10$ sec, including instrument lag time). The measured values were closer to the theoretical silo wall values after the time of flow attachment in the launch tube ($t > 0.10$ sec).

The measured total heating rates at the center of the floor of the silo are compared with the predicted values in Figure 42. The predicted (empirical) values were obtained by scaling measured Minuteman exhaust plume date to account for differences in plume geometry, temperature, and composition. No purely theoretical method was available for calculating heating rates on a flat plate when a plume or jet is impinging upon the plate. The agreement between the measured and empirical values is fairly good early in the launch period (up to .10 sec). The disagreement after 0.10 sec is caused by two factors. The vehicle is moving away from the silo floor, which tends to lower the heating rates. Also, the plume geometry changes substantially after the flow becomes attached in the launch tube, and the flow shocks down at a location well above the silo floor. The decrease in heating rate after 0.10 sec is coincident with the decrease in pressure at the center of the silo floor.

The radiometer facing downward on the pressure diaphragm apparently functioned properly, but relatively low radiant heating rates were measured. These values are compared with the theoretical average radiant heating rates within the silo in Figure 43. The radiation was much lower than the predicted average silo values. This is also believed to be due to the incomplete mixing of exhaust gases and initial silo air in the annulus formed by the silo and launch tube

walls, resulting in an average gas temperature in that region which was considerably lower than predicted. This resulted in radiant heating rates much lower than predicted because they are proportional to the fourth power of the gas temperature.

No data were obtained from the radiometer -47-ft level on the silo wall due to improper functioning of the instrument.

5.1.1.2 D-3 Launch

The total heating rates at the -8 ft level, Figure 44, were approximately one-half of the average values in the silo as derived by theoretical analysis. It is believed that this is again due to incomplete mixing of exhaust gases and air in this region, as encountered in the D-2 data.

The calorimeter at -11 ft was located on the silo wall 3 ft below the pressure diaphragm and 7 ft above the bottom of the launch tube. The measured total heating rates shown in Figure 45 for this location were substantially lower than the predicted average values in the silo. They were also lower than the measured values on the lower surface of the pressure diaphragm.

The calorimeter at -23 ft was located on the silo wall 5 ft below the bottom of the launch tube and 7 ft above the silo floor. The total heating rates at this location (see Figure 46) were much higher than the predicted average values on the silo walls. Two factors appear to be responsible for the higher than average values. The first factor is incomplete mixing of the rocket motor exhaust gases at this location. The second factor is the close proximity of the silo floor, which resulted in a flow having a velocity vector component normal to the wall. This effect significantly increases heating rates.

The measured total heating rates at the center of the silo floor are compared with the empirical values in Figure 47. The empirical values were obtained in the same manner as they were for the D-2 launch. Minutemen exhaust plume data were scaled to account for differences in plume geometry, temperature, and composition. The measured values were somewhat higher than the empirical. This is in contrast to the D-2 test results, where the measured values were somewhat lower than the empirical values. Since the only significant difference between the D-2 and D-3 measurements was the distance from the nozzle exit plane to the calorimeter, it appears that the decay of heating rate with axial distance along the exhaust plume is greater than predicted. The measured heating rates dropped substantially after the vehicle began to move because they are a strong function of the distance from the nozzle exit plane (at t + 0.09 sec., the vehicle had moved about 4 ft).

Also, the plume goemetry changes substantially after the flow becomes attached in the launch tube, and the flow shocks down at a location well above the silo floor. These effects were not accounted for in determining the predicted values.

Both silo radiometers functioned properly during the D-3 launch. The measured radiant heating rates are compared with theoretical values in Figures 48 and 49. The measured radiant heating rates were approximately one-half of the

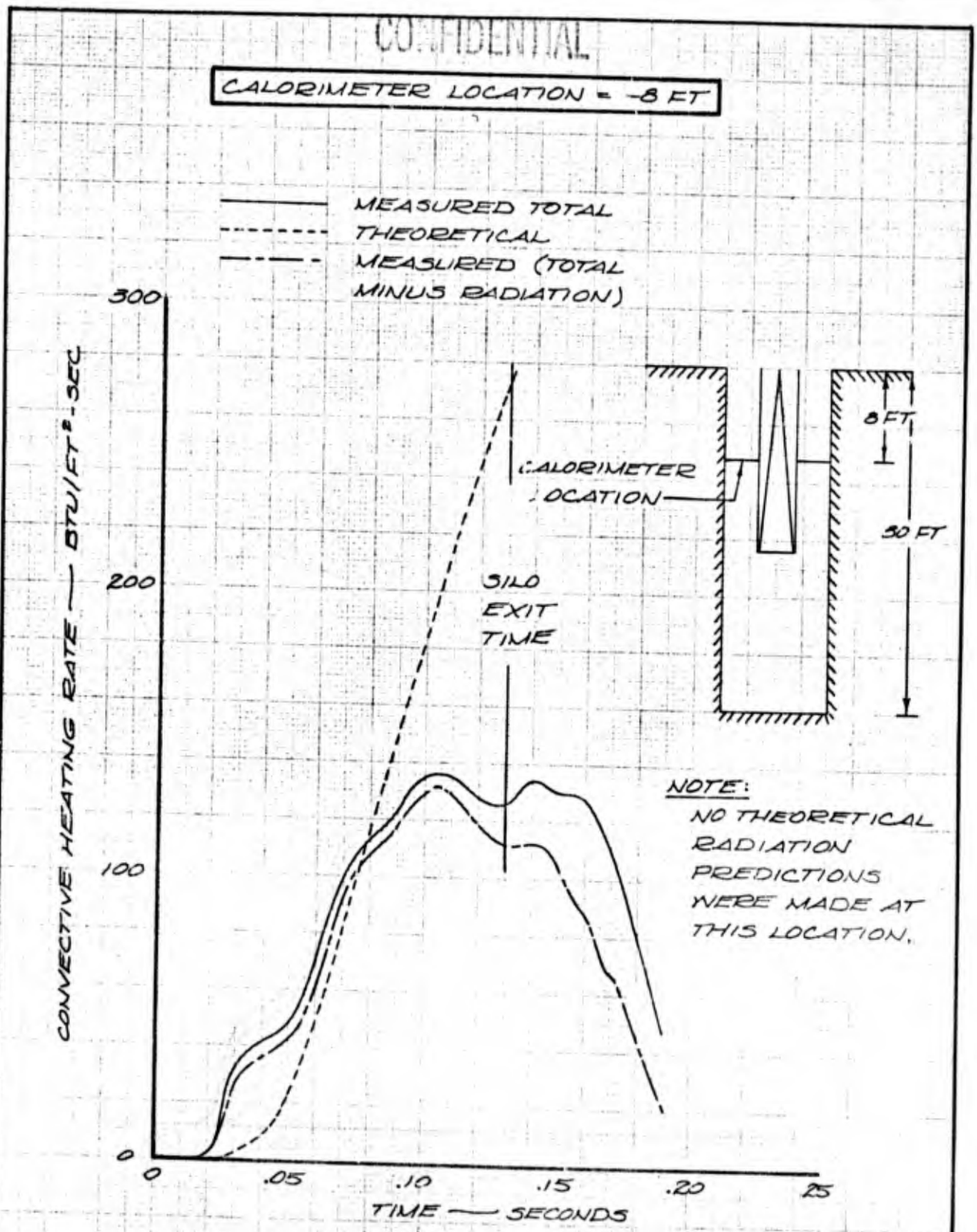

CALC			REVISED	DATE	SILO HEATING RATES DURING LAUNCH D-5 FLIGHT
CHECK					
APR					
APR					
					THE BOEING COMPANY

FIGURE 44 D2-99603-1

PAGE 91

TD 461 C-R4

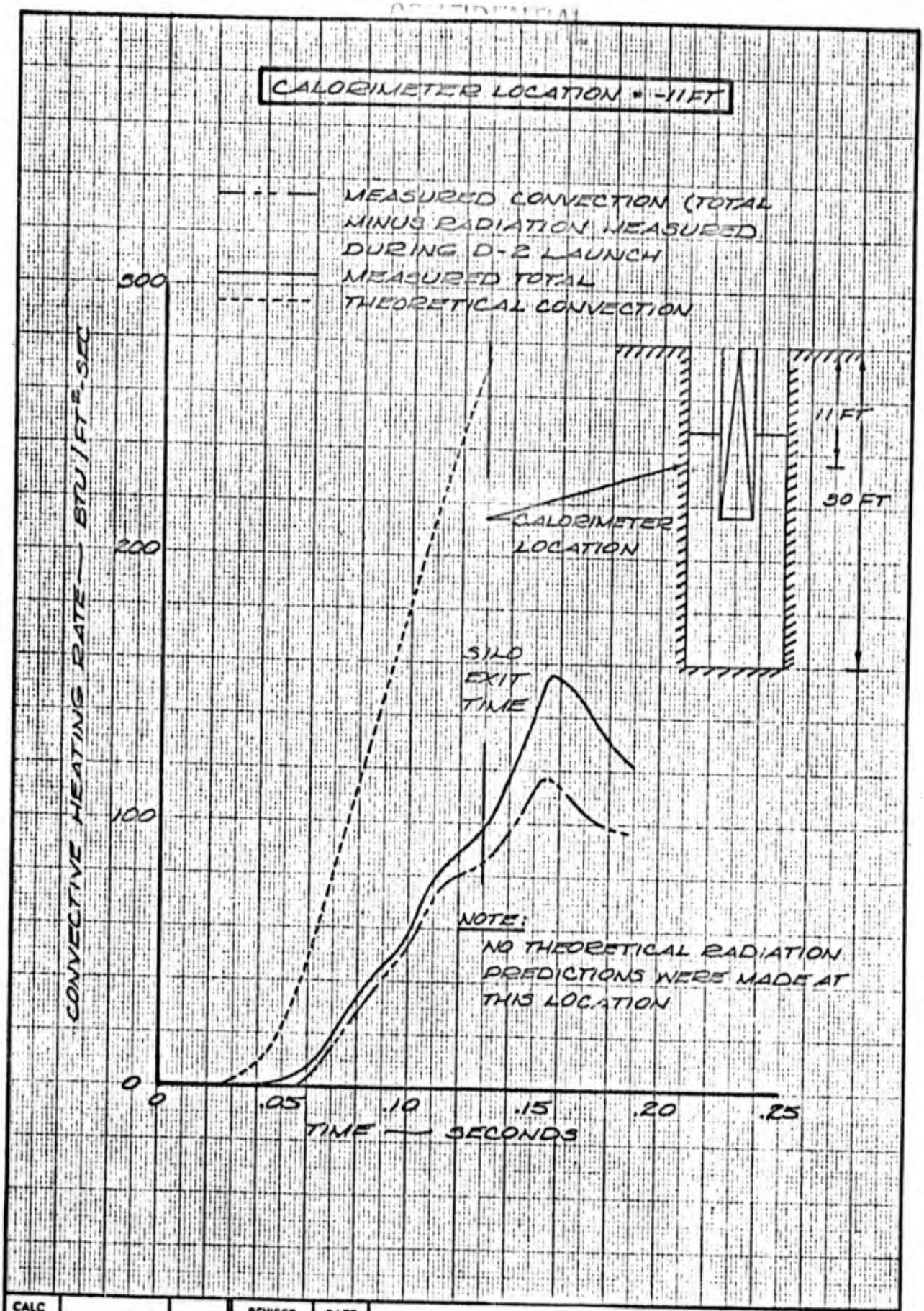

CALC			REVISED	DATE	SILO HEATING RATES DURING LAUNCH — D-3 FLIGHT FIGURE 45
CHECK					
APR					D2-99503-1
APR					THE BOEING COMPANY
					PAGE 92

TD 461 C-R4

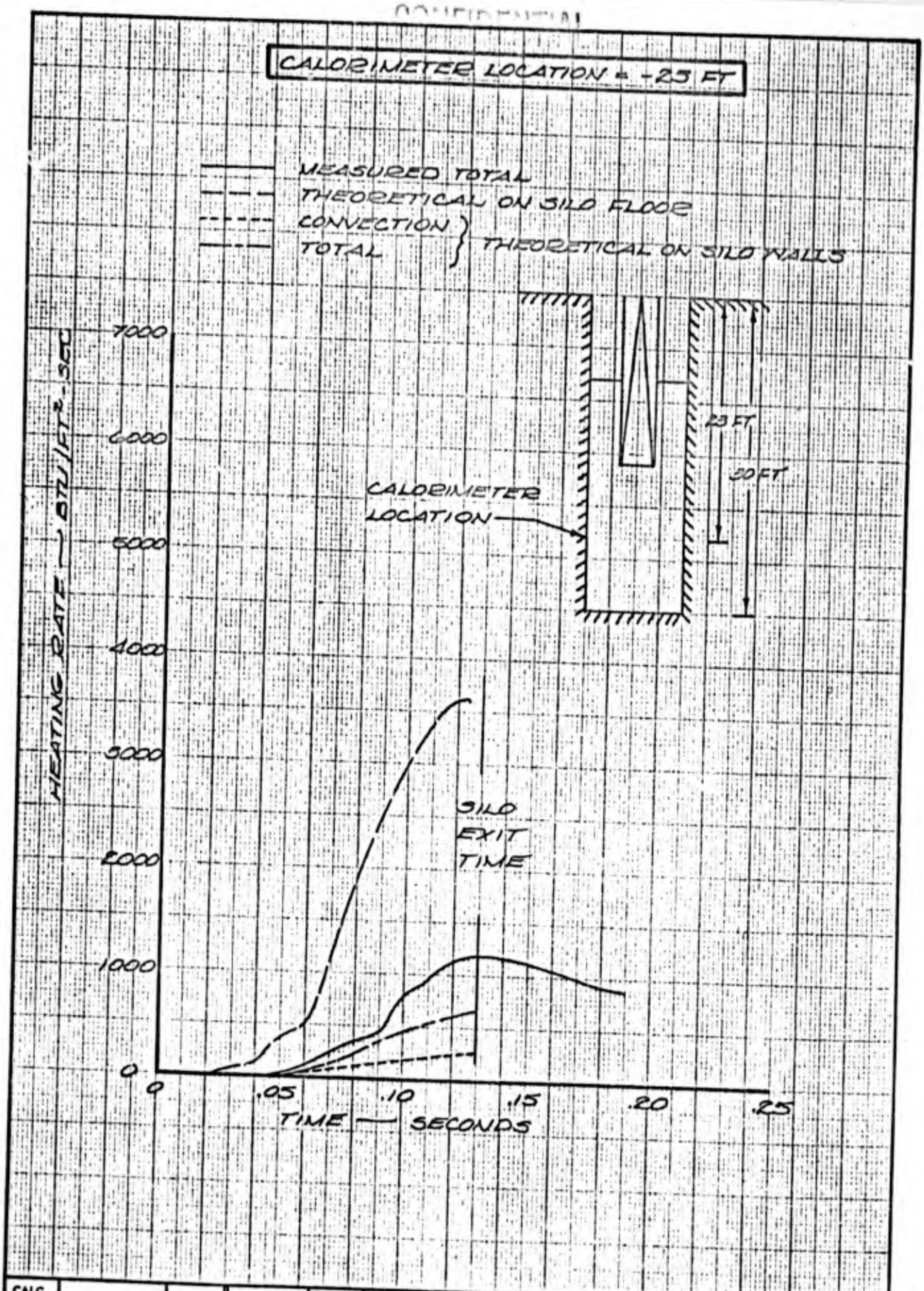

CALC			REVISED	DATE	SILO HEATING RATES DURING LAUNCH — D-3 FLIGHT FIGURE 46
CHECK					
APR					
APR					
					THE BOEING COMPANY

D2-99503-1

PAGE 93

TD 461 C-84

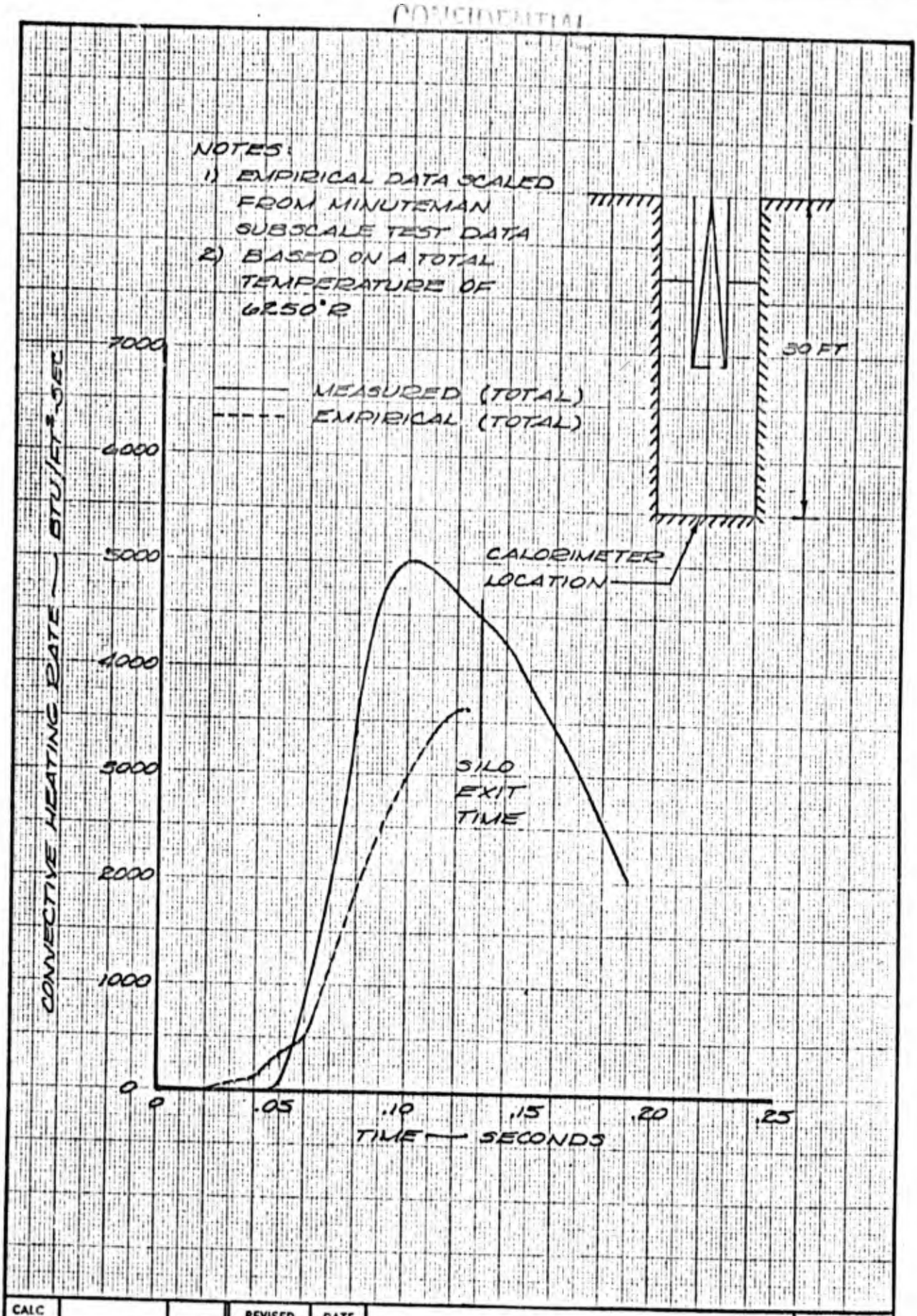

CALC			REVISED	DATE	CONVECTIVE HEATING RATES ON SILO FLOOR DURING LAUNCH — D-3 FLIGHT FIGURE 47
CHECK					
APR					D2-99603-1
APR					THE BOEING COMPANY
					PAGE 94

TD 461 C-R4

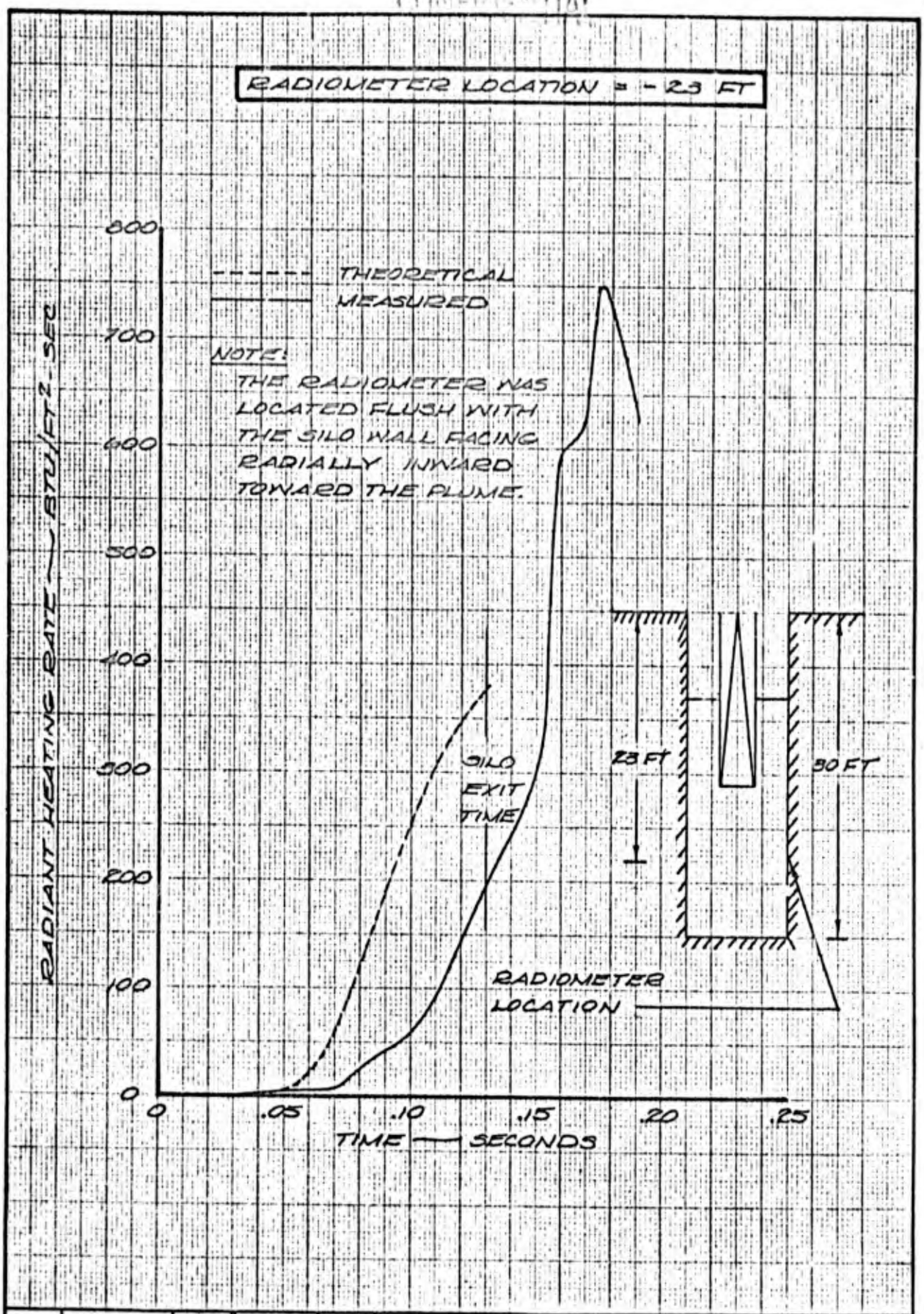

CALC			REVISED	DATE	SILO RADIANT HEATING RATES DURING LAUNCH — D-3 FLIGHT FIGURE 48
CHECK					
APR					D2-99603-1
APR					THE BOEING COMPANY
					PAGE 95

TD 461 C-R4

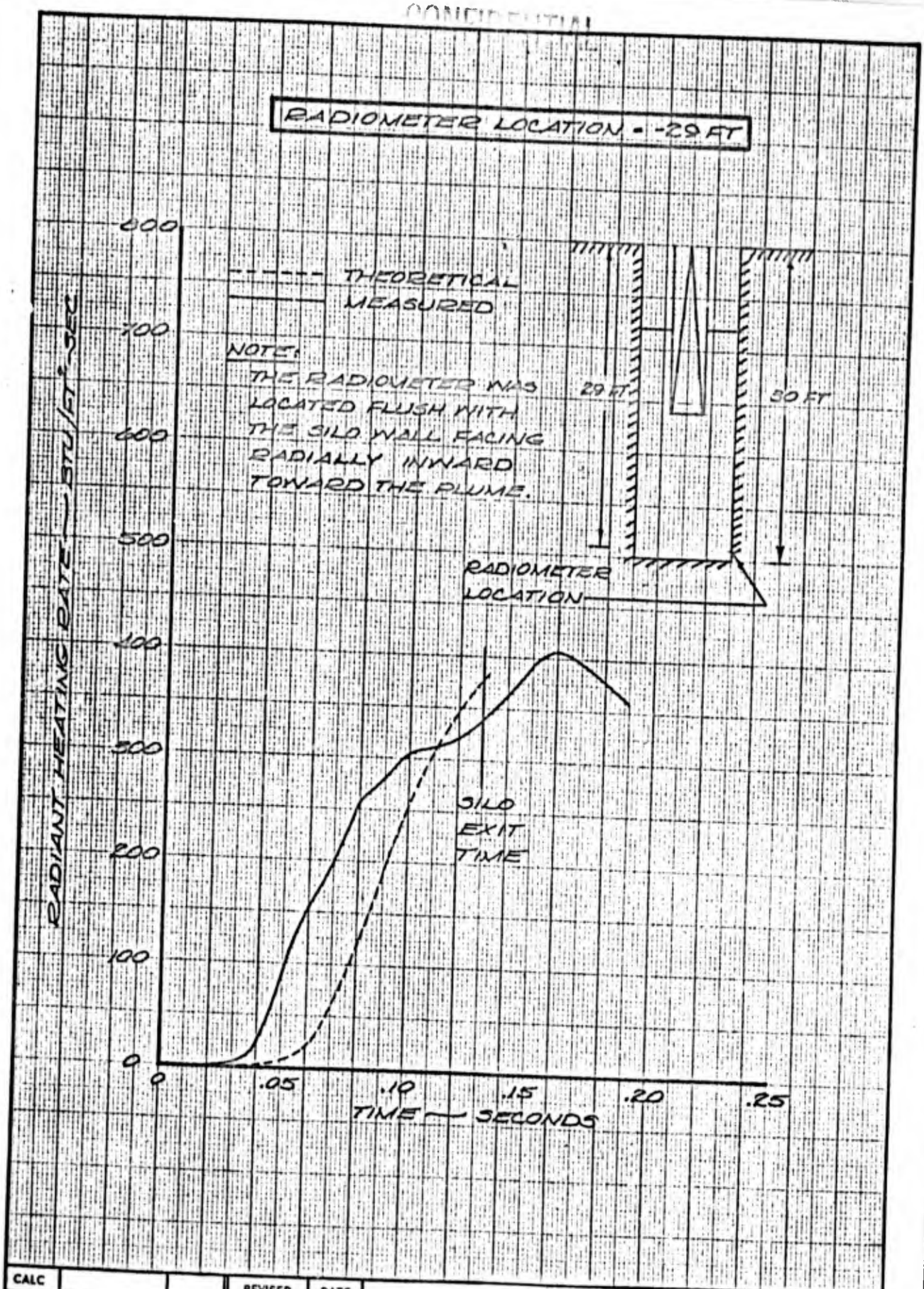

CALC			REVISED	DATE	SILO RADIANT HEATING RATES DURING LAUNCH — D-5 FLIGHT FIGURE 49
CHECK					
APR					
APR					
					THE BOEING COMPANY

D2-99503-1

PAGE 96

TD 441 C-R4

54

theoretical values at the -23 ft level. This would suggest ahat the mean particle temperature at this location was about 450°F lower than predicted when the vehicle left the launch tube, providing the cloud of particles was opaque at this location. In terms of mean particle temperature, this corresponds to a fairly small error (2550 deg R instead of 3000 deg R).

The radiant heating rates at the -29 ft level were higher than the theoretical values until T + 0.11 sec. After that time, the radiant heating rates were slightly lower than the theoretical values. This agreement is fairly good considering the fact that radiant heat transfer is proportional to the fourth power of the particle temperature, which was an estimated quantity in the theoretical analysis.

5.1.2 Silo Pressure

The measured silo pressure histories on the silo walls are shown in Figure 50 for the D-2 launch, and in Figure 51 for the D-3 launch. The calculated average silo pressure based upon the measured rocket motor chamber pressure transients, is shown on the figures for comparison.

The pressure on the silo floor was substantially higher than the pressures on the silo wall during both launches because the silo floor pressure transducer was located in the rocket motor exhaust plume and measured total pressure rather than static pressure. After the silo pressure increased to a sufficient level, the flow in the plume shocked down well above the floor and the pressure on the floor became essentially the same as the average silo pressure.

To obtain silo pressures to compare with calculated values, the values for the three silo wall measurements were averaged. The measured values on the silo floor were not used because of the large dynamic pressure component present. Figure 52 presents a comparison of the average silo pressure and the calculated silo pressure for the D-2 and D-3 launches, based upon D-2 and D-3 rocket motor chamber pressure histories, respectively. For the D-2 launch, the agreement is within 14 percent during the entire launch period and is within 5 percent as the vehicle emerged from the launch tube. For the D-3 launch, the calculated and measured values agree within 13 percent during the entire launch period, and within 6 percent at the time of vehicle exit from the silo. The average silo pressure at vehicle emergence for the D-3 launch was 254 psia, which was approximately 50 percent greater than for the D-2 launch and very near the expected pressure of 260 psia.

Silo pressure decayed slowly after vehicle exit because the driving function was then silo pressure rather than the much higher rocket motor chamber pressure. The silo pressure was approximately 150 psia 0.07 sec after the D-3 vehicle had emerged from the silo, and did not decay to ambient atmospheric pressure for more than a second after vehicle emergence.

5.1.3 Gas Dynamics During Launch

Silo pressure effects and the resultant changes in flow field are of particular interest in a closed breech silo configuration. Forces on the nozzle, sabot and launch tube result from silo pressures which in turn are a result of the interaction of the rocket motor exhaust flow with the increasing silo back pressure.

Shortly after ignition, the chamber pressure rises slightly, the nozzle closure plug is ejected, and a pressure wave moves down the nozzle. Associated with this pressure wave is a normal shock which moves down the nozzle as the rocket motor chamber pressure increases. During the short period of time that the shock wave is in the nozzle, the flow is detached from the nozzle walls downstream of the normal shock wave because of the large pressure difference between the nozzle exit and the silo. After the shock pattern moves out of the nozzle, and into the launch tube, and after the base of the sabot moves

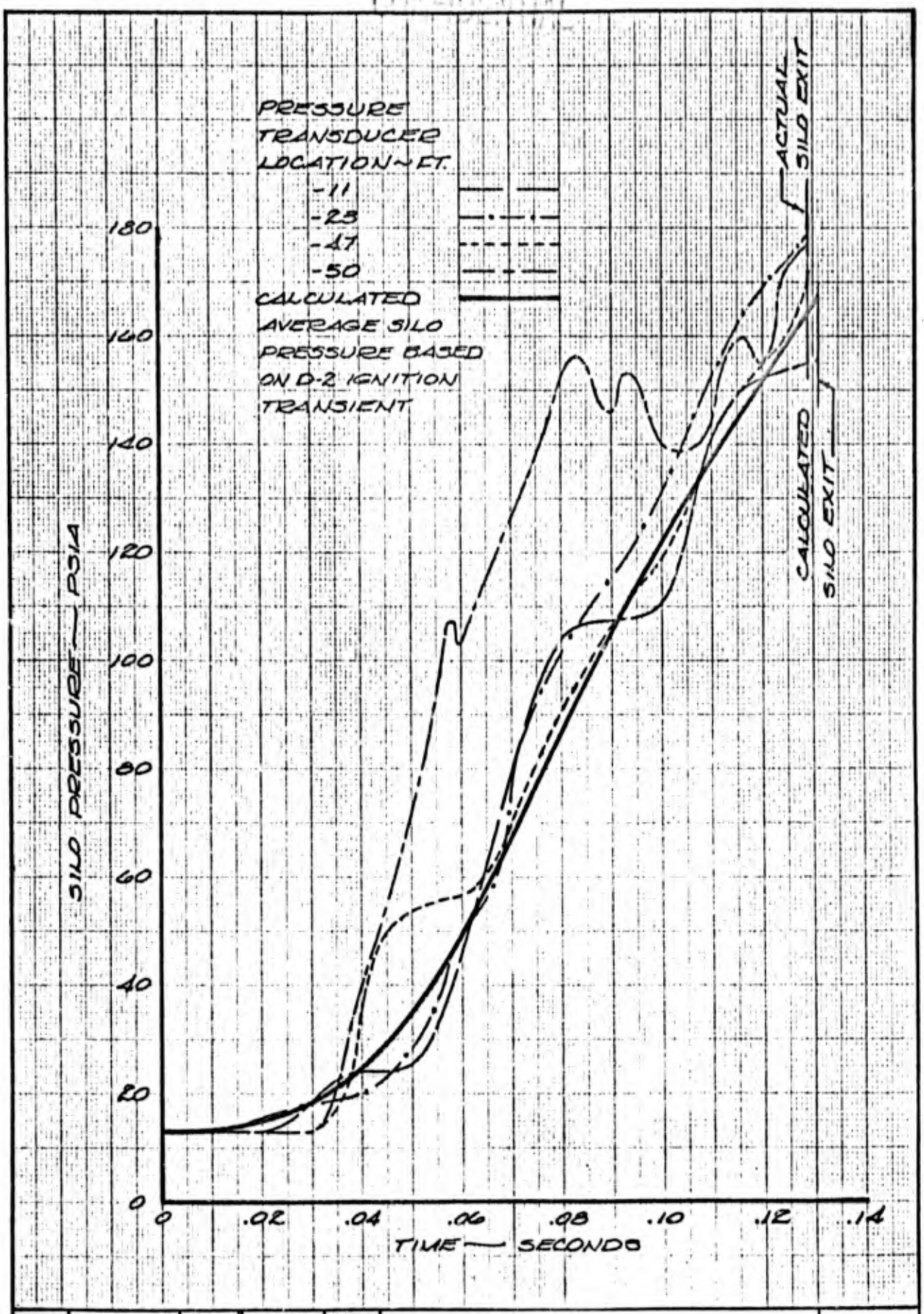

CALC			REVISED	DATE	SILO PRESSURE DURING LAUNCH — D-2 FLIGHT FIGURE 50	
CHECK						D2-99503-1
APR						
APR					THE BOEING COMPANY	PAGE 99

TD 461 C-R4

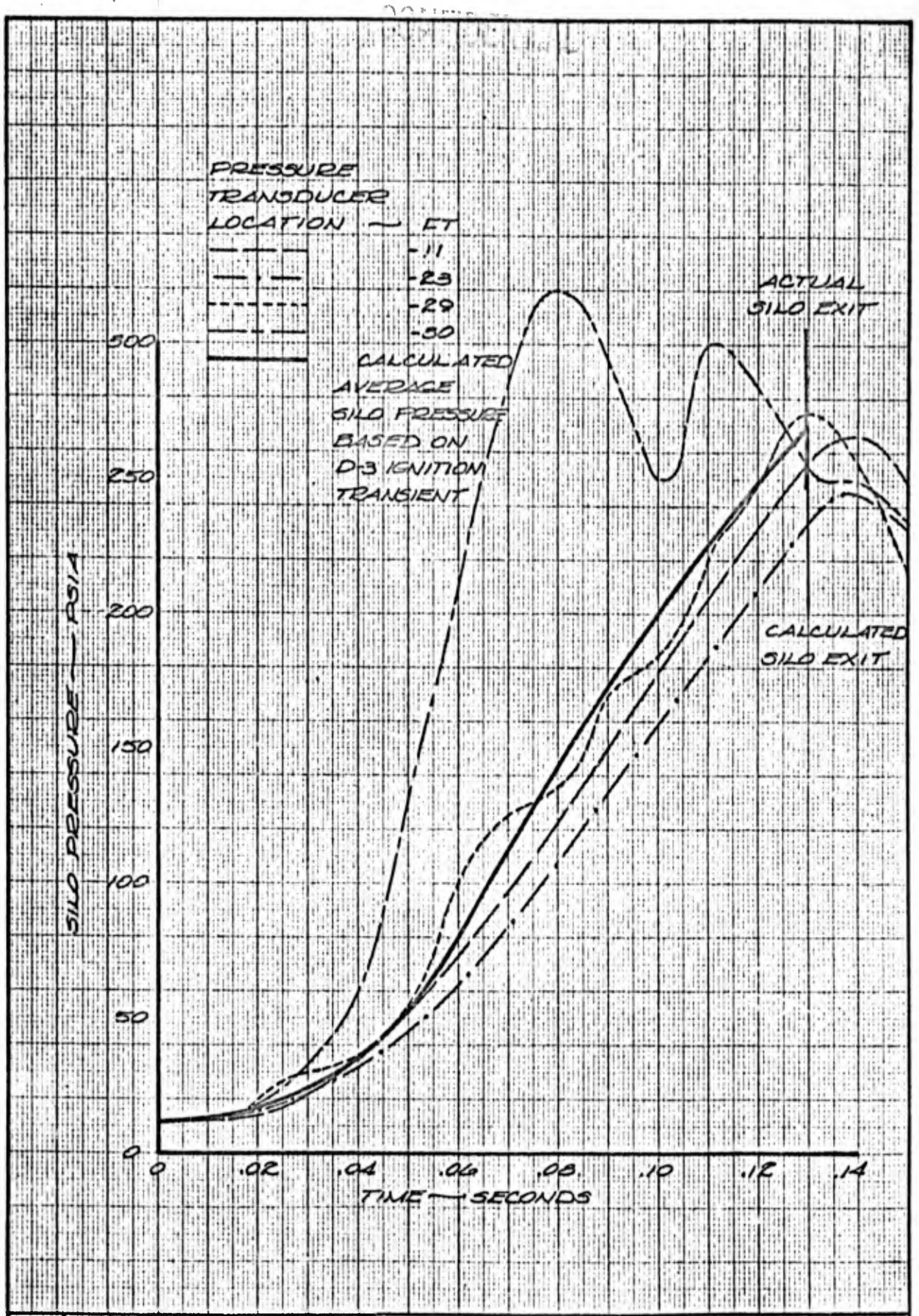

CALC			REVISED	DATE	SILO PRESSURE DURING LAUNCH — D-3 FLIGHT FIGURE 51
CHECK					
APR					02-99603-1
APR					THE BOEING COMPANY PAGE 100

TD 461 C-R4

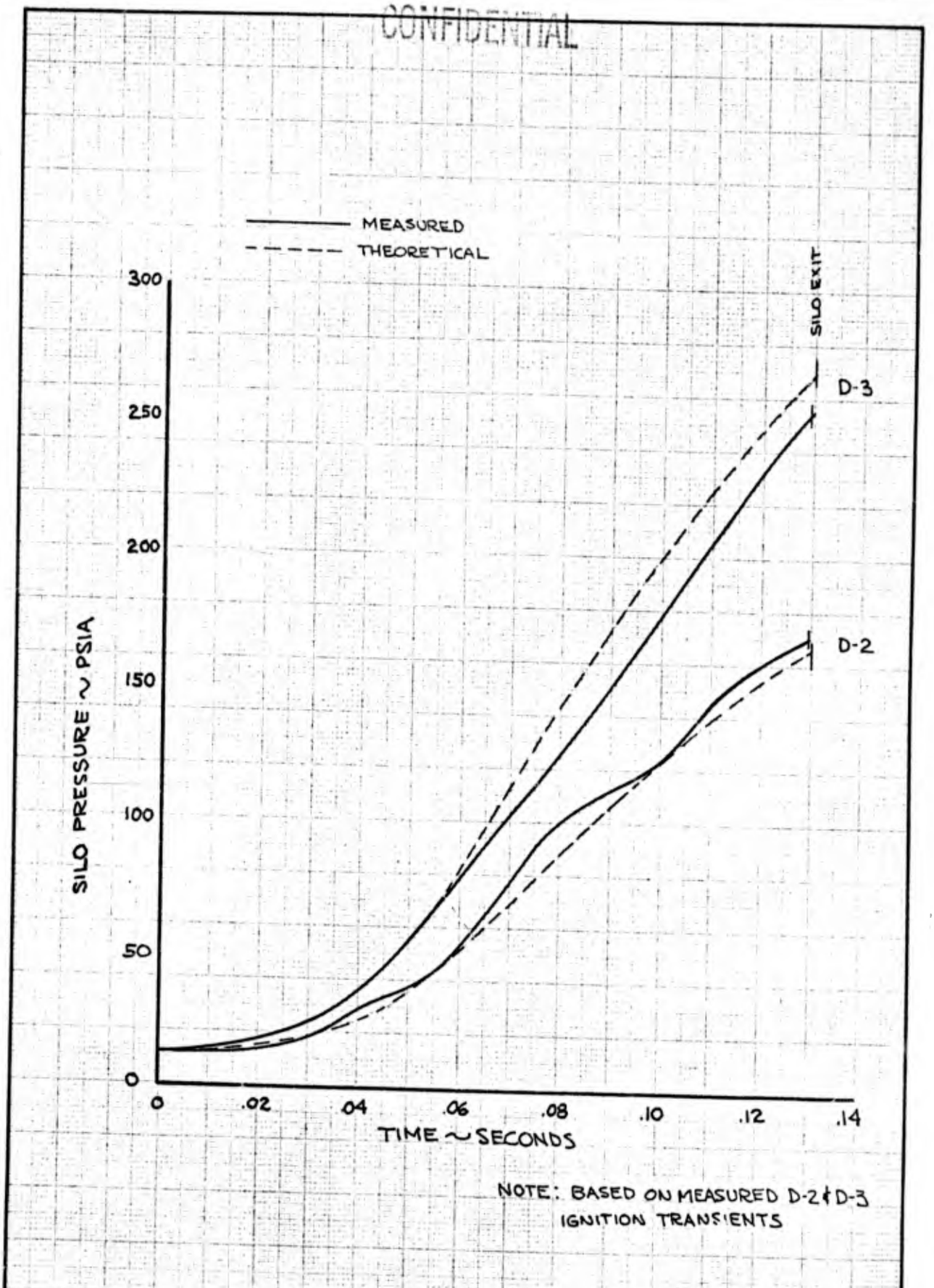

NOTE: BASED ON MEASURED D-2 & D-3 IGNITION TRANSIENTS

CALC			REVISED	DATE	COMPARISON OF MEASURED AND THEORETICAL SILO PRESSURES DURING LAUNCH	
CHECK						
APR						
APR					FIGURE 52	D2-99603-1
					THE BOEING COMPANY	PAGE 101

TD 461 C-R4

ROCKET MOTOR EXHAUST GAS FLOW DURING SILO LAUNCH

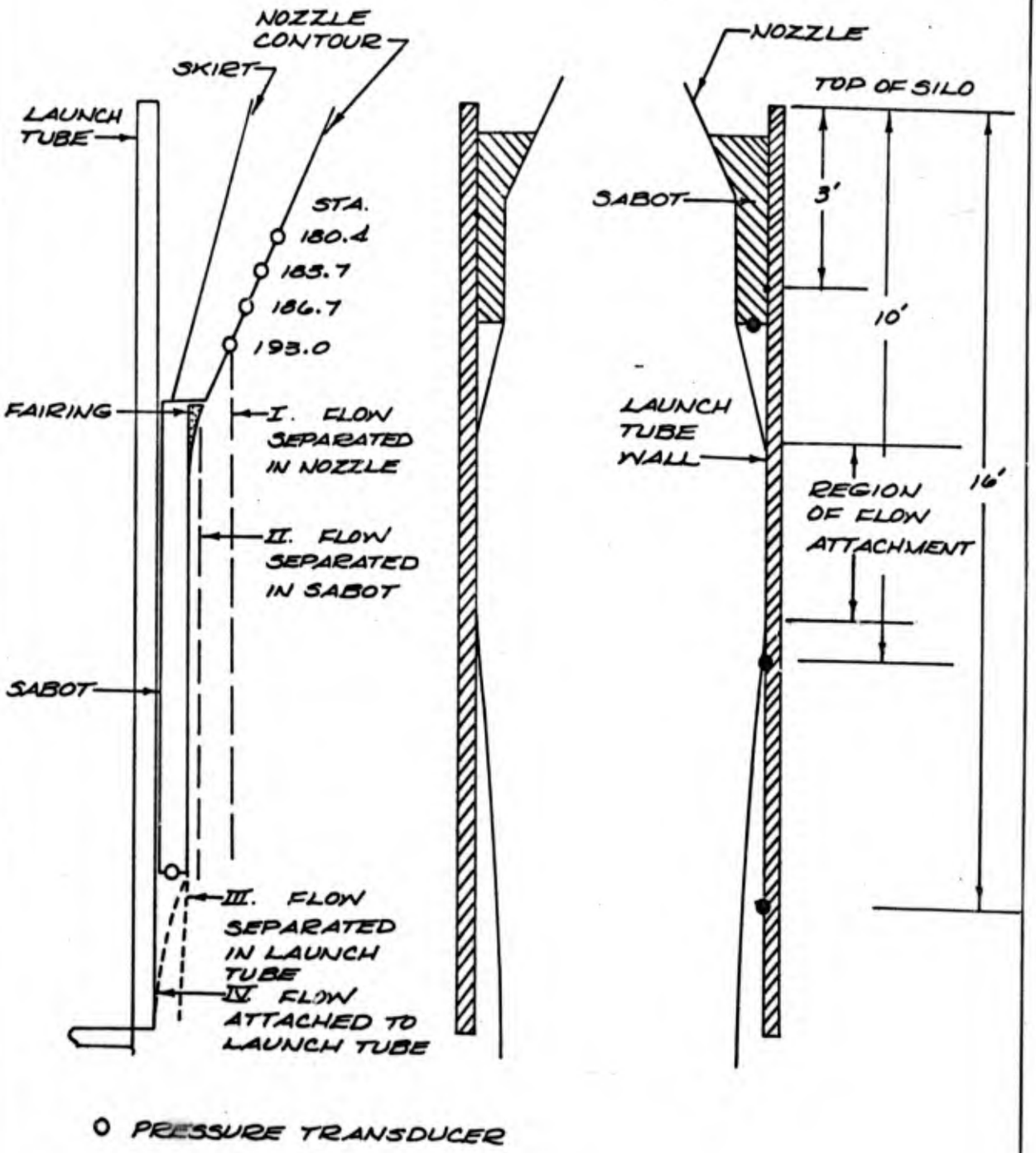

FIGURE 53

a sufficient distance, the flow becomes attached throughout the entire system. The flow is then supersonic in the exhaust plume until it shocks down to subsonic just above the silo floor. As the silo pressure increases, the exhaust plume changes shape (pinches or necks down) and the region of supersonic flow within the plume becomes reduced. A continued increase in silo pressure causes the plume to shock down to subsonic flow a short distance from the launch tube exit plane. Further increases in silo pressure produce flow separation in the launch tube, and eventually in the sabot and rocket nozzle, and a shock wave pattern re-forms in the system at the point of separation.

The nozzle wall, the inner surface of the launch tube, and the silo walls were instrumented with pressure transducers in order to establish the flow field history during the D-2 and D-3 launches.

5.1.3.1 Nozzle Wall Pressure

The nozzle wall pressure transducer locations are shown in the sketch in Figure 53. The nozzle wall pressure histories are shown in Figure 54 at stations 180.4, 183.7, 193.0, and 193.5. The average silo pressure and the pressure on the base of the sabot are shown on the same figure for reference. The nozzle wall pressure data indicate that the shock pattern moved out of the nozzle 20 ms after ignition. After the initial period of flow separation, there was a smooth pressurization transient, and the flow remained attached in the nozzle for the remainder of the launch period.

The agreement of nozzle pressure data at two diametrically opposed locations at station 193 during the D-3 launch is indicative of symmetrical flow in the nozzle. Consequently, the loads on the nozzle were no greater than for a pad launch.

5.1.3.2 Sabot Base Pressure

The sabot base pressure history was difficult to predict because the time of flow detachment could not be predicted accurately. Two sabot base pressure analyses were made. The first analysis was based on the assumption of detached flow in the launch tube during the entire launch period (until the vehicle left the silo). The second analysis was based on the assumption of attached flow in the launch tube during the entire launch period.

A comparison of the measured sabot base pressures (A3P07 and A3P08) and the predicted pressures for the D-2 launch, based on both flow analyses and the measured chamber pressure ignition transient, is shown in Figure 55. The agreement with the detached flow model curve is fairly good until about 0.08 sec. At that time the flow became attached or very close to attached to the launch tube wall and the sabot base pressure began to drop. Pressures corresponding to full flow attachment were not achieved for several milliseconds. The agreement with the theoretical attached flow curve is only fair after attachment occurred. The reason for this is probably the assumption of isentropic flow in the nozzle and sabot in the theoretical analysis.

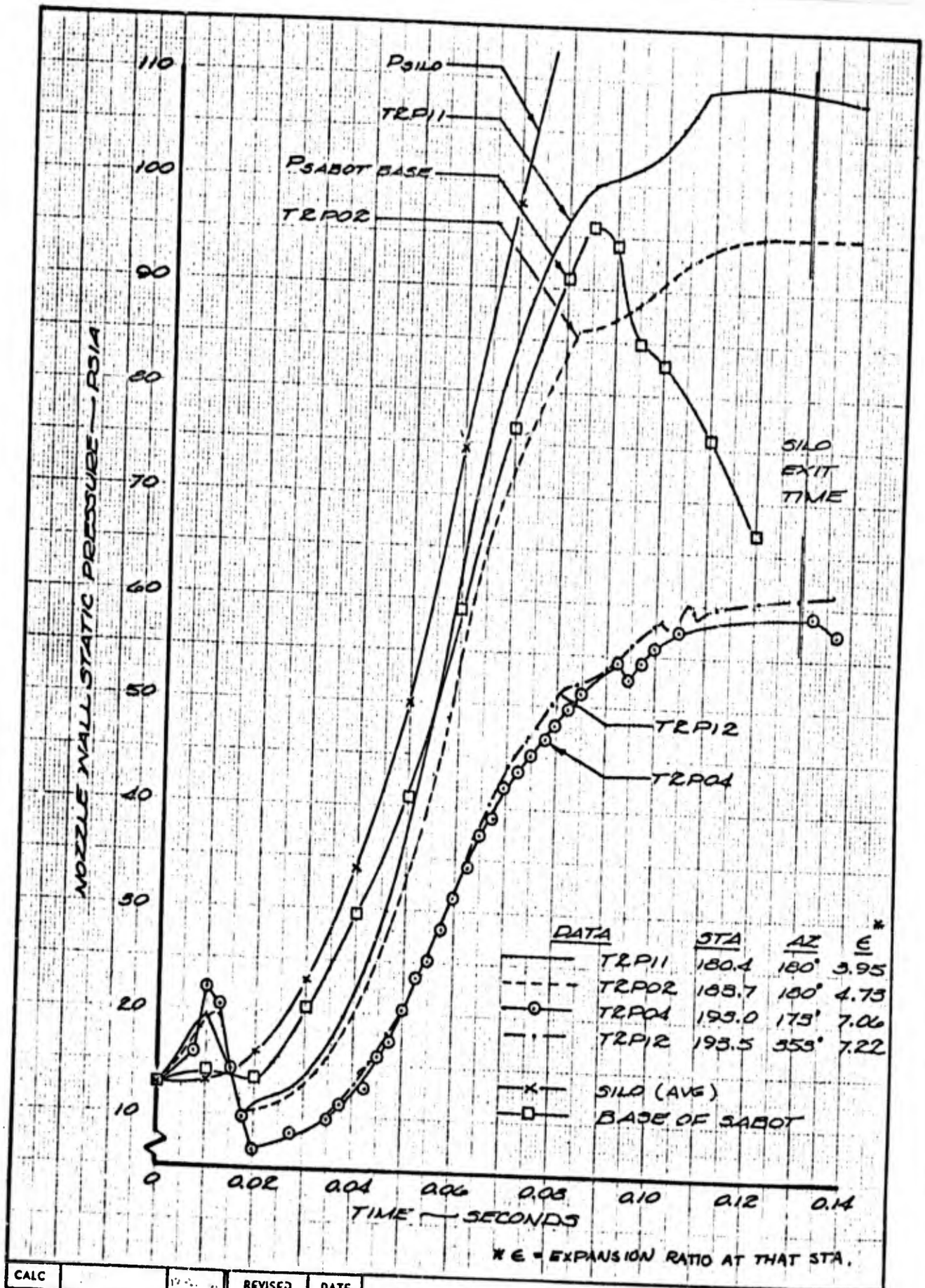

CALC			REVISED	DATE
CHECK				
APR	1			
APR				

NOZZLE WALL PRESSURES DURING IGNITION TRANSIENT
FIGURE 54 D-3 FLIGHT

D2-99603-1

THE BOEING COMPANY

PAGE 104

TD 441 C-R4

CONFIDENTIAL

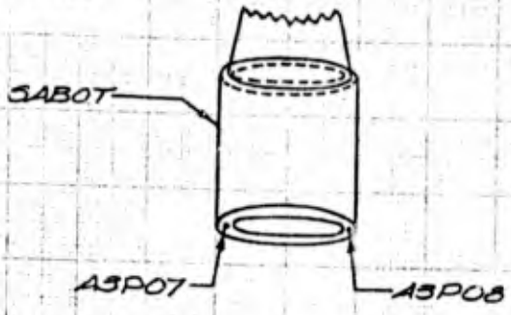

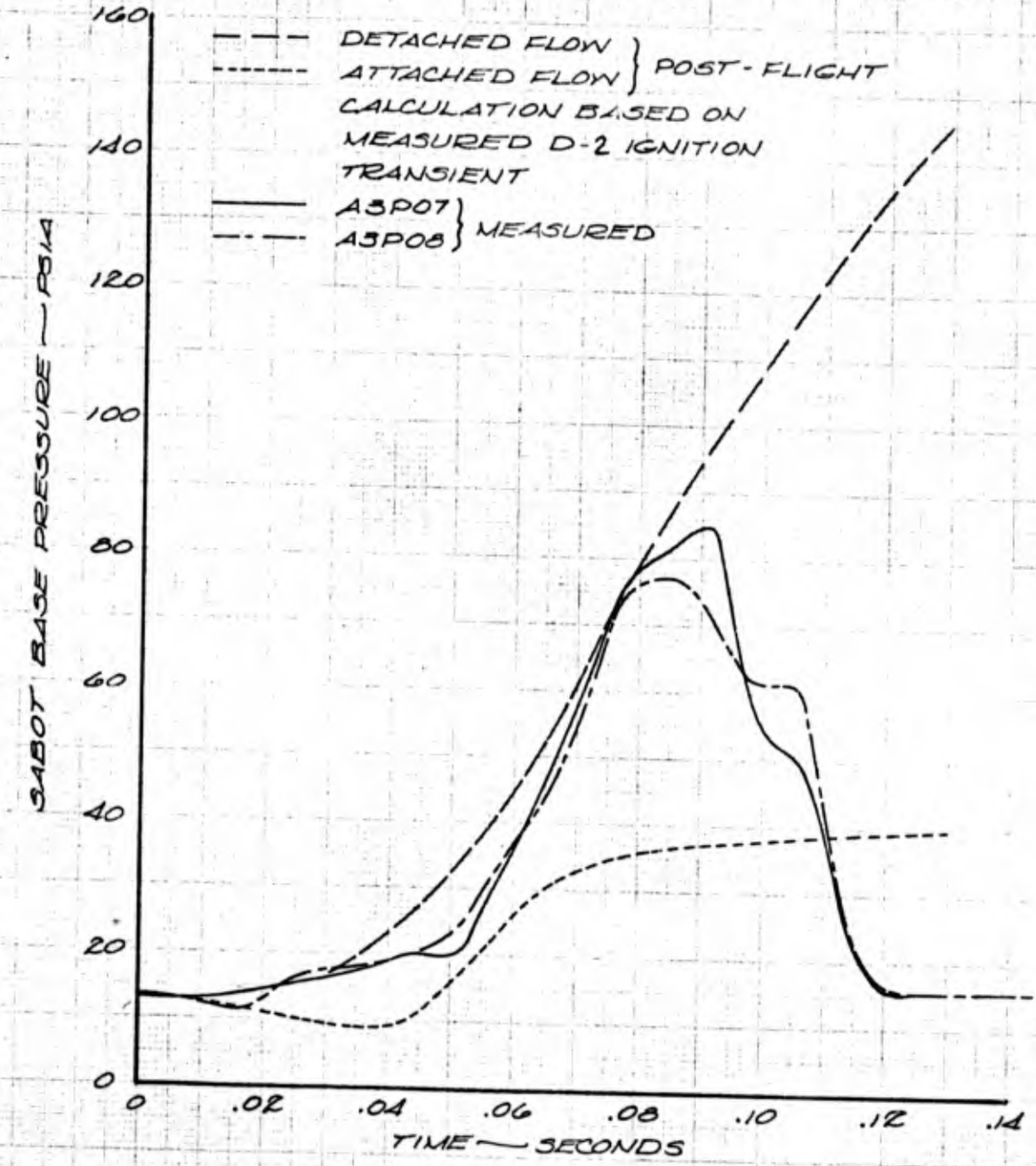

CONFIDENTIAL

CALC			REVISED	DATE	SABOT BASE PRESSURE DURING LAUNCH D-2 FLIGHT FIGURE 55
CHECK					
APR					D2-99603-1
APR					
					THE BOEING COMPANY

TD 461 C-R4

A comparison of the measured and predicted sabot base pressures for the D-3 launch, based on both flow analyses and the measured D-3 chamber pressure ignition transient, is shown in Figure 56. There is reasonable agreement between the measured and calculated detached flow values up to approximately T + 0.085 sec. At that time, the flow became attached to the launch tube wall and the pressure followed a pattern similar to that of the D-2 launch. At T + 0.122 sec, the sabot base pressure began to rise sharply, which is indicative of detachment of flow from the wall of the launch tube near the base of the sabot, just prior to vehicle emergence from the silo.

It appears that launching the HiBEX vehicle from a silo of lesser volume than the D-3 would result in a longer period of flow detachment during which high pressures from the silo plenum would act on the base of the sabot.

5.1.3.3 Launch Tube Wall Pressures

Pressure measurements were made during the D-3 launch on the inner surface of the launch tube at locations 3, 10, and 16 ft below the top of the silo. The pressure transducer at the 3 ft level did not function properly, and no data were obtained at that location. The measured pressures at the other two locations, along with the sabot base pressure and silo pressure, are shown in Figure 57.

At the -16 ft location, the bottom of the sabot passed the pressure orifice at 0.076 sec, and the pressure rose rapidly to a value corresponding to detached flow or near silo plenum pressure. The flow at this location appeared to be detached for most of the launch period after the instrument became exposed to the exhaust flow.

At the -10 ft location, the bottom of the sabot passed the pressure orifice at 0.095 sec, and the pressure rose to the attached flow value of about 40 psia. The pressure remained at that level for about 15 ms, and then rose rapidly to the level corresponding to a region of flow detachment. It can be seen from a comparison of these data and the sabot base pressure data, that the flow became detached at the -10 ft location a few milliseconds before it became detached at the base of the sabot. Therefore, the same conclusion can be made after examining the launch tube pressures as was made after examining the sabot base pressures. A slightly smaller silo volume could have resulted in a longer period of flow detachment, with much higher pressures acting on the base of the sabot.

CONFIDENTIAL

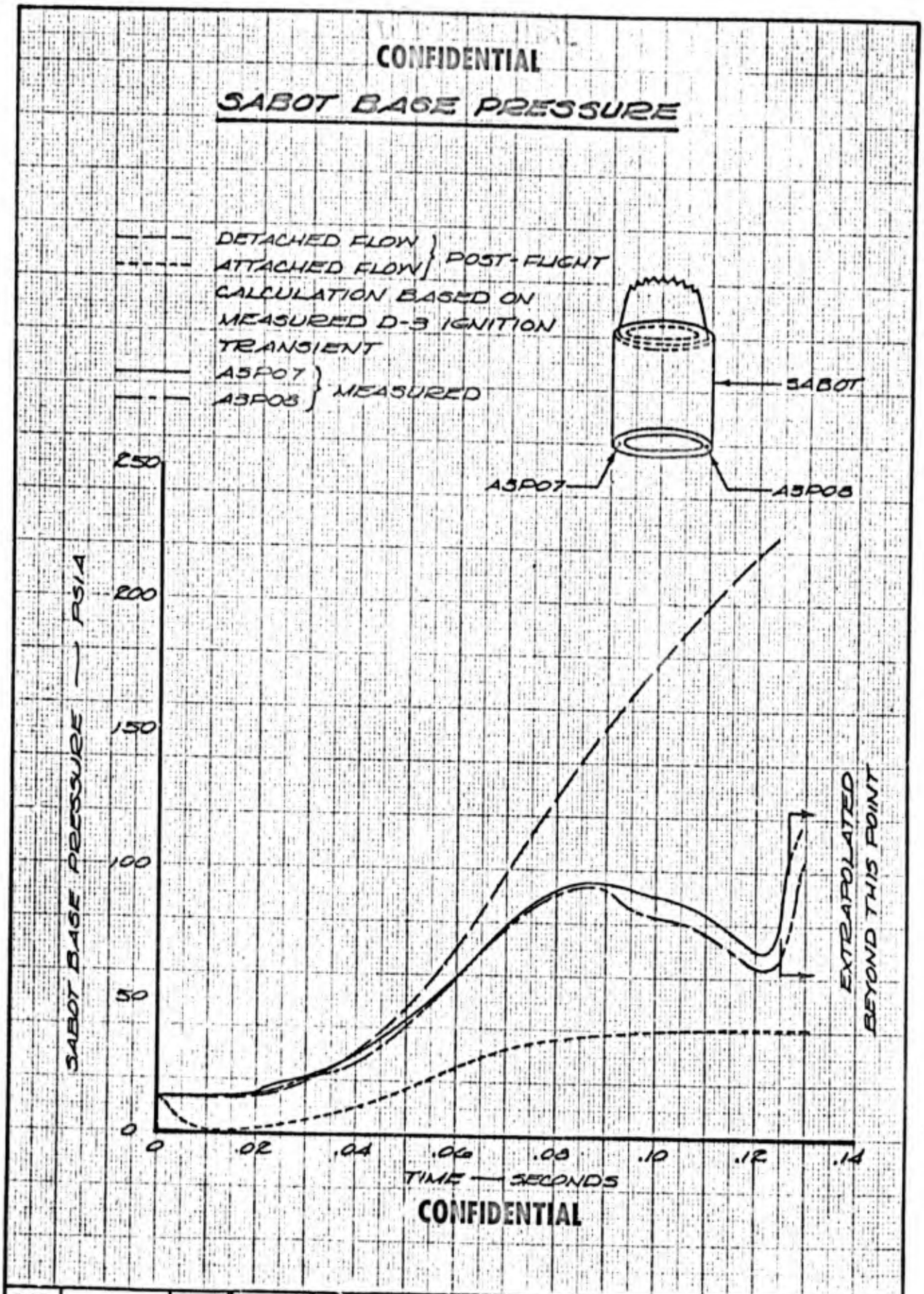

CONFIDENTIAL

CALC			REVISED	DATE	SABOT BASE PRESSURE DURING LAUNCH — D-3 FLIGHT FIGURE 56	D2-99603-1
CHECK						
APR						
APR					THE BOEING COMPANY	PAGE 107

TD 461 C-R4

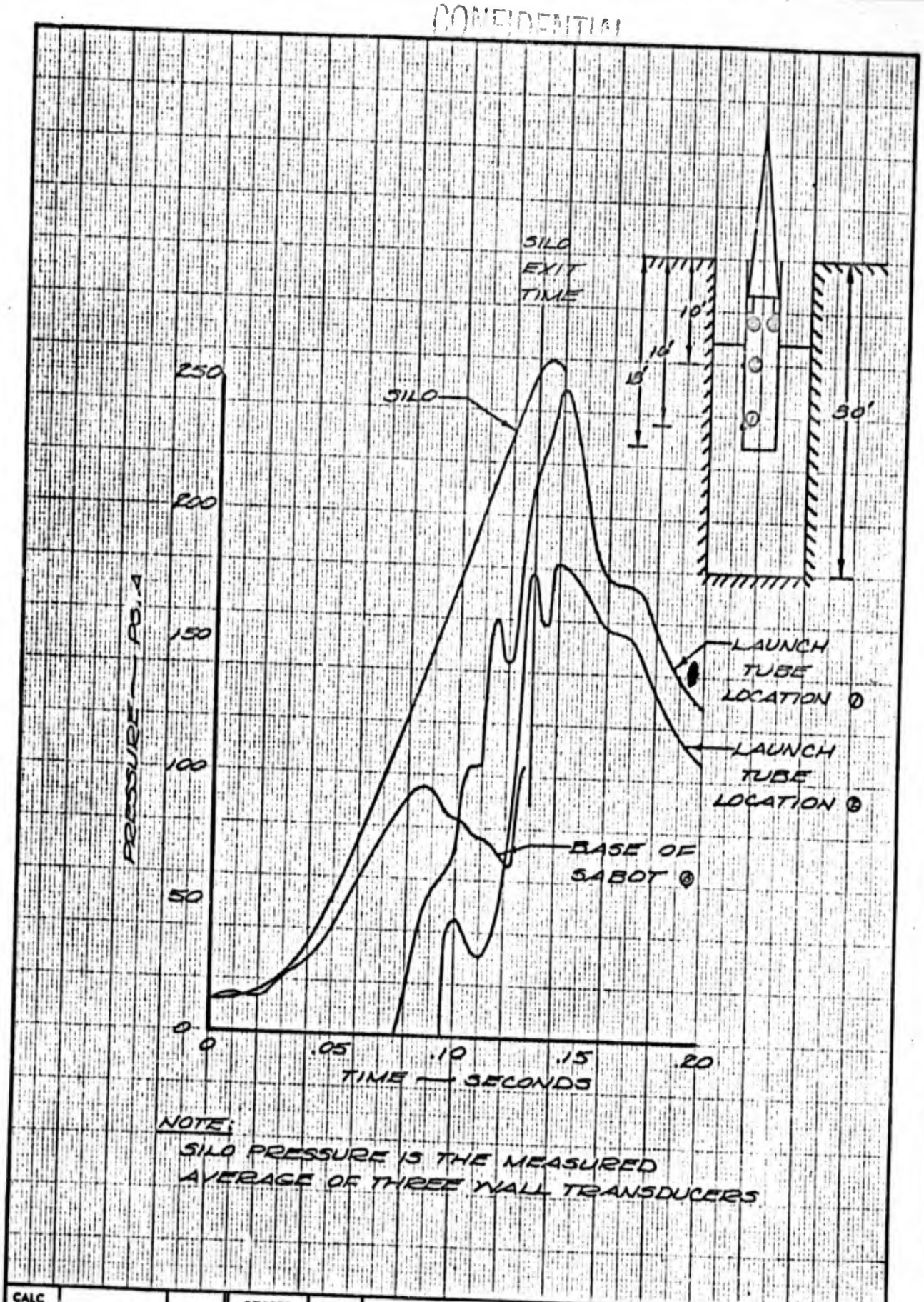

NOTE:
SILO PRESSURE IS THE MEASURED AVERAGE OF THREE WALL TRANSDUCERS

CALC			REVISED	DATE	PRESSURE HISTORIES IN LAUNCH TUBE — D-3 FLIGHT FIGURE 57	D2-99603-1
CHECK						
APR						
APR						
					THE BOEING COMPANY	PAGE 108

TD 461 C-R4

5.2 VEHICLE PERFORMANCE

Launching the HiBEX vehicle from an underground, vertical silo resulted in two distinct effects upon the vehicle performance, namely a slight increase in velocity due to higher than ambient pressures acting on the base of the vehicle and sabot during launch and a loss in vehicle velocity resulting from the delayed initiation of the pitchover maneuver.

5.2.1 Effect of Silo Back Pressure

During the time that the flow was separated in the nozzle and/or launch tube, a pressure approaching the silo plenum pressure acted on the base of the sabot and the separated portion of the nozzle. This back pressure produced a thrust increment which acted upon the vehicle.

The measured vehicle longitudinal acceleration during the D-2 launch is shown on the upper half of Figure 58, along with theoretical values based on two flow models; one based on attached flow in the launch tube, the other based on detached flow (flow fields III and IV, respectively in paragraph 5.1.3). The measured values follow the theoretical detached flow curve until about T + 0.085 sec, which was approximately the time at which the flow became attached to the launch tube wall. After this time the measured acceleration curve tended toward the theoretical curve for attached flow in the launch tube. The over-all agreement between the measured and theoretical values is good. The measured velocity and distance traveled during the D-2 launch are compared with the theoretical values on the lower half of Figure 58. The theoretical silo exit time based on either flow model differs from the measured exit time by less than two milliseconds.

The measured vehicle longitudinal acceleration during the D-3 launch is shown on the upper half of Figure 59, along with calculated values based on detached and attached launch tube gas flow models. The shape of the measured acceleration curve corresponds to that of the calculated detached flow curve until approximately T + 0.085 sec. Near that time, the slope of the measured acceleration curve changes abruptly and generally corresponds to that of the calculated attached flow curve. A slight increase in slope is apparent near T + 0.123 sec which is consistent with indications of flow detachment as indicated by the sabot base pressure measurements.

It was anticipated that the longitudinal acceleration during the D-3 launch would be slightly higher than that of the D-2 launch because of the higher pressures acting on the base of the sabot when exhaust gas flow was separated from the launch tube wall and because separated flow conditions were expected to be of greater duration due to the increased silo pressure over the D-2 test. As noted in the preceding paragraph, attached flow conditions were attained at very near the same time in both tests. However, D-3 did exhibit slightly greater longitudinal acceleration than D-2.

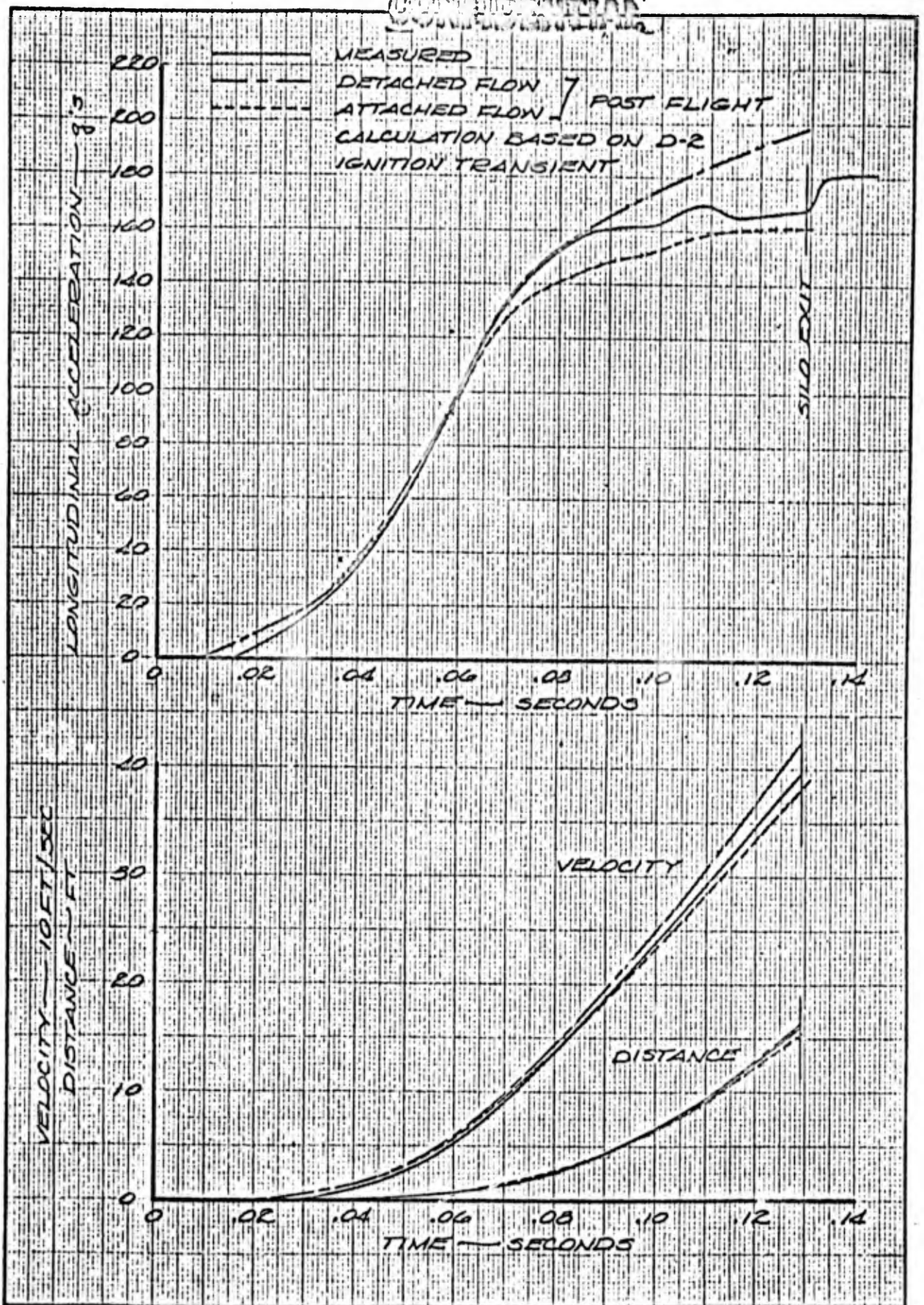

CALC			REVISED	DATE	FIGURE 58 VEHICLE PERFORMANCE DURING LAUNCH D-2 FLIGHT	D2-99603-1
CHECK						
APR						
APR					THE BOEING COMPANY	PAGE 110

ID 441 C-R4

CONFIDENTIAL

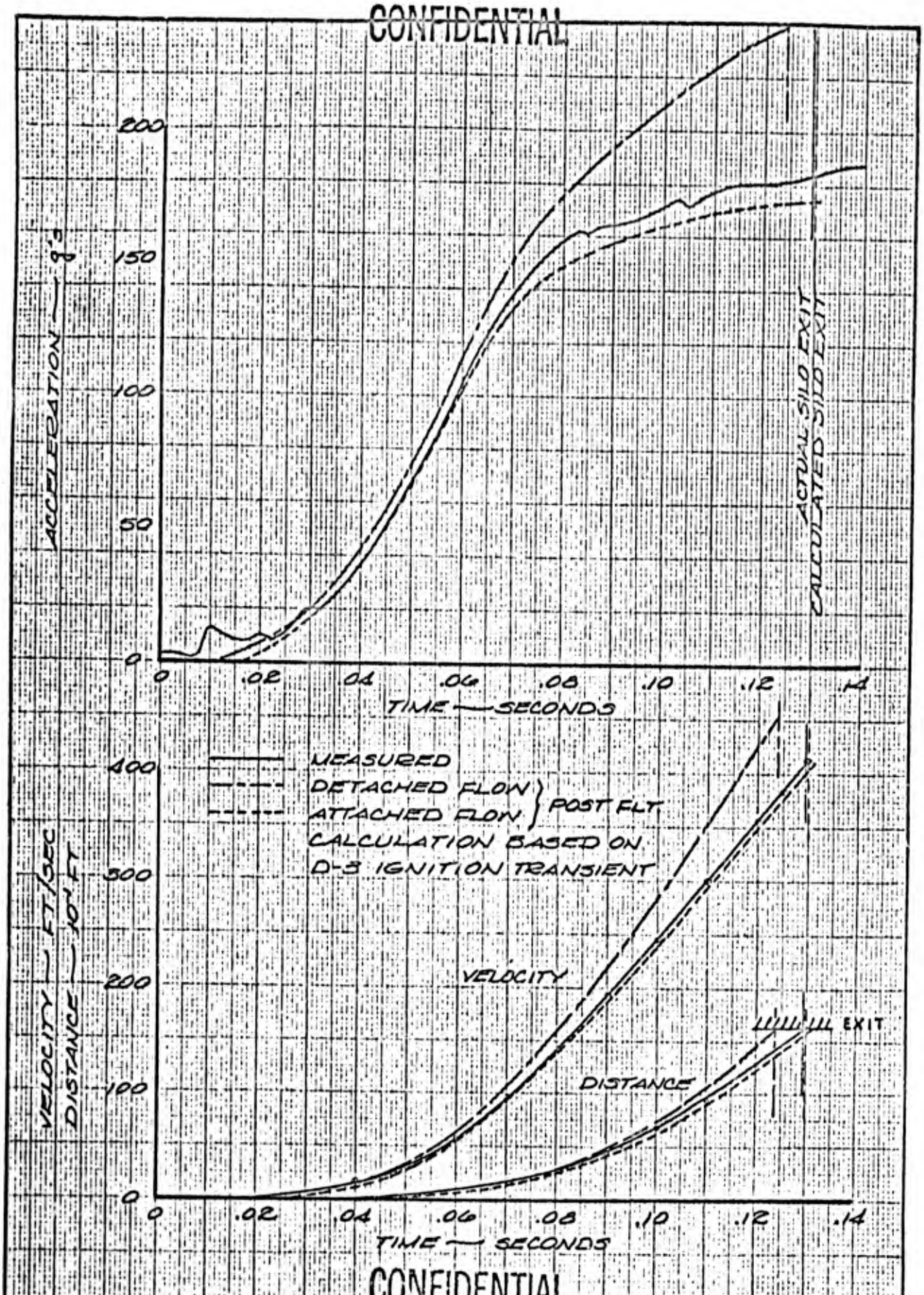

CONFIDENTIAL

CALC			REVISED	DATE	VEHICLE PERFORMANCE DURING LAUNCH — D-3 FLIGHT FIGURE 59	D2-99603-1
CHECK						
APR						
APR					THE BOEING COMPANY	PAGE 111

TD 441 C-R4

5.2.2 Effect of Delayed Pitchover

The vehicle burnout velocity after a pitchover maneuver is very strongly influenced by the time at which the maneuver is initiated since the velocity developed up to the time of pitch-over is not directed along the final trajectory angle. Therefore, initiation of the maneuver at the earliest possible time following silo exit becomes quite important.

Figure 60 shows the increase in velocity losses resulting from increased velocity at maneuver initiation. Separate curves are shown for drag loss and for thrust vector loss which are additive components. The flight weight motor burnout out weight and a vacuum specific impulse of 265 sec are assumed. For a 75 deg pitch over trajectory, the total velocity loss caused by delaying the maneuver initiation to 0.13 sec as compared to zero time is 590 fps.

Some advantage may be taken of known time delays in the vehicle flight control system to initiate the maneuver earlier than was done for HiBEX by an estimated 20 ms. This would reduce the 590 fps velocity loss by 170 fps.

From the above it would appear profitable in any design for application of silo hot launch to HARDPOINT defense to study the trades involving motor ignition transient tailoring, acceleration profile tailoring, time of maneuver initiation, and the over-all mission requirements.

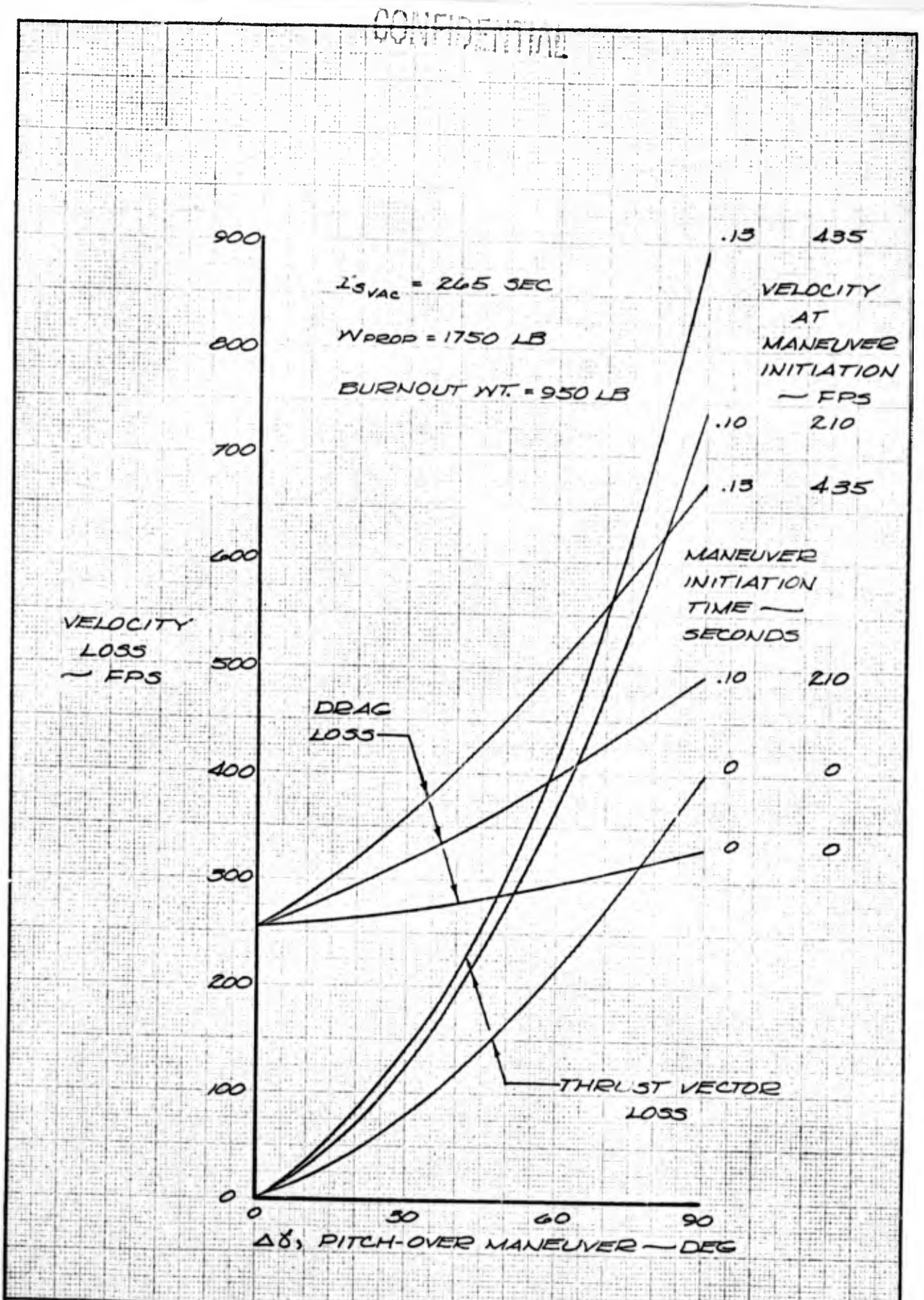

			REVISED	DATE
CALC				
CHECK				
APR				
APR				

VELOCITY PERFORMANCE
EFFECTS OF SILO LAUNCH
FIGURE 60
THE BOEING COMPANY

D2-99603-1
PAGE 113

TD 461 C-R4

5.3 EFFECTS ON EQUIPMENT AND STRUCTURE

5.3.1 Vehicle

Special strain gages were installed at Station 169 on the skirts of D-2 and D-3 to observe the effects of the silo launches on the structure. From these measurements, the bending moment plots shown in Figure 61 were obtained. The frequency of the oscillations shown in Figure 61 is approximately the same as that shown in Figure 19 before both fore and aft rings made contact with the silo walls. Therefore, only the aft ring was in contact with the silo wall during the D-3 launch, which means that the lateral motion was of small amplitude. No such conclusions can be drawn from the D-2 data. All of the information obtained from the skirt strain gages indicates that the D-2 and D-3 silo launches were accomplished with very little lateral motion and no adverse effects on the vehicle structures.

Also obtained from the strain gages were the D-2 and D-3 axial loads, which are shown in Figures 61 and 62. A tension impulse was measured by the strain gages at the impact of the sabot with the stop ring on the silo. This impulse was caused by the load required to shear the rivets in the sabot/skirt joint. The magnitude is not indicative of the actual load at the joint since the impulse was attentuated by structure between the joint and the strain gage location and also probably by the data channel. The measured loads are compared to loads calculated from flight test pressure and acceleration data before and after separation.

It was expected at the outset of the program that the variation in launch configuration from pad to silo would produce significant increases in the second stage equipment vibration levels. This prediction was made in view of the fact that in a pad launch configuration the rocket noise environment would be dissipated by natural hemispherical spreading losses while the restrained high pressure blast wave of the silo would pass over the vehicle, along with rocket noise from the engine under near maximum chamber pressure. The measured vibration data during silo launch was considerably below the pad and silo equipment test levels and did not differ significantly from the pad launch measurements. Apparently the rocket motor noise was lower than anticipated and the rocket motor exhaust plume adequately deflected the silo exhaust after the vehicle exit. For more details, see reference (6).

5.3.2 Sabot

No specific instrumentation was provided to assess the sabot structure performance. The successful vehicle performance attested to the sabot performance. Verification of clean separation of the sabot/skirt riveted joint was provided by the inspection of recovered parts of the tension tie and base skirt components.

The sabot structural breakup at impact was as expected. The massive sabot rings were stopped by the sabot stop ring, and the lighter structure buckled and was expelled from the launch tube.

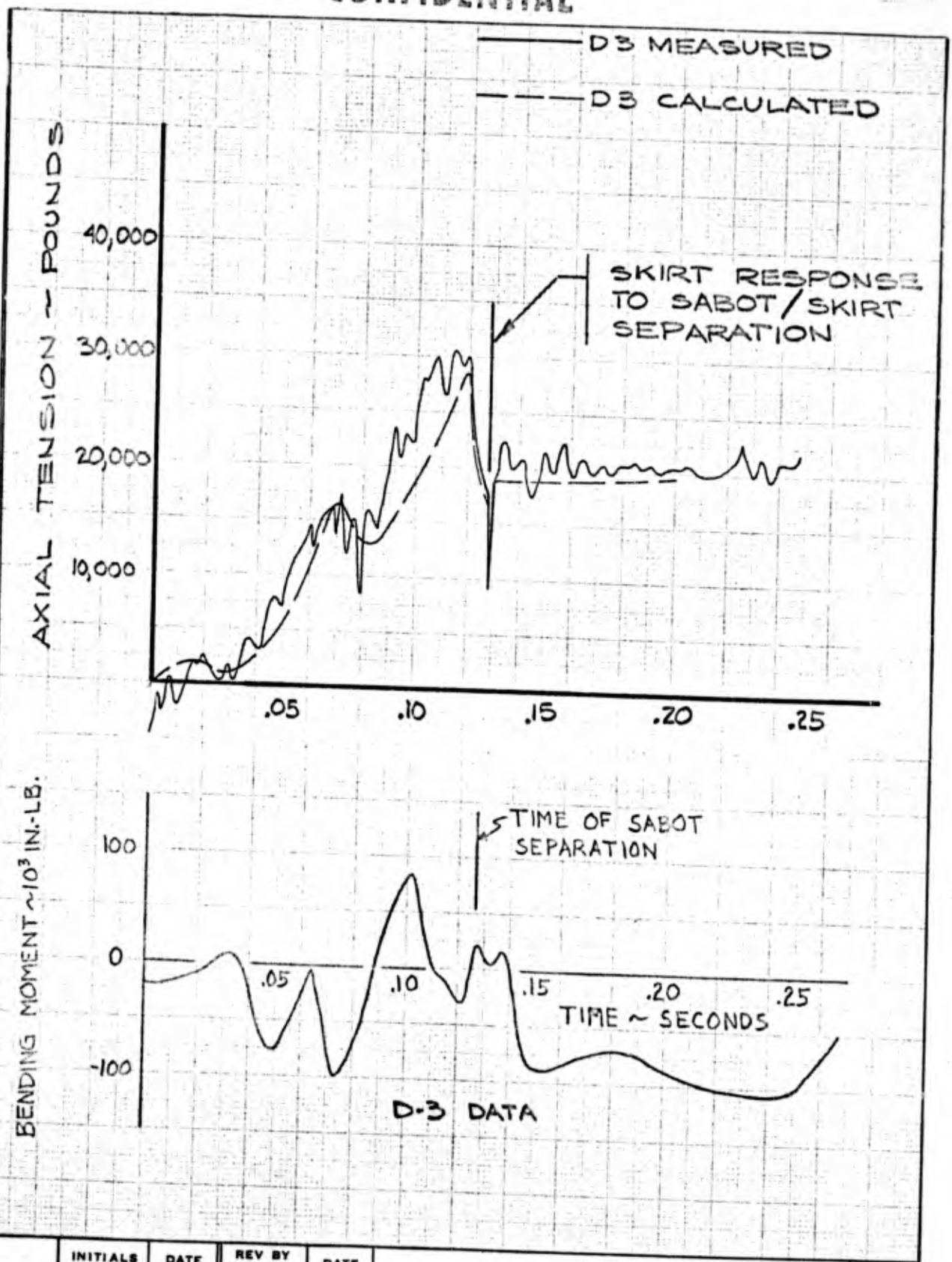

	INITIALS	DATE	REV BY INITIALS	DATE	TITLE	MODEL
CALC					AFT SKIRT MEASURED LOADS DURING SILO LAUNCH D-3 FIGURE 61	
CHECK						
APPD.						
APPD.						

U3 4013 8000 REV. 12-64

REV LTR

BOEING NO. D2-99603-1

SH

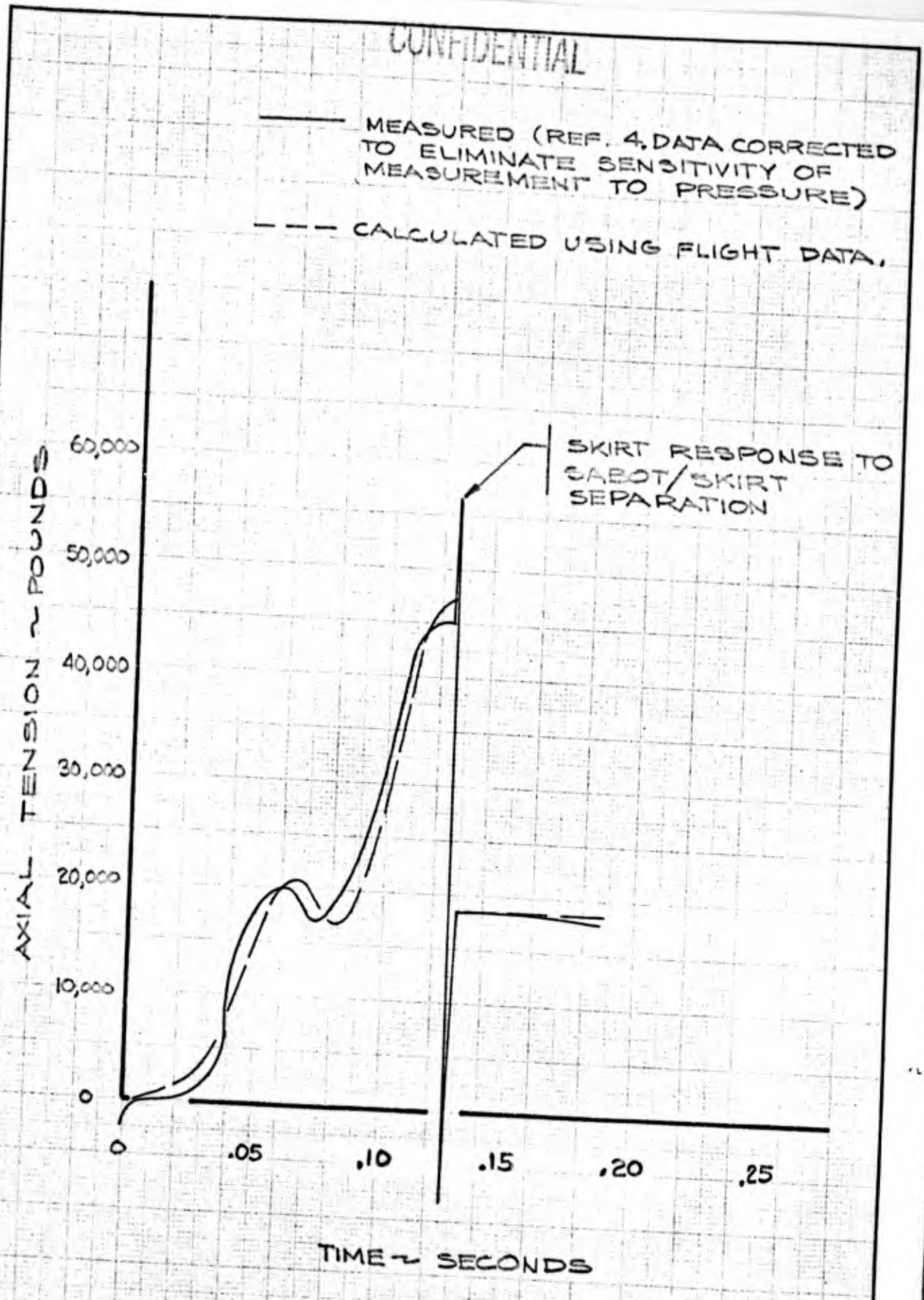

CALC			REVISED	DATE	D-2 VEHICLE AFT SKIRT AXIAL LOADS SILO LAUNCH
CHECK					
APR					
APR					
					FIGURE 62

D2-99603-1

THE BOEING COMPANY

PAGE 116

TD 461 C-R4

The Teflon thermal protection inside the sabot shell showed ablation thickness on the order of 0.005 to 0.010 in., which shows that the ablation analysis was conservative.

5.3.3 Silo

Effects of the silo launch on the silo structure were about as expected. With the exception of a stop ring nut failure on the D-2 launch and a base plate bolt failure on the D-3 launch, no structural failures occurred. Stop ring deformation was expected and occurred on both silo launches. Stop ring replacement had been provisioned for the D-3 launch. The launch tube was easily refurbished. Deposits from the motor exhaust gases were removed by hand with wire brush and emery paper. The molybdenum disulfide coating provided excellent protection. Figure 63 shows the D-3 sabot before firing and Figure 64 shows the detail of the sabot to vehicle joint after separation by the sabot stop ring at the silo lip.

Deformation of the stop ring was due to the massive sabot rings remaining essentially intact and the lack of additional bending moment capability which would have been provided if stop ring bolts with larger heads had been used.

The design did not endanger successful operation, therefore, no modification was accomplished before the D-3 launch. Deformation of the D-2 launch stop ring under the bolts indicated a peak impact force on the order of 1,600,000 lb.

The silo instrumentation on the D-3 launch was regarded as qualitative only, and showed impact time, pressure load buildup and tube and support bracket response to sabot impact. Data channels were on 2 ground tape recorders, 1 of which failed just prior to launch. As a result of the failure, only 1 stop ring gage, the 3-1/2 and 16 ft tube gages, and the support bracket gage were recorded. The 3-1/2 ft level strain gage and the stop ring strain gage saturated or failed as the sabot reached the 3-1/2 ft level and at impact respectively. No satisfactory explanation for the failure of these gages was found. The 16 ft level and support bracket strain gages whoed proper time and level response to the pressure time history and impact events during silo launch. The measurements are shown in Figure 65.

5.4 ACOUSTIC OVERPRESSURE

The measured acoustic overpressure levels from the closed breech silo launch proved to be essentially as predicted. The measurements taken during the silo launch were a combination of rocket noise and silo blast. In most cases the peak pressure recorded was the initial pressure rise felt by the instrument. This peak was caused by release of the contained silo gas on silo launches, and by motor ignition on pad launches. Measured overpressure contours are shown in Figure 66 for a silo launch, and Figure 67 for a pad launch.

The ground acoustic instrumentation also produced over-all sound level data in decibels, db, obtained by converting the root mean square acoustic pressure P_{rms}, over the duration of the pulse to decibels by the following relationship:

$$db = 20 \log (P_{rms}/0.0002 \text{ dyne/cm}^2)$$

This conventional time average relationship is given so comparisons may be

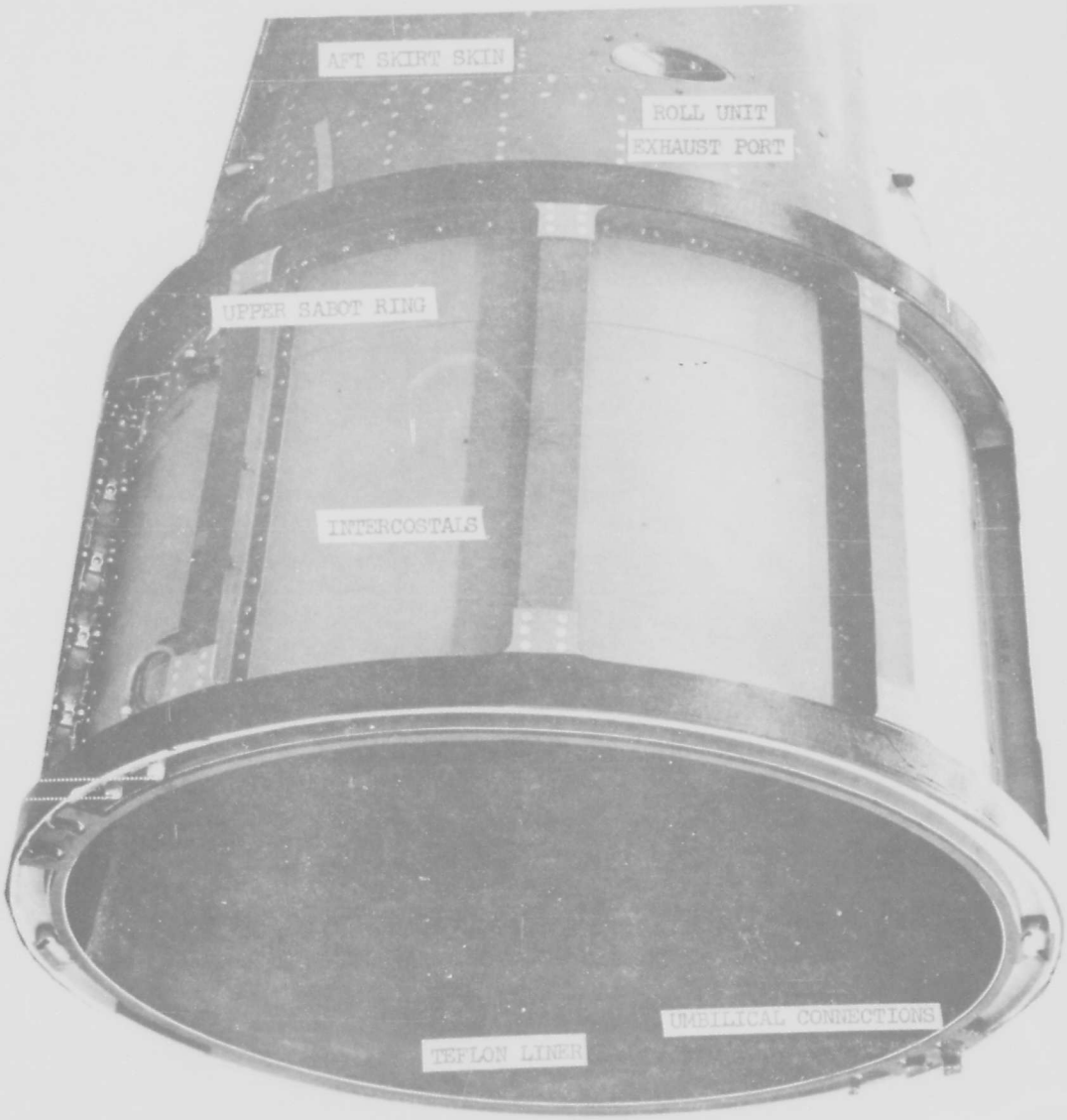

FIGURE 63 - VIEW OF SABOT ATTACHED TO D- VEHICLE - Sabot is riveted to aft skirt with 84 x 5/32 rivets which shear when upper sabot ring impacts sabot stop ring at lip of silo.

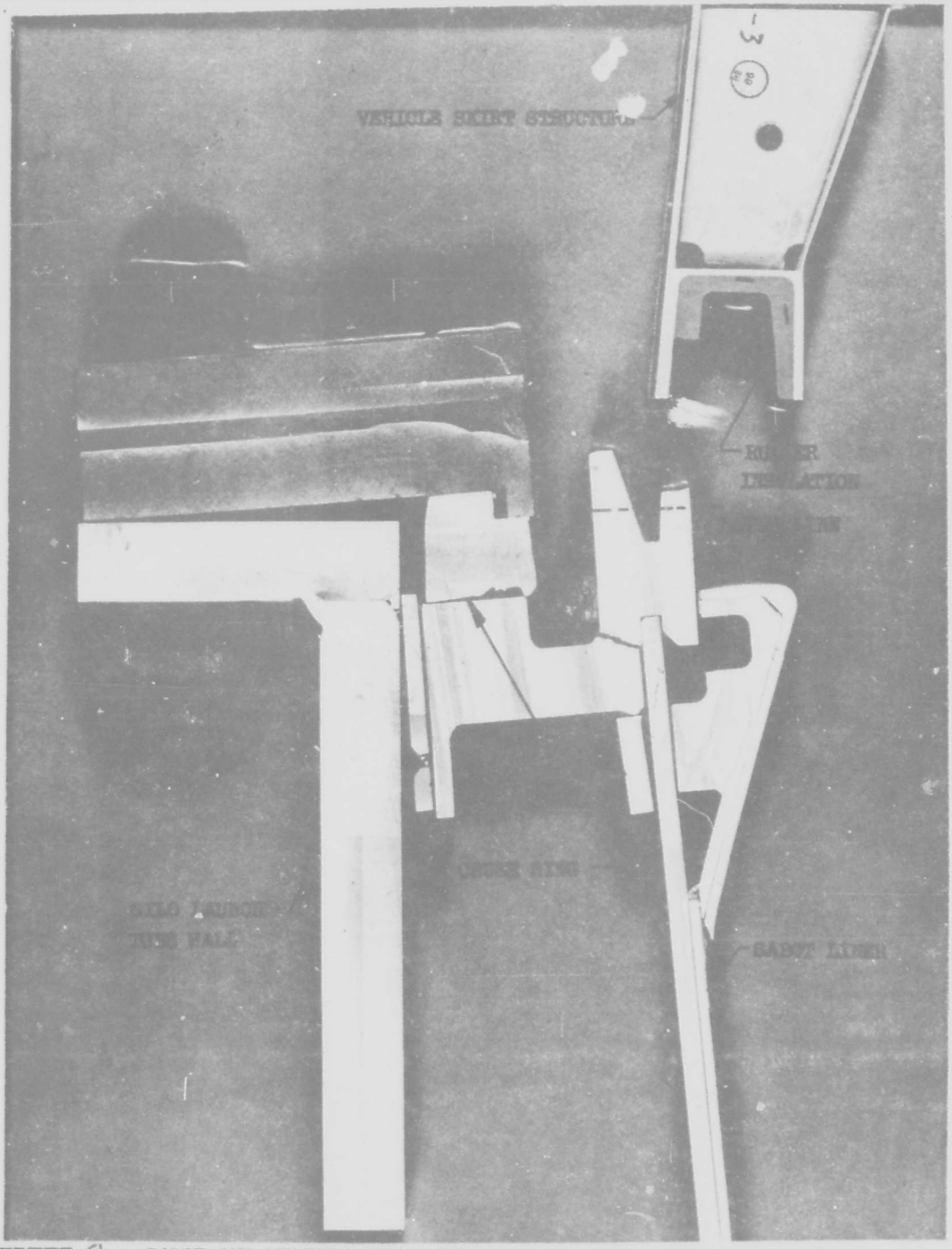

FIGURE 64 - SABOT AND VEHICLE SKIRT RELATIONSHIP JUST AFTER SABOT SEPARATION. Riveted joint between skirt and sabot is sheared when sabot impacts stop ring at silo lip. Shock is reduced by crush ring. Photo shows distortion of crush i stop rings after D-2 launch.

US 4802 1434 ORIG. 4-65

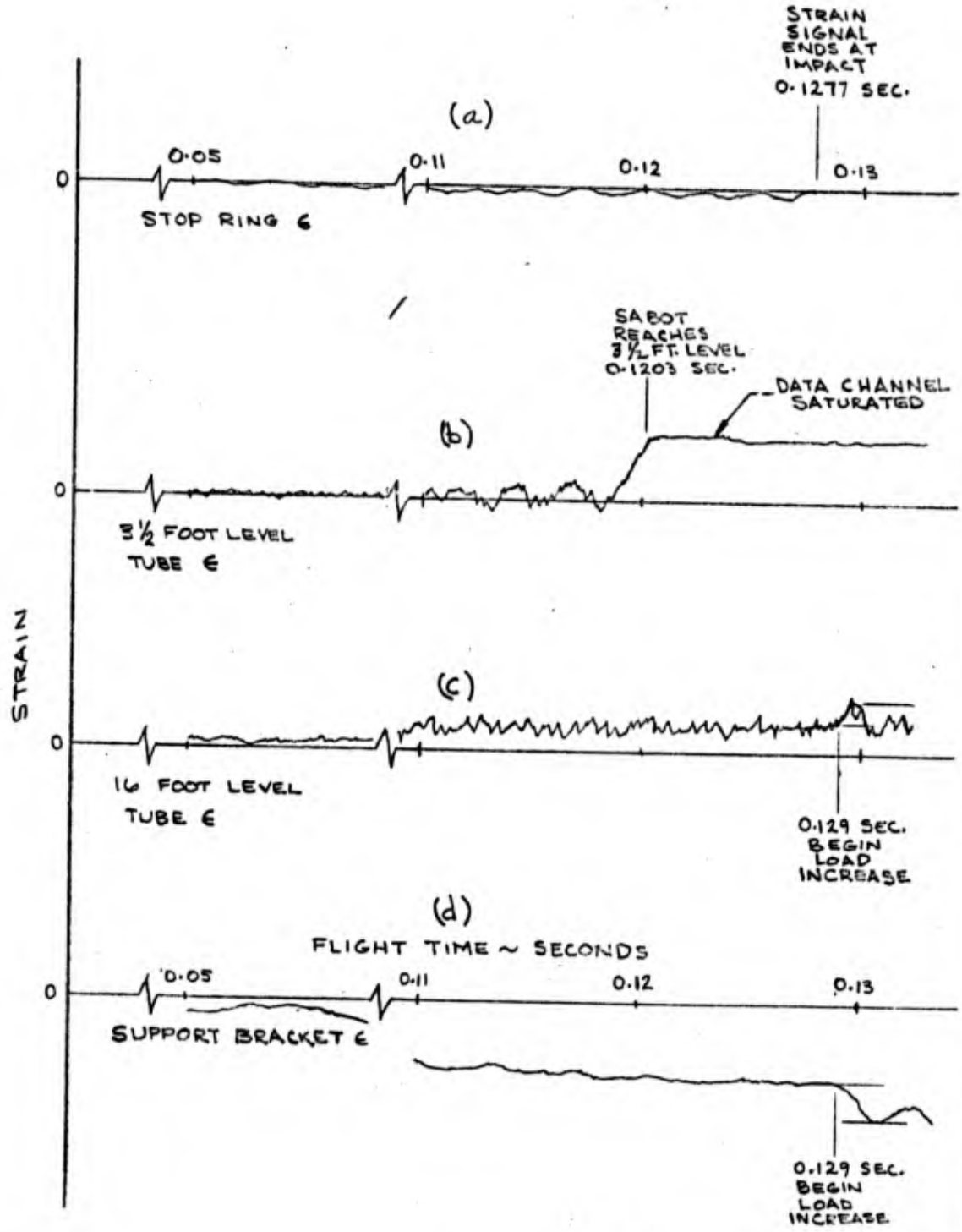

CALC		10/16/5	REVISED.	DATE
CHECK				
APPD				
APPD				

STRAIN VS TIME FOR SILO COMPONENTS
FIGURE 65

THE BOEING COMPANY

HIBEX D-3
D2-99603-1

120

U3 4036 3000 REQ 10388

FIG 3.4.3-1

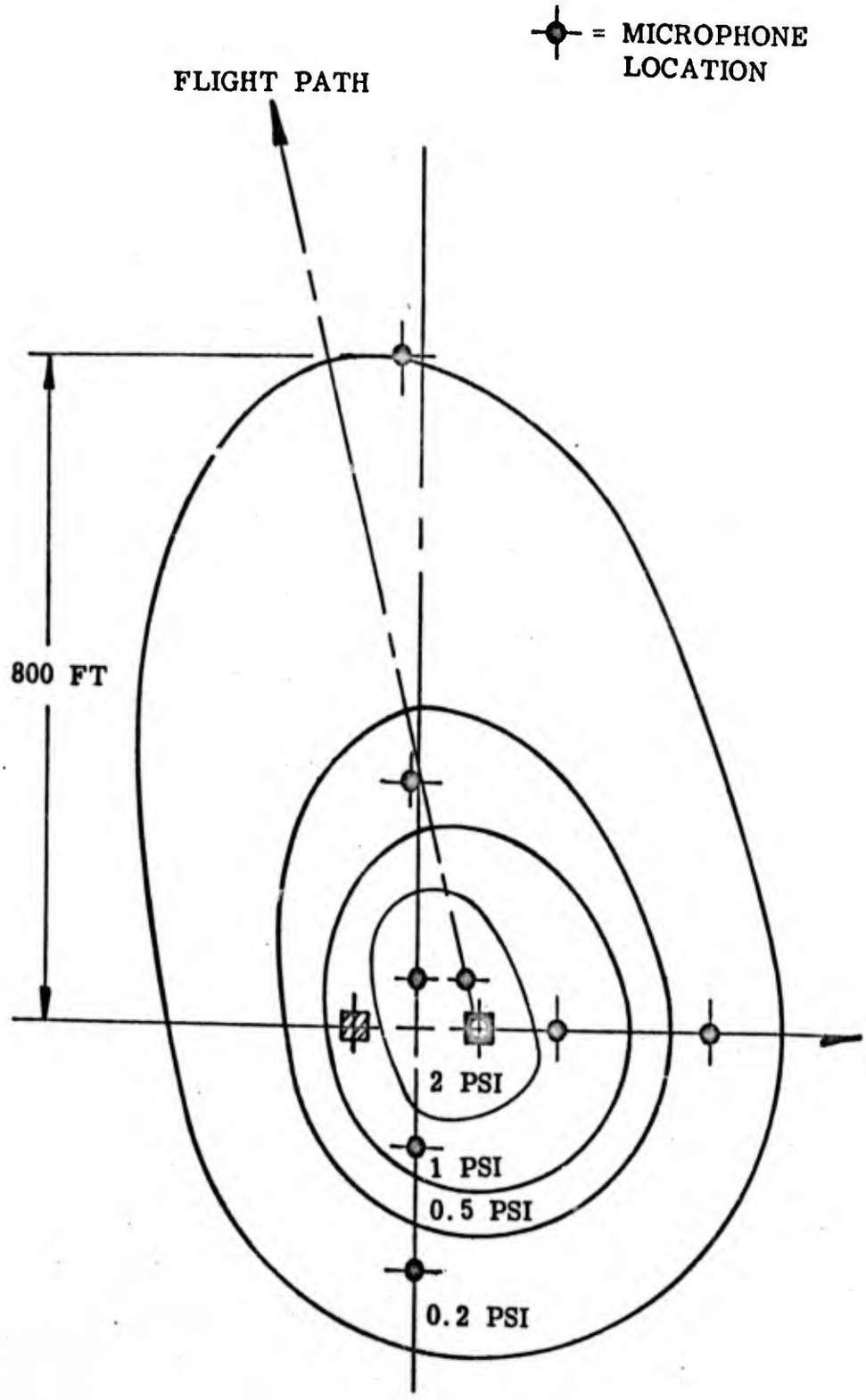

FIGURE 66 - ACOUSTIC OVERPRESSURE FOR SILO LAUNCH

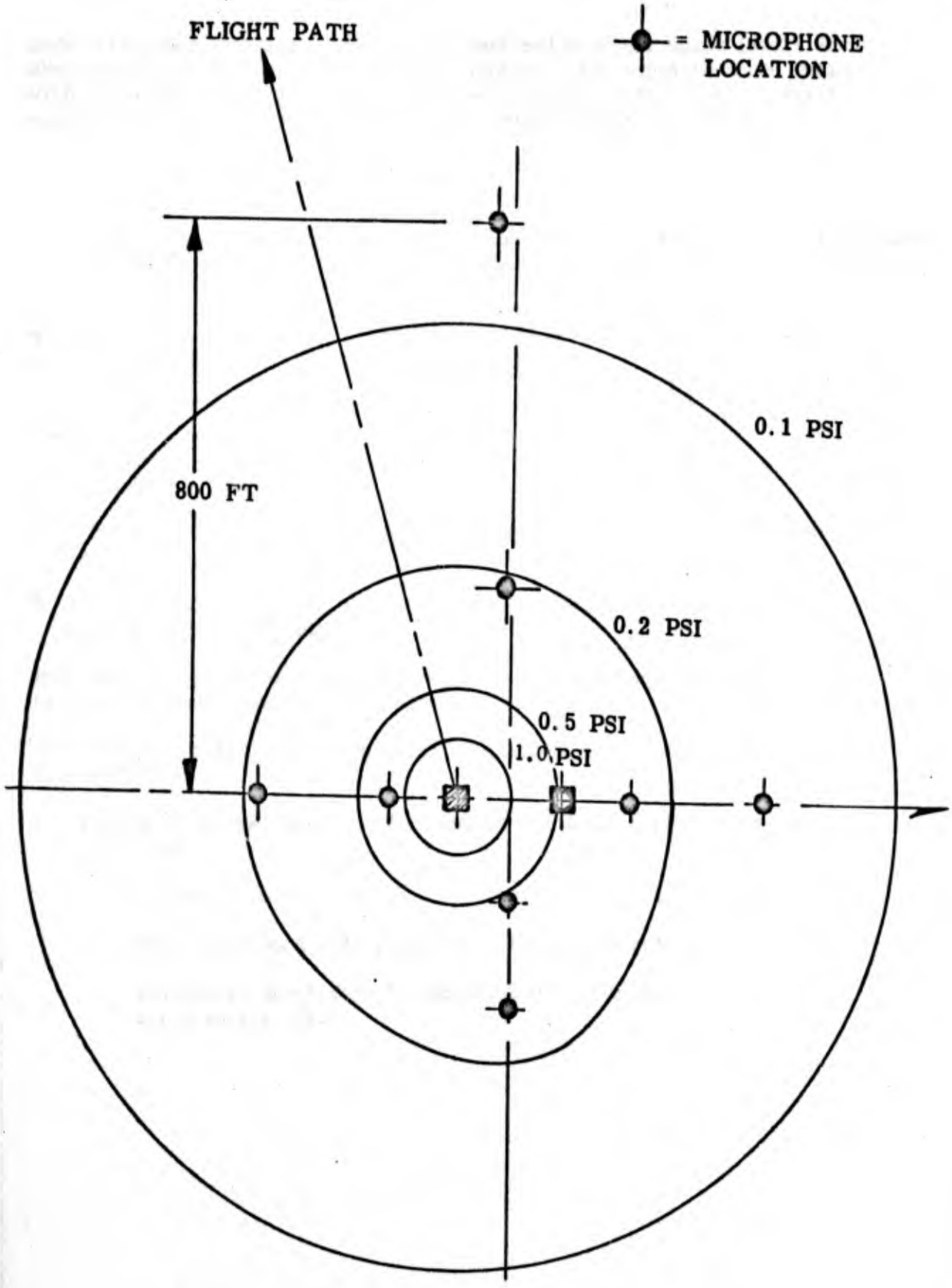

FIGURE 67 - ACOUSTIC OVERPRESSURE FOR PAD LAUNCH

made with other vehicles. The nominal measured over-all sound levels are shown in Figure 68 for a silo launched vehicle. For a pad launched vehicle with a near vertical flight the levels were roughly 8 db lower. A brief summary of peak measured and estimated levels is presented below:

	Approximate Radius ft	Elevation ft	Estimated Maximum psi	Peak psi Measured	Over-all Sound Level db	Pad Launch Peak psi
*D-3	5	2.5	200.0	224.0	191	-
	5	9	85.0	86.0	194	-
	60	2	10.0	12.4	165.5	-
*D-2	100	2	4.2	4.0	164	0.8
	166	2	2.6	1.3	155	0.5
	300	2	.8	0.75	149	0.2
	800	2	.3	0.2	137.5	0.08
	1300	2	.1	0.1	133	0.03

* D-2 had a 50 ft deep silo, 170 psia back pressure and no microphones inside of a 100 ft radius.

* D-3 had a 30 ft deep silo, 254 psia back pressure and no microphones outside of a 60 ft radius.

Peak measured pressures in the above table have not been adjusted for the difference between the D-2 and D-3 silos.

The following blast values are given to evaluate the damage potential of the measured data:

For Short Natural Periods of Vibration and Small Plastic Deformation at Failure.

Broken windows	0.5 to 1.0 psi
Failure of wood siding panels	1.0 to 2.0 psi
Failure of unreinforced concrete block wall panels.	2.0 to 3.0 psi

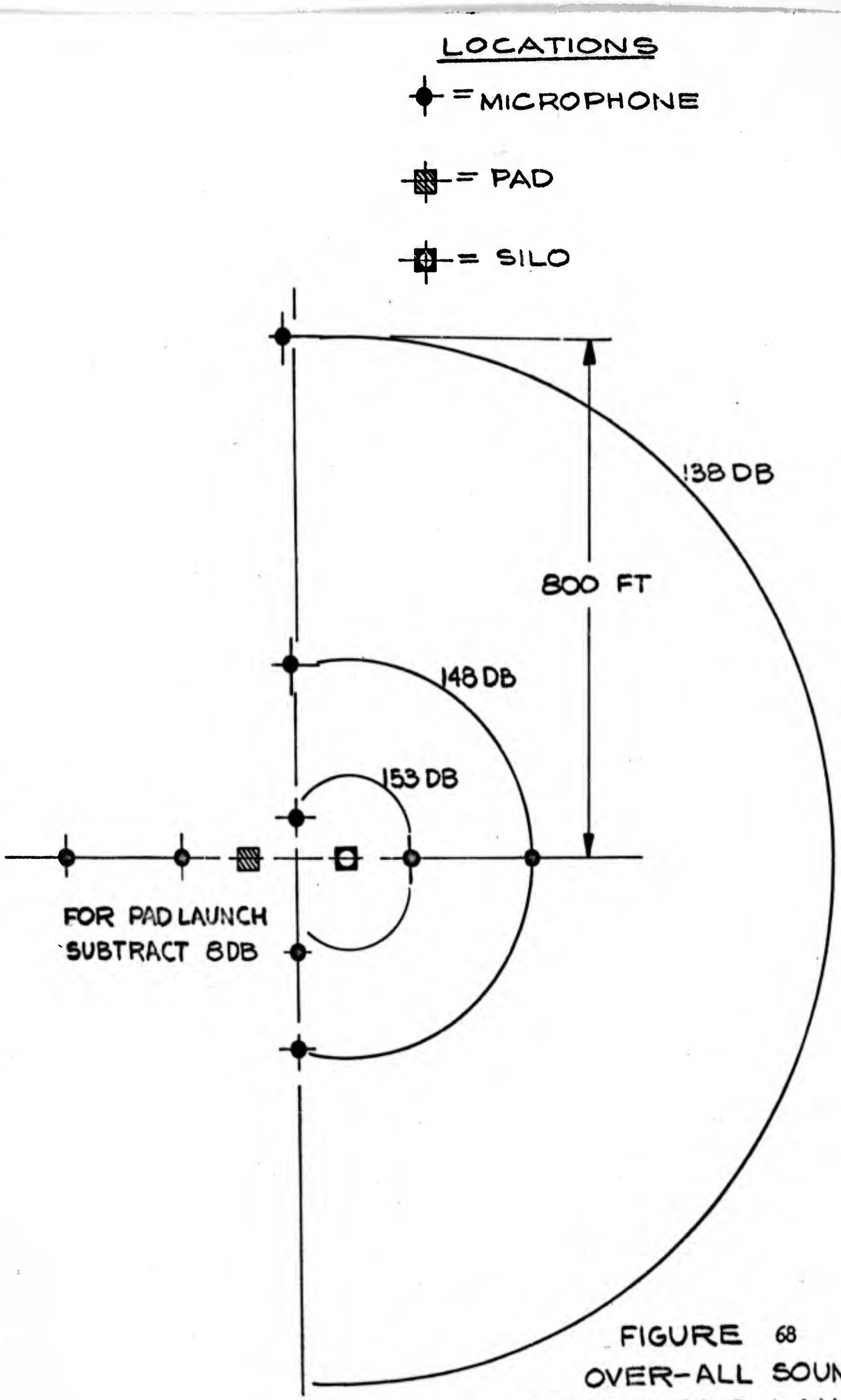

FIGURE 68
OVER-ALL SOUND
LEVELS SILO LAUNCH

ACTIVE SHEET RECORD

SHEET NO.	REV LTR	ADDED SHEETS				SHEET NO.	REV LTR	ADDED SHEETS			
		SHEET NO.	REV LTR	SHEET NO.	REV LTR			SHEET NO.	REV LTR	SHEET NO.	REV LTR
1						49					
2						50					
3						51					
4						52					
5						53					
6						54					
7						55					
8						56					
9						57					
10						58					
11						59					
12						60					
13						61					
14						62					
15						63					
16						64					
17						65					
18						66					
19						67					
20						68					
21						69					
22						70					
23						71					
24						72					
25						73					
26						74					
27						75					
28						76					
29						77					
30						78					
31						79					
32						80					
33						81					
34						82					
35						83					
36						84					
37						85					
38						86					
39						87					
40						88					
41						89					
42						90					
43						91					
44						92					
45						93					
46						94					
47						95					
48						96					

ACTIVE SHEET RECORD

SHEET NO.	REV LTR	ADDED SHEETS				SHEET NO.	REV LTR	ADDED SHEETS			
		SHEET NO.	REV LTR	SHEET NO.	REV LTR			SHEET NO.	REV LTR	SHEET NO.	REV LTR
97											
98											
99											
100											
101											
102											
103											
104											
105											
106											
107											
108											
109											
110											
111											
112											
113											
114											
115											
116											
117											
118											
119											
120											
121											
122											
123											
124											
125											
126											
127											
128											
129											